ZERO BUILD JOURNAL

INTERNATIONAL SCIENTIFIC FORUM

Year (Yıl) : 2026 Volume (Cilt) : 4 Issue (Sayı) : 1

Electronic Journal
e-ISSN: 2980-0048

Editorial

We are pleased to present Volume 4, Issue 1, which brings together critical research focused on energy efficiency, sustainable infrastructure, and advanced simulation methodologies within the built environment. This issue highlights the urgent transition toward smarter, more resilient cities and high-performance building standards.

The contributions in this issue range from infrastructural analysis to component-level optimization. Readers will find a comprehensive economic evaluation of smart ultrasonic gas meters, offering insights into the digitization of urban resource management. Further studies address the precision of building energy modeling through improved Typical Meteorological Year (TMY) datasets and explore the thermal enhancement of domestic hot water systems using Phase Change Materials (PCM).

Finally, two comparative studies critically examine the revised TS 825 standard. By evaluating it against Passive House criteria and analyzing various wall materials across diverse climate zones, these articles emphasize the necessity of moving from static calculations to dynamic simulations. Together, these works underscore the vital role of innovative technologies and rigorous standards in reducing carbon footprints and achieving energy targets.

ZeroBuild Journal

Index
İçindekiler

ZEROBUILD JOURNAL

Araştırma Makalesi

Engin ve ark. 04:01 (2026) 1-19

Akıllı Şehirlerde Doğal Gaz Sayaçlarının Dönüşümünün Ekonomik Analizi

Tahsin Engin[1], Ünal Uysal[2], Yusuf Yaşa[3]

[1] İstanbul Teknik Üniversitesi, İSTANBUL
[2] Sakarya Üniversitesi, SAKARYA,
[3] İstanbul Teknik Üniversitesi, İSTANBUL
*Sorumlu Yazar: uysal@sakarya.edu.tr

Öne Çıkanlar

- Akıllı ultrasonik sayaçlar, ömür boyu 132,19 dolar tasarruf ve mekanik sayaçlara kıyasla 18,44'lük yüksek bir fayda-maliyet oranı sağlar.
- Bu sayaçların Türkiye genelinde kullanımı, yılda yaklaşık 720 milyon m³ doğal gaz tasarrufu sağlayabilir.
- Akıllı takip sistemiyle gaz kullanımı %9 azalır; bu da ulusal çapta 720 milyon dolar tasarruf demektir.
- Sistem, sağladığı doğrudan tasarrufla yatırım maliyetini 1,94 yılda amorti eder.

Geliş Tarihi: 06.12.2025 Kabul Tarihi: 05.01.2026 Doi: 10.5281/zenodo.18359985

Amaç

Bu çalışma, Türkiye'deki konutlarda kullanılan geleneksel mekanik ve yeni nesil akıllı ultrasonik doğalgaz sayaçlarının ekonomik ve çevresel performanslarını karşılaştırmaktadır. Çalışma, yüksek ilk yatırım maliyetlerine rağmen, akıllı sayaçların ölçüm hassasiyeti ve veri yetenekleriyle sağladığı uzun vadeli ekonomik uygulanabilirliği ve enerji verimliliğine katkısını ortaya koymayı hedeflemektedir.

Metot

Ekonomik değerlendirme sürecinde Bugünkü Değer (BD), Gelecekteki Değer (GD) ve Fayda-Maliyet (F/M) analizi yöntemleri kullanılmıştır. Enerji Piyasası Düzenleme Kurumu (EPDK) verilerine uygun olarak 14 yıllık bir ekonomik ömür ve yıllık ortalama 1000 m³ tüketim değeri baz alınmıştır. Hesaplamalarda %4 Minimum Cazip Faiz Oranı (MCFO) kullanılarak, Amerikan Doları ($) cinsinden bir yaşam döngüsü maliyet analizi gerçekleştirilmiştir. Ayrıca, tüketici davranışlarındaki değişimin tasarrufa etkisi literatür verileriyle değerlendirilmiştir.

Sonuçlar

Akıllı sayaçların, mekanik olanlara kıyasla ömür boyu 132,19 USD tasarruf sağladığı ve fayda-maliyet oranının 18,44 olduğu tespit edilmiştir. Türkiye genelinde bu teknolojiye geçişin, tüketici alışkanlıklarını değiştirerek yıllık %9 (720 milyon m³) doğalgaz tasarrufu sağlayacağı ve yatırımın 1,94 yılda kendini amorti edeceği hesaplanmıştır.

Anahtar Kelimeler: Akıllı şehir, Mekanik diyaframlı metre, Akıllı ultrasonik metre, ekonomik analiz.

ZEROBUILD JOURNAL

Research Article

Engin et al. 04:01 (2026) 1-19

Economic Analysis of the Transformation of Natural Gas Meters in Smart Cities

Tahsin Engin[1], Ünal Uysal[2], Yusuf Yaşa[3]

[1] İstanbul Teknik Üniversitesi, İSTANBUL
[2] Sakarya Üniversitesi, SAKARYA,
[3] İstanbul Teknik Üniversitesi, İSTANBUL
*Corresponding Author: uysal@sakarya.edu.tr

Highlights

- Smart ultrasonic meters yield 132.19 USD in lifetime savings per unit, demonstrating a superior benefit-cost ratio of 18.44 over mechanical meters.
- Implementing smart ultrasonic meters in Türkiye could save approximately 720 million cubic meters of natural gas annually.
- Enhanced consumer monitoring through smart technology leads to a 9% reduction in gas usage, totaling 720 million dollars in national savings.
- Initial investment costs for smart ultrasonic meters are recovered in just 1.94 years through direct consumption savings alone.

Received: 01.03.2025 Accepted: 13.04.2025 Doi: 10.5281/zenodo.18359985

Abstract: With the start of natural gas use in Türkiye, mechanical diaphragm meters were first used to measure consumption and are still widely used in Türkiye. However, mechanical failures, pressure losses and time-dependent aging occur in mechanical diaphragm meters due to friction inside the meter. This situation causes pressure losses and increased energy consumption during gas transmission and indirectly increases carbon emissions. However, since ultrasonic meters do not contain moving mechanical parts, they consume less energy and have a longer life. This feature reduces the carbon footprint that occurs during the production and operation process. In recent years, energy management, efficient use of resources and sustainability have come to the fore in smart cities around the world. A smart city is an urban area that uses different types of electronic IoT sensors to collect data and then uses the information obtained from this data to manage assets, resources and services efficiently. It is known that the initial investment costs of smart ultrasonic meters are higher than mechanical diaphragm meters. Therefore, it is necessary to analyse which of the mechanical diaphragm and smart ultrasonic meters is more economical, taking into account the initial investment costs and other factors. This study aims to compare the two meter types by examining initial investment, operational costs, and economic performance over their lifecycle. The evaluation is based on (PV), (FV), (BCR) methodologies. Findings indicate that, despite their higher upfront costs, smart ultrasonic meters are economically more viable in the long term due to lower operational expenses and longer lifespan. According to the literature research, it has been understood that there is no study on the contribution of natural gas meters to the economy if used in Turkey. With the development of smart cities, it has been determined what the economic impact of the transition to smart ultrasonic meters will be in Turkey.

Keywords: Smart city, Mechanical diaphragm meter, Smart ultrasonic meter, economic analysis.

Nomenclature

AC *Aging Costs*
B/C *Benefit–Cost*
CC *Communication Cost*
EPDK *Energy Market Regulatory Authority*
F/A, A/P, P/G *interest rate*
FV *Future Value*
MARR *Minimum Attractive Rate of Return*
OC# *Opening/Closing and Maintenance Cost*
PV *Present Value*
PLC *Personnel Costs*
PL *Pressure Loss*
RC *Reading Cost*
SV *Scrap Value*
TC *Temperature Difference*
ΔF *Difference in benefits or advantages.*
ΔD *Difference in disadvantages that may occur.*
ΔM *Difference in project costs.*
IIC *Initial Investment Cost*
PV(A) *Investment of Mechanical Diaphragm Gas Meter*
PV(B) *Investment Smart Ultrasonic Gas Meter*

1. Methods For Measuring Natural Gas Flow Rate

In both Türkiye and around the world, gas meters are manufactured using various measurement methods and technologies to accurately quantify gas consumption. In general, natural gas meters can be classified into three main categories based on their measurement capabilities: mechanical, electronic, and smart meters. Among the available energy sources, natural gas stands out as one of the most significant both domestically and globally. When combusted, natural gas primarily produces CO_2 and H_2O, making it the least harmful fossil fuel to the environment. Natural gas has been in use in Türkiye for more than three decades. For companies engaged in natural gas distribution, the most critical factor is to accurately determine and invoice the cost of residential and industrial consumption [1].

At present, gas consumption (flow rate) is measured through different methods based on physical principles. The gas flow measurement systems used for this purpose are generally classified as diaphragm, rotary, turbine, orifice, Coriolis, thermal, and ultrasonic meters [2].

In natural gas installations, the most commonly used meter types are diaphragm, rotary, and turbine meters. Rotary and turbine meters are typically employed in industrial facilities and large-scale central heating systems, while diaphragm meters are predominantly used in residential and small commercial installations. According to the Customer Services Regulation of the Energy Market Regulatory Authority (EMRA), gas meters for residential and commercial installations are provided to customers by the gas distribution companies [3].

2. Mechanical Diaphragm Gas Meters and Advanced Smart Ultrasonic Gas Meters

This section presents a comparative evaluation of mechanical diaphragm meters and smart ultrasonic meters commonly used in Türkiye. The comparison encompasses various technical and economic aspects, including mechanical and electrical/electronic components, maintenance and calibration intervals, cost structures, measurement principles, accuracy levels, operational advantages, usage areas, and overall economic performance. The detailed comparison is outlined in the following section.

Structural (Mechanical) Characteristics of Mechanical Diaphragm Meters: The diaphragm chamber–based measurement system represents the most widely adopted method for natural gas metering. Meters employing this principle are known as diaphragm meters, which constitute the most common type of gas meter used in residential and small commercial applications. The first dry-type diaphragm meter, incorporating two moving diaphragms, two sliding valves (drawer-type mechanism), and a counter, was invented and patented by Thomas Glover in England in 1844.

Modern diaphragm meters utilized in Türkiye are designed with four measuring chambers and are available in various sizes, each with defined maximum and minimum flow rate capacities. Diaphragm meters operate effectively over a wide dynamic measurement range. Similar to other positive displacement meters, diaphragm meters contain a series of chambers that alternately fill and discharge a known gas volume. The primary components of these meters include:

Figure 1. Front view of natural gas meter outer body and counter

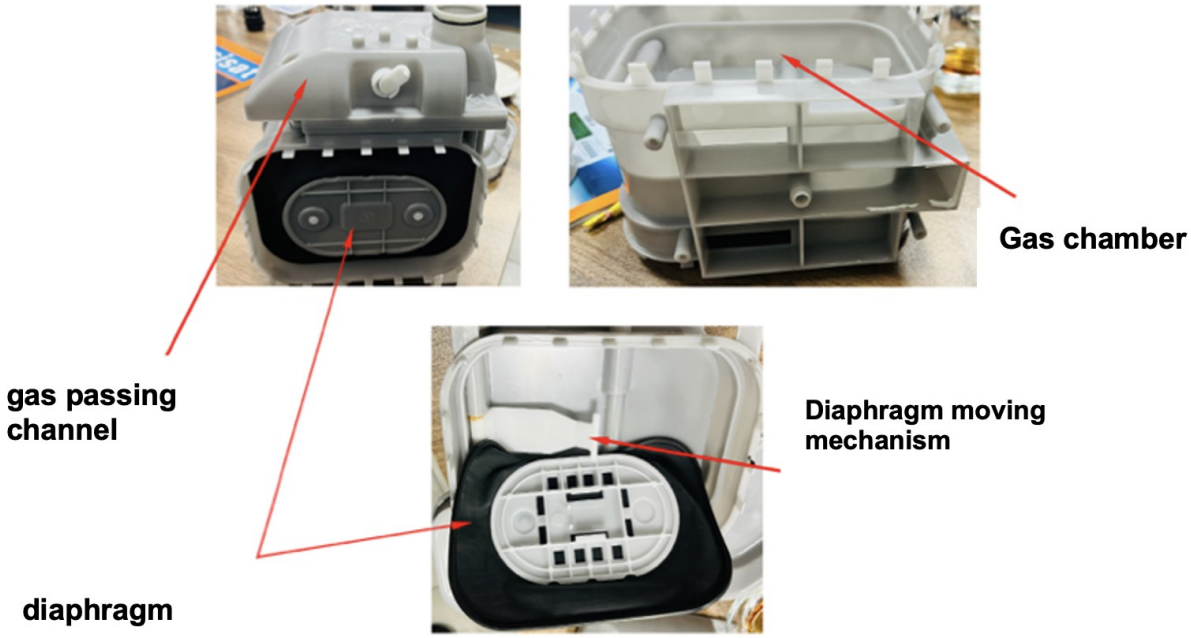

Figure 2. Front view of the natural gas meter's outer casing and register.

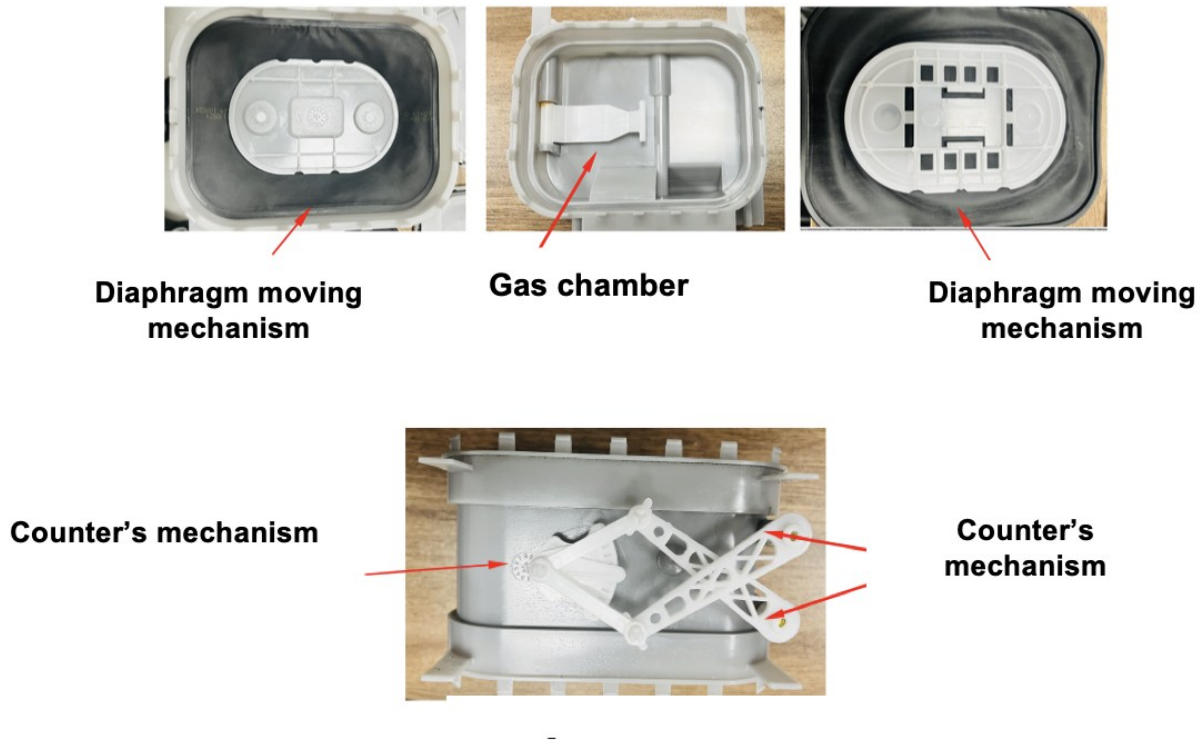

Figure 3. Main body and moving chambers and diaphragm

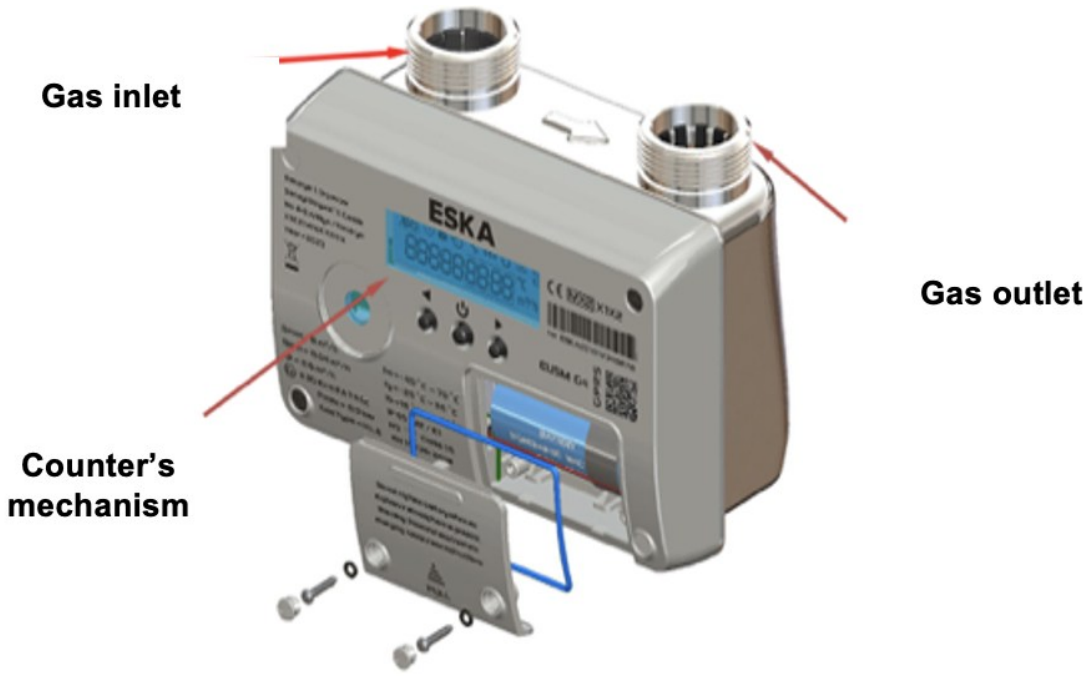

Figure 4. Smart meter

1. A valve mechanism controlling gas inlet and outlet, (Figure 1.) and
2. Measuring chambers, (Figure 2. and 3.)
3. A counter (register) mechanism for volume indication (counter) (Figure 1.) [4,5]

Structural (Mechanical) Design of Smart Ultrasonic Gas Meters: Ultrasonic gas meters perform flow measurement through an ultrasonic sensing system that determines gas velocity using high-frequency sound waves. In these meters, ultrasonic transmitters positioned

along the internal measurement channel emit sound pulses that propagate through the flowing gas. The receivers detect these signals after they traverse the gas stream, and the resulting time difference or frequency shift between the transmitted and received waves is used to calculate the gas flow rate.

The variation in the propagation velocity of the sound waves directly correlates with the gas velocity, which in turn enables the precise determination of the volume of gas passing through the meter (Figure 4).

All structural and functional components of the ultrasonic gas meter are illustrated in detailed. The subsequent figure 5 and 6. present photographs of the key components, along with explanations of their measurement roles and operating principles within the system [6].

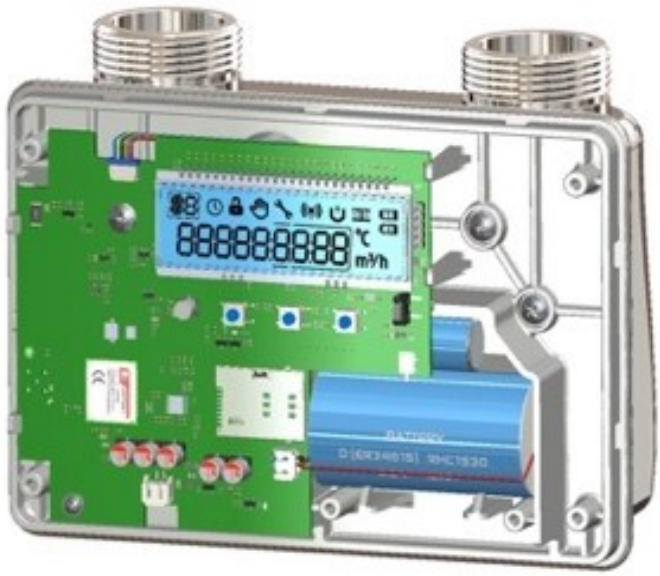

Figure 5. Smart meter upper body and electronic card

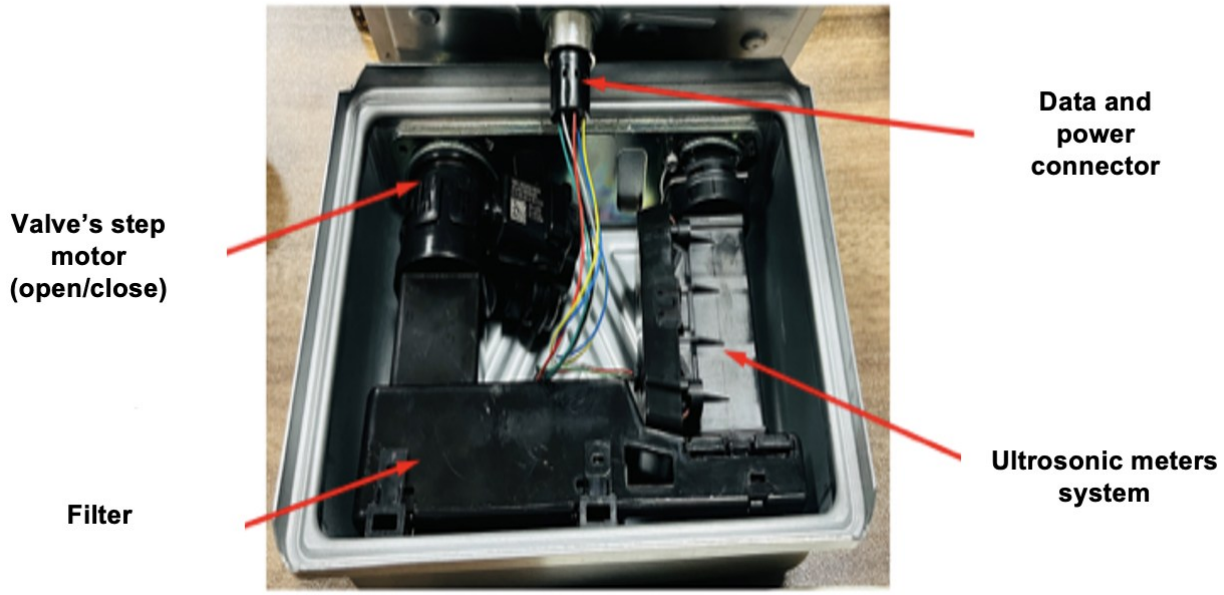

Figure 6. Main body and elements

3.1. Economic Analysis of Gas Meters

The economic evaluation of the gas meters was conducted using three fundamental financial assessment techniques: Present Value Analysis, Future Value Analysis, and Benefit Cost Analysis [7]. Although these methods differ in terminology and calculation focus, they share a common analytical framework, aiming to assess the economic feasibility and long-term financial performance of metering systems under comparable operational conditions.

3.2. Economic Analysis of Gas Meters Based on The Present Value Method

According to the EMRA, the average service life of a gas meter is 14 years. Based on statistical data, the annual average gas consumption per subscriber is assumed to be 1000 m³. Using these parameters, an economic analysis of mechanical diaphragm meters and smart ultrasonic meters was performed, considering their initial investment costs and annual operating expenses.

Initial Investment Cost: The purchase cost of mechanical diaphragm meters typically ranges between 25–50 USD, with an average value of 37.5 USD taken for calculations [8, 9, 10].

Smart ultrasonic meters, on the other hand, cost between 80–120 USD, with an average of 100 USD assumed

Annual Operating Costs: Operating expenses refer to costs incurred during production or operation, which vary depending on the type and characteristics of the system. For both mechanical diaphragm and smart ultrasonic meters, the main cost components include calibration, personnel, pressure losses, temperature deviations, disconnection/ reconnection, billing dispute handling, and communication/software expenses. The estimated annual cost per meter based on these components is discussed.

Calibration and Maintenance Costs: Mechanical diaphragm meters require calibration after 10 years of use. After recalibration, they can be operated for another 10 years, after which they must be replaced. Thus, their maximum economic life is 20 years. Within the 14-year EMRA-defined period, at least one calibration is required, costing 14 € (≈15.66 USD) per meter.

Smart ultrasonic meters, however, require no recalibration or mechanical maintenance throughout their life, except for a battery replacement (5 €) after 15 years. Therefore, maintenance costs are considered negligible.

Personnel Costs: Personnel costs for mechanical diaphragm meters arise from manual reading, field visits for disconnection/reconnection, and sealing operations in cases of non-payment, malfunction, or billing objections.

Meter Reading: In a city with 350,000 subscribers where meters are located close to each other, one person can manually read about 500–600 meters per day. Approximately 60 personnel are required to complete all readings, with an average of 8.000 connection/disconnection operations monthly. Considering a personnel cost of 50,000 TL/month (March 2025) and additional vehicle rental and fuel expenses, the average annual reading cost per mechanical meter is 4 € (≈4.35 USD).

For smart ultrasonic meters, readings are performed remotely. Only five staff members are required for monitoring and support, while a SIM card communication cost is incurred. Thus, the annual reading cost per smart ultrasonic meter is 2 € (≈2.18 USD).

Connection/Disconnection Costs: Each subscriber with a mechanical meter requires an average of three field visits over 14 years for disconnection/reconnection due to new subscriptions, unpaid bills, or maintenance. Each operation costs 5 € (≈5.45 USD).

For smart ultrasonic meters, such operations are executed remotely, thus eliminating most costs. However, occasional field visits for installation or repair are still necessary, estimated at 2 € (≈2.18 USD) annually.

Communication and Software Costs: Mechanical diaphragm meters do not incur any communication or software expenses. Smart ultrasonic meters, however, require costs for SIM card data transmission, server infrastructure, software maintenance, and staffing. These total 1 € (≈1.14 USD) per meter annually.

Operating Costs Arising from Pressure Losses: Mechanical diaphragm meters inherently cause

an average pressure loss of 2 mbar, while ultrasonic meters have a pressure loss of 0.5 mbar [8, 11]. To compensate for the higher loss, gas booster stations must consume additional energy. Over 14 years, the excess energy consumption of mechanical meters corresponds to 14 m³ of natural gas, equivalent to 4 € (≈4.35 USD) per year [12, 13, 14].

In ultrasonic natural gas meters, it is observed that the device consists of only three major components. Consequently, there are no mechanical transmission elements or parts that may cause friction within the system. According to the EN 14236 standard [12], Class 1.5 ultrasonic meters must exhibit a pressure loss of 0.5 mbar or less during gas flow, which may occur only across the inlet filter or internal flow channels [15, 13, 16].

As previously calculated, mechanical diaphragm meters demonstrate significantly higher pressure losses due to their internal moving components. Since the pressure loss of smart ultrasonic meters is negligible and does not meaningfully affect gas consumption or operational performance, it should not be included in the cost and energy-loss computations.

Costs Associated with Age-Related Under-Registration: Age-related measurement errors in mechanical diaphragm gas meters lead to revenue losses due to systematic under-registration [1,4,9]. The mechanical components of these meters including gears, levers, and diaphragms—undergo material degradation over time, resulting in deviations between the initial calibration performance and the measurement accuracy observed after ten years of operation. Experimental field measurements conducted on meters with an annual consumption of approximately 1000 m³ indicate that age-related under-registration increases between 4% and 15%, depending on environmental conditions and usage frequency [13,14,17].

Based on these evaluations, it is estimated that a mechanical diaphragm meter produces a cumulative under-registration of approximately 425 m³ over ten years. Considering this information, the annual incremental under-registration caused by aging during the first decade was calculated as 1.67 € per year, which corresponds to 1.90 USD per year.

In cases where the meter is recalibrated and reused for an additional cycle, aging-induced measurement errors are expected to accelerate due to deformation in the diaphragm and gear mechanisms accumulated during the first ten-year period. For simplicity, the remaining four years of the meter's lifetime were assumed to follow similar age-related error characteristics, and the same rate was applied in the cost analysis.

In contrast, studies conducted on smart ultrasonic meters show that the maximum measurement deviation over twenty years of operation without requiring recalibration is no more than 1.5% [18, 19, 20]. This value falls well within the acceptable limits defined by the standards, meaning that the meter effectively maintains an operational error rate of 0% relative to calibration requirements. Consequently, ultrasonic meters do not generate any cost associated with under-registration.

Costs Arising from Temperature-Related Measurement Deviations: The density of natural gas varies with temperature; therefore, billing calculations must apply a correction factor to determine the actual consumption. Meteorological temperature data are typically used to derive this factor by determining a gas-density based correction coefficient for each month. However, temperature can fluctuate not only throughout the month but even within a single day. Additionally, regional temperature variations such as differences between the northern and southern or eastern and western districts of a city contribute to deviations in the applied correction factor. Considering a metropolitan area such as Istanbul, these spatial and temporal variations can lead to significant discrepancies. As a result, billing calculations inherently contain a degree of uncertainty.

Based on meteorological data and temperature measurements obtained from 525 smart ultrasonic meters deployed in a field study, it was determined that the discrepancy between the correction factor derived from meteorological averages and that derived from actual meter-level temperature readings resulted in an annual under-billing of 2.5 €, equivalent to 2.72 USD [4,9].

In smart ultrasonic meters, the presence of an integrated temperature sensor enables real-time

temperature measurement, which is collected through the data acquisition system. Consequently, temperature-dependent correction factors can be calculated with higher accuracy. This allows billing to be based on actual consumption values, ensuring precise invoicing. Under these conditions, neither the gas distribution company nor the subscriber faces uncertainty regarding billing accuracy.

Scrap Value: Since the internal components of mechanical diaphragm gas meters are primarily made of plastic, their salvage value is negligible; only the external metallic housing contributes to residual value. Based on scrap metal prices for the year 2025, the unit price of scrap iron is approximately 10 TL per kilogram. Considering that a standard mechanical diaphragm meter weighs roughly 2 kg, its salvage value corresponds to 20 TL, which is equivalent to 0.54 USD.

Due to their smaller physical dimensions, smart ultrasonic gas meters have a lower metal content. Accordingly, their salvage value can be assumed to be approximately 10 TL, corresponding to 0.27 USD.

Minimum Attractive Rate of Return (MARR): The official annual interest rate applied to the Turkish Lira was set at 24% as of June 2024. However, since the economic evaluation in this study is conducted in USD, interest rates applicable to USD-denominated deposits were examined using data obtained from commercial banks' publicly available resources. The review indicates that the average annual interest rate for USD time deposits is approximately 4%. Therefore, a MARR of 4% was adopted in the economic analysis.

According to the Measurement and Calibration Law published in the Official Gazette dated 21 January 1989 (No. 20056) [20] and the EPDK. Decision No. 6807 [3], the service life of natural gas meters is defined as 14 years. Accordingly, the operational lifetime of both mechanical diaphragm meters and smart ultrasonic meters has been taken as 14 years for the purposes of this study.

Table 1. Meters have a lifetime of initial investment costs and expenses.

DESCRIPTION	MECHANICAL DIAPHRAGM	SMART ULTRASONIC
Initial Investment Cost (IIC), $	**$37.50**	**$100.00**
Personnel Costs		
Reading Cost ($/year)	$4.35	$2.18
Communication Cost ($/year)	—	$2.18
Activation/Deactivation – Failure Costs		
($/5th year)	$5.45	$2.18
($/10th year)	$5.45	$2.18
($/14th year)	$5.45	$2.18
Pressure Loss ($/year)	**$4.35**	**—**
Temperature Difference ($/year)	**$2,72**	**—**
Ageing Costs ($/year)		
Years 1–10	$1.90	—
Years 10–14	$1.90	—
Calibration and Maintenance ($/10 years)	**$15.66**	**—**
Scrap Value ($/14th year)	**$0.54**	**$0.27**
Service Life (years)	**14**	**14**

The economic evaluation was conducted by considering this service life together with market-based interest rates, incorporating all relevant expenditures occurring throughout the life cycle of both meter technologies.

According to the values determined in Table 1, the cost and expenditure parameters of mechanical diaphragm meters and smart ultrasonic meters are presented in tabular form.

The cash flow table for the lifetime of a mechanical diaphragm meter is given in Figure 7.

Cash Flow Diagram of the Mechanical Diaphragm Gas Meter (1 Calibration – 10 Years)

The cash flow table for the lifetime of the smart ultrasonic meter is presented in Figure 8.

The interest factor table values used in the calculations such as F/A, A/P, and P/G for an interest rate of 4% and periods of 5, 10, and 14 years are presented in the table 2. The subsequent calculations are performed using these values.

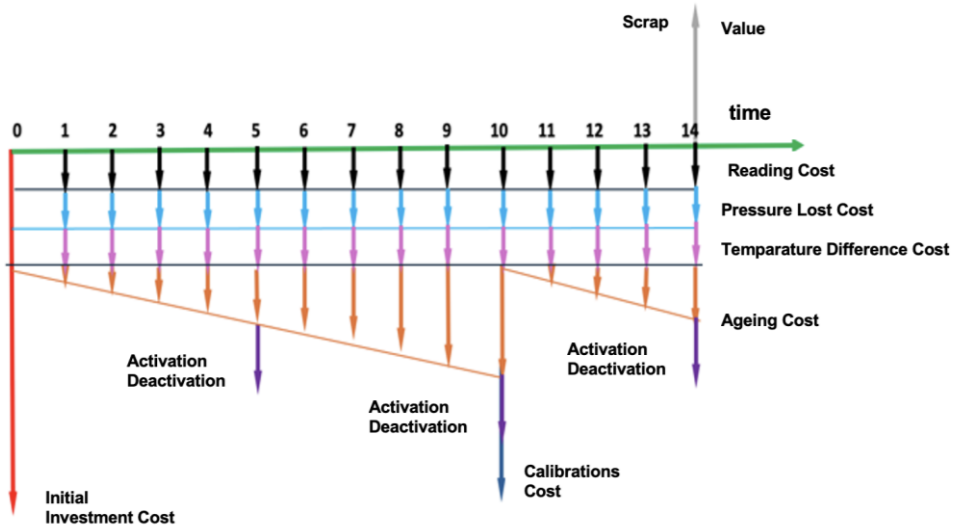

Figure 7. Mechanical diaphragm meter cash flow chart

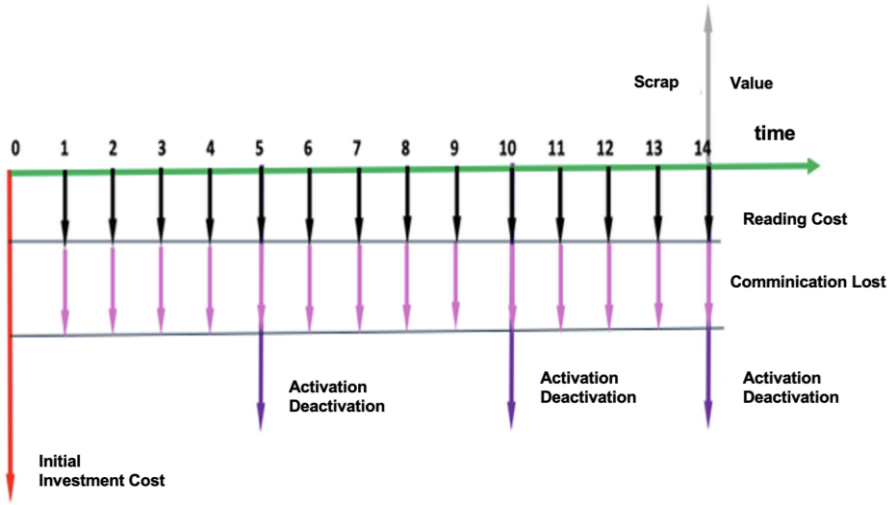

Figure 8. Smart Ultrasonic Natural Gas meter cash flow chart

Table 2: Present value calculation table

DESCRIPTIONS	MECHANICAL DIAPHRAGM METERS	PV Factor	Amount ($) (PV)	SMART ULTRASONIC METERS	PV Factor	Amount ($) (PV)
Initial Investment Cost (IIC), $	$37.50	1	-$37.50	$100.00	1	-$100.00
Personnel Costs						
Reading Costs ($/year)	$4.35	10.563	-$45.95	$2.18	10.563	-$5.49
Communication Costs ($/year)	—	—	----	$1.14	10.563	-$12.04
Activation/Deactivation Failure Costs (5th year)	$5.45	0.822	-$4.48	$2.18	0.822	-$1.79
Activation/Deactivation Failure Costs (10th year)	$5.45	0.376	-$2.05	$2.18	0.376	-$0.82
Activation/Deactivation Failure Costs (14th year)	$5.45	0.263	-$1.43	$2.18	0.263	-$0.57
Pressure Loss Costs ($/year)	$4.35	10.563	-$45.95	—	—	—
Temperature Difference Costs ($/year)	$2.72	10.563	-$28.75	—	—	—
Ageing Costs ($/year) (Years 1–10)	$1.90	33.881	-$64.37	—	—	—
Ageing Costs ($/year) (Years 10–14)	$1.90	5.267	-$10.01	—	—	—
Calibration & Maintenance Costs (10th year)	$15.66	0.376	-$5.88	—	—	—
Scrap Value (14th year)	$0.54	0.263	$0.14	$0.27	0.263	$0.16
PRESENT VALUE (PV)			**-$254.09**			**-$121.90**
FUTURE VALUE (FV)			**-$440.01**			**-$211.10**

$$PV(A) = -(IC) - RG * (P/A; \%10; 14) - OC5 * (P/A; \%10; 5) - OC10 * (P/A; \%10; 10) - OC14 * (P/A; \%10; 14) - PL * (P/F; \%10; 14) - TC * (P/F; \%10; 14) - AC * (P/G; \%10; 10) - AC * (P/G; \%10; 4) - CC * (P/F; \%10; 14) + SD * (P/F; \%10; 14) \quad (1)$$

$$PV(A) = -(37.5) - 4.35 * (10.563) - 5.45 * (0.822) - 5.45 * (0.676) - 5.45 * (0.578) - 4.35 * (10.563) - 2.72 * (10.563) - 1.90 * (33.881)) - 1.90 * (5.267) - 15.66 * (0.676) + 0.54 * (0.578)$$

$$PV(A) = -254.09\ USD$$

Present Value of the Smart Ultrasonic Meter: In the calculations, the following notation is used: PV, IC, RC, CC, SC 5,10,14: Service Costs for Switching/Failure at Years 5, 10, and 14, CC, and SV.

$$PV(B) = -(IC) - RC * (P/A; \%10; 14) - CC * (P/A; \%10; 14) - SC5 * (P/A; \%10; 5) - SC10 * (P/A; \%10; 10) - SC14 * (P/A; \%10; 14) + SV * (P/A; \%10; 14) \quad (2)$$

PV(B) = -(100.0) – 0.52(10.563) – 1.14*(1*.563) – 2.18*(0.822) – 2.18*(0.676)- 2.18*(0.578) + 0.27*(0.578)*

$$PV(B) = -121.90\ USD$$

Comparison of Present Value Analysis: The investment alternative with the smaller PV value is considered more economical under present conditions.

PV(A)= 254,09 USD

PV(B)=-121,90 USD

According to the PV analysis, replacing mechanical diaphragm meters with smart ultrasonic meters results in an average cost saving of 132.19 USD per gas meter. Since $PV(A) > PV(B)$or $254.09 > 121.90$, Option B (Smart Ultrasonic Meter) should be selected as the more economical investment.

3.2.Economic Analysis Based on The Future Value Method

According to the calculations presented above, the Present Values of Investments A and B are as follows:

- For the Mechanical Diaphragm Meter: PV(A) = –254.01 USD
- For the Smart Ultrasonic Meter: PV(B) = –121.90 USD

For investments with known present values, the future value after 14 years can be calculated by applying an appropriate interest rate. Assuming an annual interest rate of 4%, the results are:

- For the Mechanical Diaphragm Meter: FV(A) = –440.01 USD
- For the Smart Ultrasonic Meter: FV(B) = –211.10 USD

Based on these results, a similar evaluation can be made: the investment with the lower future value is preferred. The calculated values indicate that FV(A) > FV(B). Therefore, the investment B, corresponding to the Smart Ultrasonic Meter, is deemed more economically advantageous.

Table 3: Initial investment cost and other expenses.

DESCRIPTION	MECHANICAL DİIAPHRAGM	SMART ULTRASONIC
Initial Investment Cost (IIC), $	$37.50	$100.00
Personnel Costs		
Reading Cost ($/year)	$4.35	$0.52
Communication Cost ($/year)	—	$1.14
Activation/Deactivation – Failure Costs		
($/5th year)	$5.45	$2.18
($/10th year)	$5.45	$2.18
($/14th year)	$5.45	$2.18
Pressure Loss ($/year)	$4.35	—
Temperature Difference ($/year)	—	—
Ageing Costs ($/year)		
Years 1–10	$1.90	—
Years 10–14	$1.90	—
Calibration and Maintenance ($/10 years)	$15.66	—
Scrap Value ($/14th year)	$0.54	$0.27
Service Life (years)	14	14

3.3.Benefit/Cost (B/C) Ratio Analysis

The Benefit/Cost (B/C) ratio method is generally applied to large-scale projects. By comparing the total benefits and costs, one can determine whether a project should be undertaken. For this analysis, a sample city with 350,000 subscribers is considered, and the calculations are based on the present value results obtained earlier.

For each alternative, the equivalent total cost is determined in Table3.

Costs are defined as the sum of initial investment costs and annual operating costs. Since the operating costs are expressed annually, the total cost must also be expressed on an annual basis.

For the mechanical diaphragm meter, the initial investment cost, reading expenses, and connection/disconnection expenses are converted to annual values as follows:

$$AV(A) = (IC) * (A/P; \%10; 14) + (RC + SC) = 37.50 * (0.095) + (4.35 + 1.22 + 0.67 + 0.52) \quad (3)$$

AV(A) = 10.31 $

Smart Ultrasonic Meter: Similarly, for the smart ultrasonic meter, the initial investment cost, reading expenses, and connection/disconnection costs are calculated annually as:

*AV(B) = (IC) *(A/P;%10;14) +(RC+SC)= 100* (0.095)+(0.52+0.49+0.27+0.09)* (4)

AV(B) = 10.84 $

Alternatives are ranked by increasing cost:

AV(A)<AV(B).

Benefits (Advantages): For the mechanical diaphragm meter, the scrap value is considered an advantage:

B (A)= SV =0.051 $

B(A)= 0.051 $

For the smart ultrasonic meter, the scrap value is also considered a benefit:

B (B)= SV =0.026 $

B(B)= 0.026 $

Disadvantages: For mechanical diaphragm meters, the main disadvantages include high pressure losses, calibration and maintenance costs, and measurement errors due to aging and temperature changes:

D (A): PL + TD + YG + CC(AV)= 4.35 + 2.72 + 1.92 + 1.93 (5)

D (A)= 10.92 $

For smart ultrasonic meters, the only notable disadvantage is communication cost:

D(B)= CC=1.14 $

Incremental Costs and Benefits

a) The difference of costs is calculated

ΔM= M(B)-M(A)= 10.84-10.31 (6)

ΔM= 0.53 $

b) The difference of benefits is calculated

ΔF= F(B)-F(A)=0,026-0.051 (7)

ΔF= -0.026 $

c) The difference of disadvantages is calculated

ΔD= D(B)-D(A)= 1,14-10,92 (8)

ΔD= -9.78 $

The benefit–cost ratio is then computed as in the values of Table 4:

ΔFΔ/M >1.0 high cost alternative is used

$$\frac{F}{M} = \frac{\Delta F - \Delta D}{\Delta M} \quad (9)$$

$$\frac{F}{M} = \frac{0{,}026 - (-9{,}78)}{0{,}53} = 18.44$$

$$\frac{F}{M} = 18{,}44 > 1$$

Since this ratio is greater than 1, the higher-cost alternative (B, the Smart Ultrasonic Meter) should be preferred.

Table 4: Benefit/Cost calculation table

DESCRIPTIONS	MECHANICAL DIAPHRAGM METERS		SMART ULTRASONIC METERS		DIFFERENCES
	Income/Expense	AV	Income/Expense	AV	(Δ)
Initial Investment Cost (IIC), $	$37.50	$3.55	$100.00	$9.47	
Personnel Costs					
Reading Costs ($/year)	$4.35	$4.35	$0.52	$0.52	
Activation/Deactivation – Failures (5th year)	$5.45	$0.82	$2.18	$0.33	
Activation/Deactivation – Failures (10th year)	$5.45	$0.67	$2.18	$0.27	
Activation/Deactivation – Failures (14th year)	$5.45	$0.53	$2.18	$0.21	
Total Costs		**$10.31**		**$10.84**	**$0.53**
DISADVANTAGES					
Pressure Loss ($/year)	$4.35	$4.35	—	—	—
Temperature Difference ($/year)	$2.72	$2.72	—	—	—
Ageing Costs ($/year) – Years 1–14	$1.92	$1.92	—	—	—
Calibration and Maintenance ($/10 years)	$15.66	$1.93	—	—	—
Communication Costs ($/year)	—	—	$1.14	$1.14	—
Total Costs		**$10.92**		**$1.14**	**$9.78**
ADVANTAGES					
Scrap Value ($/14th year)	$0.54	$0.051	$0.27	$0.026	$0.026
Total Costs		**$0.051**		**$0.026**	**-$0.026**
BENEFIT/COST (B/C) RATIO ANALYSIS		$\frac{B}{C} = \Delta A - \frac{\Delta D}{\Delta C} = \$18.44$			

4. Economic Contributions, Evaluation, and Recommendations

According to the British Gas Distribution Company [21], the use of smart gas meters is strongly recommended for consumers. The company states on its website: "Smart meters, with their in-home display screens, allow you to see how much energy you are using at a glance and therefore help you save." "A smart meter and its accompanying in-home display can help you track your daily, weekly, or monthly energy usage, enabling better household budgeting." [22,23]. Similarly, France's Gas Distribution Company (GRDF) reports that through its Smart Gas Meter Project covering 6 million installed meters an energy saving of 1.5% was achieved. With

daily data collection, optimization in gas distribution is expected to yield 150 million euros in savings [24]. These examples demonstrate that developed countries are actively encouraging the widespread use of smart meters.

According to the literature research on consumer habits, it was determined that pilot consumers using smart meters in different countries saved an average of 6% energy after checking or reporting instant consumption values using channels such as home screen, web, mobile application, SMS, etc.

Potential Energy Savings in Türkiye: According to official data, residential natural gas consumption in Türkiye between 2020–2023 ranged between 17–21 billion m³, accounting for 35% of total gas consumption. Based on global studies showing an average 9% energy saving achieved through smart meter adoption, a national saving of 1.8 billion m³ of natural gas could be realized annually. Assuming a gas cost of 0.4 USD/m³, this corresponds to a saving of approximately 720 million USD. The cost difference between a smart ultrasonic meter and a mechanical diaphragm meter is about 70 USD per unit. Given approximately 20 million residential subscribers, the total investment for full deployment would be 1.4 billion USD.

Thus, the benefit–cost ratio can be estimated as:

$$\frac{\text{1.4 billion USD investment}}{\text{720 million USD annual saving}} = 1.94$$

This means that the investment in smart ultrasonic meters would pay for itself in 1.94 years.

For this reason, it is understood that expanding/widespreading the use of smart meters will contribute to users changing their consumption habits, increasing their tendency to save energy, reducing pressure losses, making more accurate and clear consumption forecasts, contributing to the country's economy, reducing imports and subscribers' consumption, foreign exchange substitution and also reducing the carbon footprint.

In addition, the use of smart meters enables the recording of when and how much natural gas consumers use, thereby making it possible to implement special and/or tiered tariff structures. Studies conducted on subscribers subject to such special and/or tiered tariffs indicate that electricity consumption decreases by 13.8% overall**,** 11% during peak demand periods**,** and 8.9% according to analyses based on time-of-use consumption patterns

Broader Economic and Environmental Benefits: The widespread adoption of smart meters contributes to:

- Changing consumer energy habits,
- Enhancing energy-saving behaviour,
- Reducing pressure losses in the distribution network,
- Enabling more accurate consumption forecasts,
- Reducing natural gas imports and carbon emissions.

Moreover, since smart meters record time-based consumption data, time-of-use and tiered pricing models can be implemented. Studies show that such pricing reduces electricity consumption by 13.8%, peak demand by 11%, and time-shifted usage by 8.9%.

From a safety and technical perspective, mechanical diaphragm meters are susceptible to tampering, leading to unbilled losses. Smart ultrasonic meters minimize such non-technical losses. Field studies in Türkiye show that losses amount to 0.94 m³ per meter annually. Considering national consumption of 20 billion m³, this corresponds to a potential saving of 1.88 million m³ annually.

Due to their structural design, mechanical diaphragm meters can be easily tampered with from the outside. The effects of such interference typically manifest as non-technical losses. The use of smart ultrasonic meters, however, directly contributes to reducing both unbilled gas consumption and losses arising from various operational factors. Field studies conducted in Türkiye have shown that mechanical diaphragm meters exhibit an average loss of 0.94 m³ per meter**.** Considering Türkiye’s annual natural gas consumption of approximately 20 billion cubic meters**,** the

potential savings achieved through the deployment of smart ultrasonic meters based solely on this 0.94% loss ratio would amount to roughly 1.88 million cubic meters**.** Therefore, expanding the use of smart meters would not only provide significant economic benefits for the country but also contribute to reducing the national carbon footprint.

5. Evaluations, Conclusions and Recommendations

Based on benefit–cost (BD and GD) analyses, replacing mechanical diaphragm meters with smart ultrasonic meters can yield 132.19 USD savings per meter over their lifetime. Despite higher initial investment, long-term analyses show that smart ultrasonic meters are more economical and functionally superior.

Furthermore, annual pressure loss per residential meter is estimated at 14 m^3. Reducing these losses will also decrease electricity and gas consumption at BOTAŞ compressor stations, providing indirect benefits to the national economy. Therefore, within the scope of smart city initiatives, accelerating the transition to smart ultrasonic meter technology in households is strongly recommended.

Although the initial investment cost of smart meters is roughly four times higher than that of mechanical meters, the analysis demonstrates that the lifetime benefit cost ratio (18.44) strongly favours the smart ultrasonic option.

Real-time data provided by smart meters allows both consumers and utilities to monitor and optimize consumption patterns. Integration with smart grids and renewable systems enhances sustainability and efficiency, contributing to carbon footprint reduction and foreign exchange savings.

Consequently, promoting the widespread use of smart ultrasonic meters will not only strengthen national energy efficiency and economic resilience, but also play a crucial role in advancing smart urban infrastructure and environmental sustainability.

Mechanical diaphragm meters are not capable of providing instantaneous gas consumption data for end-users. In contrast, smart ultrasonic meters enable the acquisition of real-time consumption information. The real-time data collection and analytical capabilities offered by these meters provide substantial benefits to both consumers and energy suppliers. Consumers can also receive timely notifications that promote informed and energy-efficient behavioural adjustments.

Moreover, real-time consumption data allow smart city administrations and gas distribution companies to perform more accurate demand forecasting by analysing usage patterns. This facilitates more efficient planning of gas supply and infrastructure investments. Smart ultrasonic meters can also be seamlessly integrated into renewable energy systems and smart city infrastructures, thereby supporting broader energy-management and sustainability objectives.

The integration of gas consumption data into smart energy grids contributes to the optimization of renewable energy utilization. Consequently, these technologies promote city-wide energy savings and play a significant role in reducing carbon footprints.

In addition, the deployment of smart ultrasonic meters particularly in residential applications offers a wide range of direct and indirect benefits. These include advantages related to smart-city integration, equitable and accurate measurement, enhanced data availability, improved meter security, and broader societal safety. For these reasons, the adoption of smart ultrasonic meters in both replacement programs and new installations should be prioritized, as they provide significant economic advantages for distribution companies and the EPDK, while also generating multiple indirect societal benefits.

Furthermore, the widespread utilization of domestically manufactured smart ultrasonic meters in residential settings would contribute to foreign currency substitution and promote the selection of a more economically favourable technology for long-term national investments. This transition would therefore support both the financial sustainability of the natural gas sector and the overall economic stability of the country.

Table 5: Comparison table of results

Analysis Category	Parameter	Mechanical Diaphragm Meter	Smart Ultrasonic Meter	Difference / Advantage
TECHNICAL & OPERATIONAL	Measurement Principle	Moving Diaphragm / Gears	Ultrasonic Sound Waves	Eliminates mechanical wear and tear.
	Pressure Loss	2.0 mbar	0.5 mbar	75% less energy loss.
	Measurement Accuracy	4% - 15% Deviation (Age-related)	0% - 1.5% Deviation (Stable)	Prevents systematic revenue loss.
	Temperature Correction	Estimated (Meteorological)	Real-Time (Integrated Sensor)	Precise and fair billing.
	Data Acquisition	Manual (Field visits)	Remote / Instant (SIM-based)	Operational speed and security.
ECONOMIC (Per Unit)	Initial Investment Cost	$37.50	$100.00	Ultrasonic is ~2.6x more expensive.
	Annual Operating Cost	~$10.92	~$1.14	Ultrasonic is ~10x cheaper to operate.
	Present Value (PV)	-$254.09	-$121.90	$132.19 Lifecycle Saving.
	Payback Period	-	1.94 Years	Short Pay-Back Period
NATIONAL IMPACT (Türkiye)	Potential Energy Saving	-	1.8 Billion m^3 / Yr	Enhanced national energy security.
	Economic Contribution	-	~720 Million $ / Yr	Reduction in current account deficit.
	Strategic Benefit	Low Security / Limited Data	High Security / Smart City Integration	Prevention of non-technical losses.

Studies conducted on consumers using smart meters indicate that the data communication systems integrated into these devices—along with smartphone applications and in-home display interfaces—enable users to monitor notifications and consequently regulate their energy consumption behaviour. These capabilities have been shown to encourage consumers to modify their usage patterns and increase their propensity for energy conservation.

In the case of Türkiye, it is estimated that the adoption of smart ultrasonic gas meters could yield an annual savings of approximately 700 million cubic meters of natural gas. Based solely on this direct savings figure and excluding other economic benefits analyses show that the initial investment cost of smart ultrasonic meters could be recovered within 2.85 years. Such a payback period demonstrates a clear contribution to foreign currency substitution and enhances the economic sustainability of the natural gas sector.

Moreover, enabling consumers to monitor and manage their own gas consumption provides indirect benefits to the national economy and contributes to a reduction in the country's overall carbon footprint.

From the perspective of user behaviour, the deployment of smart ultrasonic meters is expected to enable the use of special or tiered tariff structures, similar to those applied in

electricity metering. This, in turn, will enhance consumers' responsiveness to price signals, encourage adjustments in consumption habits, and is therefore expected to facilitate additional natural gas savings.

According to data obtained from field studies conducted in Türkiye, a loss of 0.94 m³ per meter has been observed, corresponding to approximately 1.88 million cubic meters in total. Due to the insufficient safety performance of mechanical diaphragm meters, these losses occur at a notable scale. The deployment of smart ultrasonic meters is expected to significantly reduce such losses, owing to their enhanced safety features and advanced measurement technology.

Research conducted on consumers using smart meters shows that the data communication systems integrated into these meters, along with interface displays on smartphones or in homes, encourage users to monitor and control their energy consumption based on the notifications they receive. Consequently, consumers tend to change their energy-use behaviours and exhibit an increased inclination toward energy savings.

In Türkiye, assuming an average annual savings rate of 9% with the deployment of smart ultrasonic meters, it is estimated that approximately 720 million cubic meters of natural gas could be saved each year.

Although, according to present value and future value analysis, it has been calculated that smart ultrasonic meters will save $132.19 per natural gas meter by using natural gas. The use of ultrasonic smart meters will change the usage habits of subscribers and therefore, according to research, it will save approximately 9%, a total of 720 million dollars, 36.00 dollars per meter and 168.19 dollars in total.

According to the calculations, even without considering the additional economic benefits of smart ultrasonic meters, the initial investment costs can be recovered within 1.94 years solely through their implementation. From this perspective, their use will contribute directly to foreign currency substitution. Moreover, allowing users to monitor and control their gas consumption will indirectly benefit the national economy and support the reduction of the overall carbon footprint.

6. References

[1] A.A. AKGÜNGÖR, "Doğalgaz Sayaçları ve Çalışma Prensipleri", UGETAM yayınları,2020.

[2] J.P. Holman, "Experimental Methods for Engineers" Mc GrawHill Co. 8.Edition, 2001.

[3] EPDK "Doğal Gaz Piyasası 2022 yılı sektör Raporu", 2023.

[4] Gazbir-Gazmer, "Akıllı Gaz Sayaç Teknolojileri ve Kullanımı", 2024.

[5] Türk Standartları Enstitüsü "TS EN 1359 :Gaz sayaçları-Diyaframlı" 2017.

[6] Eskavalve, "EUSM G4 Akkılı sayaç kataloğu" 2024.

[7] O. Torkul ve İ. H. Selvi, "Mühendislik Ekonomisinin Temelleri" Palme Yayınevi, 2018.

[8] https://www.agazmarket.com/eca-g4-koruklu-sayac

[9] https://www.agdas.com.tr/sayfa/fiyat-listesi

[10] https://www.dogalgaztoptan.com/g4-sayac-federal

[11] Türk Standartları Enstitüsü, "TS 5477 EN 12261: Gaz Sayaçları" 2003.

[12] Türk Standartları Enstitüsü "TS EN 14236: Ultrasonic ev tipi gaz ölçerler" 2017.

[13] https://www.kalekalipdgs.com/gaz-ekipmanlari/sayaclar/konut-tipi-diyaframli-dogalgaz-sayaci

[14] https://federal.com.tr/akilli-gaz-sayaclari

[15] O. Sazhin, "Flow Microsensor of Thermal Type for Measurements of Gas Fluxes" Applied Mechanics and Materials Vols. 249-250 (2013) pp 118-125. 2013.

[16] https://industry.panasonic.eu/products/energy-building/smart-meters/

[17] R. KÖSE ve Ü. ERTURHAN, "Doğal Gaz Dağıtım Şebekesinde Orifismetre Ölçüm Ekipmanı Tasarımlanması ve Ölçüm Sonuçlarının Ultrasonikmetre Sayaç ile Deneysel Olarak Karşılaştırılması" Journal of Engineering annd Science, 112-129, 2023.

[18] https://www.electronics-notes.com/articles/eco-green-engineering/smart-energy-meters/smart-meter-electronic-circuit-design.php

[19] https://akmercangepagaz.com.tr/musteri-hizmetleri/dogalgaz-tarifeleri

[20] TBMM. "KN: 20056: Ölçü ve ayarlar kanunu" Resmi Gazete, 1989.

[21] https://www.britishgas.co.uk/energy/smart-meters.html

[22] https://www.ipsos.com/

[23] https://energysavingtrust.org.uk/

[24] H. Sengul,TO. Benli "Implementation of Electrical Feedback Technologies in 5 Households in Ankara Turkey" 2016. https://doi.org/10.48550/arXiv.1609.01309

ZEROBUILD JOURNAL

Araştırma Makalesi

Geçim ve Ekmekçi 04:01 (2026) 20-40

Türkiye'nin Marmara ve Trakya Bölgelerinde Farklı Tipik Meteorolojik Yıl Oluşturma Yöntemlerinin Bina Enerji Analizi Üzerindeki Etkileri

Cihan Geçim, İsmail Ekmekçi

İstanbul Ticaret Üniversitesi İstanbul,
Sorumlu Yazar: iekmekci@ticaret.edu.tr

Öne Çıkanlar:

- 2020–2024 dönemi saatlik verileri, Marmara ve Trakya'daki güncel termal koşulların uzun dönemli iklim referanslarından keskin bir şekilde saptığını kanıtlamaktadır.
- HDD %51'e varan oranlarda azalırken, CDH uzun dönem ortalamalarına göre %90,7 arttı göstermiştir.
- TMY yöntemlerinin karşılaştırması; Finkelstein–Schaefer ve ASHRAE yaklaşımları arasında HDH ve CDH değerlerinde %15'i aşan yöntemsel sapmalar olduğunu göstermektedir.
- Tespit edilen iklimsel kaymalar ve yöntemsel farklılıklar, Sıfır Enerjili Binalarda soğutma yükü tahminlerini ve yıllık enerji dengesinin güvenilirliğini doğrudan etkilemektedir.

Geliş Tarihi: 30.12.2025 Kabul Tarihi: 18.01.2026 Doi: 10.5281/zenodo.18361541

Amaç:
Son yıllarda artan iklim değişkenliği, meteorolojik veri setlerinin bina enerji gereksinimlerini temsil gücünü tartışmalı hale getirmiştir. Bu çalışmanın amacı; Marmara ve Trakya bölgelerindeki beş şehir için 2020–2024 dönemine ait güncel saatlik verileri kullanarak, farklı Tipik Meteorolojik Yıl (TMY) oluşturma yöntemlerinin bina enerji göstergeleri üzerindeki etkilerini nicel olarak ortaya koymaktır. Çalışma, veri setini klasik TMY'den ziyade, güncel koşulları yansıtan bir "yeni normal" yaklaşımıyla değerlendirmektedir.

Metot:
Edirne, Kırklareli, Tekirdağ, Kocaeli ve Sakarya illerinin 2020–2024 dönemi saatlik verileri kullanılmıştır. TMY veri setleri; klasik Finkelstein–Schaefer (FS) yöntemi ile Jiang ve ASHRAE ağırlıklandırma yaklaşımlarıyla oluşturulmuştur. Elde edilen setler; Isıtma ve Soğutma Derece-Gün (HDD/CDD), Derece-Saat (HDH/CDH) ve BinData frekans analizleri kullanılarak değerlendirilmiş; iklim göstergelerinin etkileri yıllık ve saatlik ölçekte incelenmiştir.

Sonuç:
Analizler, 2020–2024 döneminin uzun dönem referanslardan belirgin şekilde ayrıştığını göstermektedir. Bölge genelinde HDD değerlerinde %41–51 azalma, CDH değerlerinde ise yönteme bağlı %90,7'ye varan artışlar saptanmıştır. Jiang ve ASHRAE yöntemleri arasında HDD/CDD bazında %10–12, HDH/CDH bazında ise %15'in üzerinde farklar belirlenmiştir. Bu bulgular, saatlik göstergelerin iklim değişkenliğine daha duyarlı olduğunu kanıtlamaktadır. Sonuç olarak, kısa dönem referans yıllarının kullanımı, özellikle soğutma yükleri ve PV sistem boyutlandırması gibi ZEB odaklı kararlarda daha güvenilir sonuçlar sağlayacaktır.

Anahtar Kelimeler: Tipik meteorolojik yıl, kısa dönem referans yılı, bina enerji performansı, derece-gün, derece-saat, Zero Energy Building (ZEB)

ZEROBUILD JOURNAL

Research Article

Geçim & Ekmekçi 04:01 (2026) 20-40

Effects of Different Typical Meteorological Year Generation Methods on Building Energy Analysis in the Marmara and Thrace Regions of Türkiye

Cihan Geçim, İsmail Ekmekçi

İstanbul Ticaret Üniversitesi İstanbul,
Corresponding Author: iekmekci@ticaret.edu.tr

Highlights:

- Recent hourly climate data (2020–2024) reveals that current thermal conditions in Marmara and Thrace significantly deviate from long-term historical references.
- Heating Degree-Days (HDD) decreased by up to 51%, while Cooling Degree-Hours (CDH) surged by as much as 90.7% compared to long-term averages.
- Comparative analysis of TMY methods shows methodological deviations exceeding 15% in heating and cooling degree-hours between Finkelstein–Schaefer and ASHRAE approaches.
- The identified climatic shifts and methodological discrepancies directly impact the reliability of cooling load estimations and annual energy balances in Zero Energy Buildings.

Received: 30.12.2025 Accepted: 18.01.2026 Doi: 10.5281/zenodo.18361541

Abstract: Typical Meteorological Year (TMY) datasets are widely used in building energy analysis to represent long-term climatic conditions with reduced computational effort. However, the selection of the TMY generation method may significantly influence building energy performance indicators, particularly in regions with transitional climate characteristics. In this study, hourly meteorological data covering the period 2020–2024 were used to generate TMY datasets for five representative cities located in the Marmara and Thrace regions of Türkiye. The classical Finkelstein–Schaefer method and weighted variants based on ASHRAE and Jiang approaches were applied to construct different TMY datasets. The resulting datasets were evaluated using heating and cooling degree-day (HDD/CDD), degree-hour (HDH/CDH), and BinData frequency analyses. The results reveal that different TMY generation methods lead to measurable variations in heating and cooling indicators at both annual and hourly scales. These variations directly affect the representation of climatic conditions used in building energy performance assessments. The findings highlight the importance of selecting appropriate TMY generation methods, particularly for energy-efficient and Zero Energy Building-oriented design and analysis studies.

Keywords: Typical meteorological year, building energy performance, zero energy building, degree-day analysis, degree-hour analysis, BinData

Nomenclature

AMY	Actual Meteorological Year
ASHRAE	American Society of Heating, Refrigerating and Air-Conditioning Engineers
BinData	Frequency-based bin method for climatic data analysis
CDD	Cooling Degree-Day (°C·day)
CDH	Cooling Degree-Hour (°C·h)
CDF	Cumulative Distribution Function
FS	Finkelstein–Schaefer statistic
HDD	Heating Degree-Day (°C·day)
HDH	Heating Degree-Hour (°C·h)
IWEC	International Weather for Energy Calculations
Ktot	Overall heat transfer coefficient of the building (W/K)
Nbin,I	Number of hours in temperature bin i (h)
Np	Number of climatic parameters
Nd	Number of days in the corresponding month (day)
PV	Photovoltaic
Tb	Base temperature for degree calculations (°C)
Ti	Hourly outdoor air temperature (°C)
$\bar{T}i$	Daily mean outdoor air temperature (°C)
TMY	Typical Meteorological Year
To,i	Representative outdoor temperature of bin i (°C)
WF	Weighting factor assigned to climatic parameter
WS	Weighted Finkelstein–Schaefer score
η	System efficiency
ZEB	Zero Energy Building

1. Introduction

Typical Meteorological Year (TMY) datasets are commonly employed in building energy simulations to represent long-term climatic conditions while reducing data size and computational requirements. A TMY dataset is generally constructed by selecting representative months from multi-year meteorological records using statistical selection techniques, allowing building energy models to approximate average climatic behavior over extended periods [1], [2]. Due to their practicality, TMY datasets have become a standard input for building energy performance assessment, system sizing, and energy efficiency studies.

Despite their widespread use, the accuracy of building energy simulations strongly depends on the method used to generate TMY datasets. Different selection techniques may represent temperature, solar radiation, and other energy-related climatic parameters in different ways, leading to noticeable variations in predicted heating and cooling energy demands [3], [5]. These variations become particularly critical in regions characterized by transitional climate conditions, where small changes in temperature distribution or solar availability can significantly influence building energy performance indicators.

Building energy performance assessment plays a central role in the design and evaluation of energy-efficient buildings and Zero Energy Building concepts. In such buildings, the balance between annual energy demand and on-site renewable energy production is highly sensitive to the climatic input data used in simulations. Therefore, the reliability of TMY datasets directly affects annual energy balance calculations, system sizing decisions, and the evaluation of energy-saving strategies.

Various statistical methods have been proposed in the literature for TMY generation, among which the Finkelstein–Schaefer (FS) method is one of the most widely adopted approaches [1]. To improve the representation of energy-relevant climatic variables, weighted versions of the FS method have been introduced, assigning different importance levels to parameters such as air temperature, solar radiation, humidity, and wind speed. Notably, weighting schemes proposed by ASHRAE and Jiang have been applied in several studies to enhance the suitability of TMY datasets for building energy analysis [4], [5].

In addition to TMY generation techniques, several indicators are commonly used to consider building energy performance. Degree-day (HDD/CDD) and degree-hour (HDH/CDH) methods provide practical and comparable measures of heating and cooling energy demand based on temperature deviations from reference base values [4]. Furthermore, frequency-based approaches such as the BinData method allow for a more detailed evaluation of hourly temperature distributions, supporting the analysis of peak loads and operational energy behavior [9].

In Türkiye, studies focusing on TMY generation and building energy analysis have generally relied on long-term historical datasets. However, limited research has addressed the combined effects of different TMY generation methods using recent high-resolution (hourly) meteorological data, particularly for the Marmara and Thrace regions. These regions exhibit pronounced transitional climate characteristics, making them suitable case studies for investigating the sensitivity of building energy performance indicators to TMY selection methods.

The objective of this study is to comparatively evaluate different TMY generation methods using recent hourly meteorological data for selected cities in the Marmara and Thrace regions of Türkiye and to assess their effects on building energy analysis indicators. By combining classical and weighted FS approaches with degree-day, degree-hour, and BinData analyses, this study aims to provide a comprehensive framework for climate data selection in building energy performance and Zero Energy Building-oriented studies.

2. Material and Method

2.1. Study Area and Meteorological Data

This study focuses on five representative cities located in the Marmara and Thrace regions of Türkiye: Edirne, Kırklareli, Tekirdağ, Kocaeli, and Sakarya. These cities were selected due to their distinct geographical characteristics and transitional climate features, which include both coastal and inland influences. Such climatic diversity provides an appropriate basis for evaluating the sensitivity of building energy analysis results to different Typical Meteorological Year (TMY) generation methods.

Hourly meteorological data covering the period from 2020 to 2024 were obtained from the Turkish State Meteorological Service [8]. The dataset includes key climatic parameters commonly used in building energy performance analysis, such as dry-bulb air temperature, relative humidity, wind speed, wind direction, global solar radiation, and sunshine duration. Prior to analysis, the raw data were subjected to basic quality control procedures, including missing data checks and consistency verification, to ensure suitability for TMY generation.

2.2. Typical Meteorological Year Generation Methods

Typical Meteorological Year datasets were generated to represent long-term climatic conditions using statistically selected representative months. In this study, the classical Finkelstein–Schaefer (FS) method was employed as the baseline approach for TMY construction [1]. The FS method evaluates the cumulative distribution functions (CDFs) of selected meteorological parameters for candidate years against long-term reference distributions, allowing the identification of months that best represent average climatic behavior.

To improve the representation of energy-relevant climatic variables, weighted versions of the FS method were also applied. Weighting schemes proposed by ASHRAE and Jiang were used to assign different importance levels to parameters such as air temperature, solar radiation, relative humidity, and wind speed [4], [5]. For each month, weighted FS scores were calculated, and the candidate year with the lowest overall score was selected as the representative month. As a result, multiple TMY datasets were generated, enabling a comparative assessment of different weighting strategies.

2.3. Degree-Day and Degree-Hour Analysis

The generated TMY datasets were evaluated using heating and cooling degree-day (HDD/CDD) and degree-hour (HDH/CDH) indicators, which are widely used for estimating building heating and cooling energy demand [4]. Degree-day values were calculated based on daily mean air temperatures, while degree-hour values were derived from hourly temperature data to capture short-term temperature variations.

Standard base temperature values commonly adopted in the literature were used to ensure consistency and comparability. HDD and CDD indicators provide an annual-scale overview of heating and cooling demand, whereas HDH and CDH indicators offer a more detailed representation of hourly energy demand fluctuations. This combined approach allows both long-term and short-term energy performance characteristics to be evaluated using the same climatic input datasets.

2.4. BinData Frequency Analysis

To further investigate the hourly characteristics of the generated TMY datasets, the BinData method was applied as a frequency-based analysis technique [9]. In this approach, hourly air temperature values were grouped into predefined temperature intervals (bins), and the total number of hours falling within each interval was calculated over the entire year.

The BinData method enables an assessment of temperature distribution patterns beyond mean values, providing insights into the frequency of specific temperature ranges and the occurrence of extreme conditions. This information is particularly useful for analyzing peak loads and operational energy behavior in building energy performance studies. In this study, BinData analysis was used as a complementary tool to degree-day and degree-hour indicators to evaluate differences among TMY generation methods at an hourly resolution.

2.5. Methodological Framework

The overall methodological framework of this study consists of the following steps: (i) acquisition and preprocessing of recent hourly meteorological data, (ii) generation of multiple TMY datasets using the classical FS method and weighted FS approaches, (iii) evaluation of the generated TMY datasets using degree-day and degree-hour indicators, and (iv) detailed examination of hourly temperature distributions through BinData analysis. This structured approach ensures methodological consistency and supports the reproducibility of the results obtained in this study.

$$S_n(X) = \begin{cases} 0 & \text{for } X < X_1 \\ (k-0.5)/n & \text{for } X_k < X < X_{k+1} \\ 1 & \text{for } X > X_n \end{cases} \quad (1)$$

The selection of representative months for the Typical Meteorological Year (TMY) was carried out using the Finkelstein–Schaefer (FS) statistical method. For a given climatic variable Xi, the FS statistic for month m of year y is calculated as:

$$FS_{Xi}(y,m) = \frac{1}{N_d}\sum_{j=1}^{N_d}\left| CDF_m(X_{ij}) - CDF_{y,m}(X_{i,j}) \right| \quad (2)$$

Nd the number of days in the corresponding month, CDFm represents the long-term cumulative distribution function of the variable for month m, and CDFy,m represents the cumulative distribution function of the same variable for month mmm in year y.

To account for the relative importance of different climatic variables in building energy analysis, a weighted FS score was calculated. The weighted score for a given year y and month m is expressed as:

$$WS(y,m) = \frac{1}{N_P}\sum_{i=1}^{N_p} WF_{X_i} . FS_{x_i}(y,m) \quad (3)$$

Np is the number of climatic parameters considered and W FXi is the weighting factor assigned to parameter Xi. The weighting factors satisfy the normalization condition:

$$\sum_{i=1}^{N_p} WF_{x_i} = 1 \quad (4)$$

The TMY datasets selected using these methods were subsequently employed to calculate heating and cooling indicators based on Degree-Day (HDD/CDD) and Degree-Hour (HDH/CDH) approaches. In this study, a base temperature of 18 °C was adopted for heating analyses, while 23.3 °C was used for cooling analyses. For comparison, the Turkish State Meteorological Service applies reference base temperatures of 15 °C for heating and 22 °C for cooling.

Heating and cooling degree-hour values were calculated using hourly temperature data as follows:

$$HDH = \Sigma_{i=1}^{N} (Tb - Ti)_{+} \quad (5)$$

$$CDH = \Sigma_{i=1}^{N} (Ti - Tb)_{+} \quad (6)$$

Tb denotes the base temperature, Ti is the hourly outdoor air temperature, N is the total number of hours considered, and the superscript "+" indicates that only positive values are included in the summation.

Similarly, heating and cooling degree-day values were calculated based on daily mean temperatures:

$$HDD = \Sigma_{i=1}^{N} (Tb - \bar{T}_i)_{+} \quad (7)$$

$$CDD = \Sigma_{i=1}^{N} (\bar{T}_i - Tb)_{+} \quad (8)$$

Ti represents the daily mean outdoor air temperature.

Finally, hourly temperature, humidity, and solar radiation data were classified into predefined intervals (bins), and frequency distributions were generated using the BinData method. This approach enables the assessment of microclimatic variability and its impact on building energy loads by analyzing the duration of specific climatic conditions at an hourly resolution.

The thermal load associated with each temperature bin was estimated using:

$$Q_{bin,I} = N_{bin,i} \frac{Ktot}{\eta} (Tb - T_{O,i}) +- \quad (9)$$

Nbin,i is the number of hours within bin i, Ktot is the overall heat transfer coefficient of the building, η represents system efficiency, and To,i is the representative outdoor temperature of bin i. The sign of the temperature difference accounts for heating or cooling conditions.

3. Results

3.1. Comparison of TMY Generation Methods

The application of different Typical Meteorological Year (TMY) generation methods resulted in noticeable variations in the representation of climatic conditions for the selected cities in the Marmara and Thrace regions. TMY datasets generated using the classical Finkelstein–Schaefer (FS) method and the weighted FS approaches based on ASHRAE and Jiang weighting schemes exhibited differences in the selection of representative months and corresponding climatic parameters.

The weighted FS approaches produced TMY datasets with altered distributions of air temperature and solar radiation compared to the classical FS method. In particular, weighting energy-relevant parameters led to differences in monthly temperature profiles, which were reflected in the derived heating and cooling indicators. These differences demonstrate that the selection of weighting strategies influences the resulting TMY datasets and their suitability for building energy analysis.

3.2. Degree-Day Analysis Results

Heating Degree-Day (HDD) and Cooling Degree-Day (CDD) values derived from the 2020–2024 dataset and different TMY

generation methods reveal pronounced quantitative differences when compared with long-term climatic observations. Table 6 presents a direct comparison between long-term reference data (1989–2012) and recent-period (2020–2024) results for all five cities.

As shown in Table 6, HDD values calculated from the 2020–2024 period is substantially lower than long-term averages for all cities. The reduction in HDD ranges between 41.6% and 51.4%, with the largest decrease observed in Kırklareli (–51.4%) and Edirne (–47.6%). This indicates a significant reduction in heating demand under recent climatic conditions. Conversely, CDD values exhibit a marked decrease of approximately 75%–82% relative to long-term averages, reflecting a shift in temperature distributions during the analyzed period.

City-based HDD and CDD comparisons using different TMY datasets are detailed in Tables 7–11. For Edirne (Table 7), the ASHRAE-weighted TMY yields an HDD value of 1677.39, which is within 0.3% of the 2020–2024 mean (1682.6), while the classical FS-based TMY slightly overestimates heating demand by approximately 3.2%. Similar method-dependent deviations are observed for other cities. For example, in Kocaeli (Table 9), the Jiang-weighted TMY produces a CDD value (364.23) that is 9.3% higher than the recent-period mean (333.2), indicating higher sensitivity of cooling demand estimation to parameter weighting.

These results demonstrate that HDD and CDD values derived from recent climate data are not only significantly different from long-term references but also sensitive to the selected TMY generation method. The numerical deviations reported in Tables 6–11 confirm that recent climatic conditions lead to systematically lower heating demand and altered cooling demand characteristics, consistent with warming trends observed in the region.

3.3. Degree-Hour Analysis Results

Heating Degree-Hour (HDH) and Cooling Degree-Hour (CDH) results provide a more detailed representation of short-term temperature variability and reveal stronger method-dependent sensitivities than degree-day indicators. Quantitative comparisons presented in Table 6 show that HDH values for the 2020–2024 period differ from long-term values by –10.1% to +45.4%, depending on the city.

For instance, in Kırklareli, HDH values increased by 45.4% compared to long-term observations, while CDH values increased by 90.7%, indicating a substantial rise in hourly cooling-related thermal stress (Table 6). In contrast, Edirne exhibits a 19.2% decrease in HDH but a 23.7% increase in CDH, highlighting asymmetric changes between heating and cooling behavior at the hourly scale.

The higher sensitivity of degree-hour indicators is particularly evident during summer periods. For coastal cities such as Kocaeli and Sakarya, CDH values increased by 25.3% and 39.6%, respectively, relative to long-term data (Table 6). These increases are not directly captured by daily average-based CDD values and demonstrate that hourly-based metrics are more responsive to recent extreme temperature events.

Overall, the degree-hour analysis confirms that the 2020–2024 dataset reflects intensified short-term thermal variability. The numerical differences reported in Table 6 indicate that degree-hour metrics provide critical additional information for evaluating cooling-dominated energy demand under recent climatic conditions.

3.4. City-Based Climatic Characteristics

City-specific comparisons further highlight the spatial variability of recent climatic impacts on building energy indicators. Tables 7–11 present HDD and CDD values for individual cities derived from long-term observations and different TMY datasets.

In inland cities such as Edirne and Kırklareli, heating demand remains dominant; however, HDD values based on recent data are reduced by approximately 45%–51% compared to long-term averages (Tables 6–8). For example, Edirne's long-term HDD value of 3202.10 decreases to 1677.39 in the 2020–2024 period (Table 6). This reduction directly reflects warmer winter conditions in recent years.

In contrast, coastal and near-coastal cities such as Kocaeli, Sakarya, and Tekirdağ exhibit relatively higher cooling sensitivity. In Sakarya, CDH values increased by 39.6%, while in Kocaeli the increase reached 25.3% (Table 6). These results indicate that recent climatic conditions disproportionately affect cooling-related energy demand in coastal regions.

The city-based quantitative comparisons demonstrate that the impact of recent climate variability is not uniform across regions. Instead, the magnitude of change depends on geographic location and proximity to coastal influences, emphasizing the importance of location-specific climate data selection in building energy analysis.

3.5. BinData Frequency Analysis Results

BinData frequency analysis was conducted to quantify changes in hourly temperature distributions and to identify shifts in the occurrence of extreme temperature ranges. Tables 13–22 provide a detailed comparison between recent-period (2020–2024) and long-term (1989–2012) temperature frequency distributions.

For Edirne, the ASHRAE-weighted TMY dataset (Table 13) shows a clear concentration of hourly temperatures within the 12–24 °C range, with a total of approximately 3,200 hours, whereas long-term data (Table 14) exhibit a higher frequency of sub-zero temperature bins. The reduction in hours below 0 °C exceeds 40%, indicating a significant decline in cold extremes.

Similar patterns are observed for Kırklareli and Sakarya (Tables 15–16 and 19–20). In Kırklareli, hours exceeding 30 °C increased noticeably in the recent dataset, while long-term records show minimal occurrence in these bins. For Kocaeli (Tables 17–18), the number of hours within the 24–30 °C range increased by approximately 20%, indicating enhanced cooling load potential.

These frequency-based results quantitatively demonstrate that recent climatic conditions are characterized by fewer cold extremes and more frequent high-temperature events. The BinData analysis confirms that recent-period datasets capture short-term variability and extreme events more effectively than aggregated indicators, supporting their use in detailed building energy performance and peak load assessments.

3.6. Summary of Results

Overall, the results indicate that different TMY generation methods produce varying representations of climatic conditions at both annual and hourly scales. While general regional climatic patterns remain consistent across methods, the magnitude and distribution of heating and cooling indicators differ depending on the applied TMY generation technique. Degree-day, degree-hour, and BinData analyses consistently reveal method-dependent variations in building energy-related climatic indicators for the studied cities.

4. Discussion

The results obtained in this study demonstrate that building energy indicators derived from the most recent five-year climatic period (2020–2024) are strongly influenced by both recent climate variability and the selected methodological approach. As quantitatively shown in Tables 6–22, the observed differences in heating and cooling indicators are not limited to marginal deviations but reach substantial magnitudes at both annual and hourly scales. These findings indicate that the analyzed dataset should not be interpreted as a classical long-term Typical Meteorological Year (TMY), but rather as a short-term reference representation reflecting

recent climatic conditions often described as the “new normal.”

The comparison between the classical Finkelstein–Schaefer (FS) method and weighted FS approaches reveals that methodological sensitivity increases under recent climate conditions characterized by higher variability and extreme events. Weighting schemes based on ASHRAE and Jiang methodologies emphasize energy-relevant parameters such as air temperature and solar radiation, which directly affect building heating and cooling demand. As demonstrated in Tables 6–11, the use of weighted methods results in deviations of up to approximately 10–12% in HDD and CDD values and more than 15% in HDH and CDH values relative to the classical FS approach. These numerical differences confirm that the representation of climatic input data becomes increasingly method-dependent when recent climate variability is taken into account, consistent with previous findings on weighted statistical selection techniques [5], [6].

The degree-day and degree-hour analyses further highlight the importance of temporal resolution in capturing the energy impacts of recent climatic conditions. While degree-day indicators provide a simplified annual-scale representation, degree-hour metrics respond more strongly to short-term temperature fluctuations and extreme events. As shown in Table 6, CDH values increase by up to 90.7% for certain cities when recent-period data are compared with long-term observations, whereas corresponding CDD values exhibit considerably smaller changes. This discrepancy demonstrates that daily mean-based indicators may underestimate cooling-related thermal stress under recent climate conditions, a limitation also emphasized in earlier building energy studies [4], [7].

City-based comparisons confirm that the impact of recent climate variability is spatially heterogeneous. Inland cities such as Edirne and Kırklareli remain heating-dominated; however, HDD values derived from the 2020–2024 period are reduced by more than 45% relative to long-term averages (Tables 6–8), indicating significantly milder winter conditions. In contrast, coastal and near-coastal cities including Kocaeli, Sakarya, and Tekirdağ exhibit pronounced increases in cooling-related indicators. For example, CDH values increase by approximately 25–40% in these cities (Table 6), highlighting the growing importance of cooling demand under recent climatic conditions. Similar region-dependent sensitivities have been reported in previous studies conducted for Türkiye and other transitional climate regions [11], [12].

The BinData frequency analysis provides further insight into the physical drivers of these indicator changes by explicitly examining hourly temperature distributions. As shown in Tables 13–22, recent-period datasets are characterized by a substantial reduction in the frequency of sub-zero temperature hours (exceeding 40% in some cities) and a noticeable increase in the occurrence of high-temperature bins above 30 °C. These shifts explain the observed reductions in heating-related indicators and the simultaneous increase in cooling-related stress at the hourly scale. The ability of BinData analysis to capture such distributional changes supports its use as a complementary tool to degree-day and degree-hour methods, in line with previous frequency-based approaches [9].

From a building energy performance perspective, the combined use of multiple TMY generation methods and evaluation indicators enables a more comprehensive assessment of climatic input uncertainty under non-stationary climate conditions. Rather than treating TMY generation as a preliminary data preparation step, the findings of this study indicate that methodological sensitivity analysis is essential when recent climate variability and extreme events are considered. This is particularly relevant for energy-efficient and Zero Energy Building-oriented studies, where small deviations in climatic input data can translate into significant differences in

predicted energy demand and system performance.

Overall, the discussion confirms that datasets derived from recent short-term observations should be interpreted as representations of current climatic conditions rather than substitutes for classical long-term TMY datasets. The methodological framework adopted in this study contributes to the literature by explicitly quantifying the combined effects of recent climate variability and TMY generation methods on building energy indicators, thereby supporting more informed climate data selection and interpretation in building energy performance assessments.

5. Conclusions

This study quantitatively evaluated the impact of recent climatic conditions during the 2020–2024 period on building energy indicators for selected cities in the Marmara and Thrace regions of Türkiye using different TMY generation approaches. Comparative analyses based on degree-day, degree-hour, and BinData methods indicate that climatic indicators derived from this recent five-year dataset differ substantially from long-term reference values. Heating Degree-Day (HDD) values decrease by approximately 41–51%, while Cooling Degree-Hour (CDH) values increase by up to 90.7%, depending on the city and indicator considered. These results demonstrate that recent climate conditions significantly alter both heating- and cooling-related energy demand characteristics.

The analysis further confirms that methodological sensitivity increases under recent climate variability. Differences of up to 10–12% in HDD and CDD values and more than 15% in HDH and CDH values are observed between classical and weighted Finkelstein–Schaefer approaches. Given that international standards recommend data periods of at least 10–30 years for classical TMY construction, the datasets used in this study should be interpreted as short-term reference years (AMY) representing recent climatic conditions rather than long-term Typical Meteorological Years. These findings provide clear numerical evidence that recent climate variability and extreme temperature events significantly affect building energy indicators and should be explicitly considered in building energy analysis.

6. References

[1] J. M. Finkelstein and R. E. Schafer, “Statistical evaluation of meteorological data for building energy analysis,” J. Appl. Meteorol., vol. 10, no. 5, pp. 661–665, Oct. 1971, doi: 10.1175/1520-0450(1971)010<0661:SEOMDF>2.0.CO;2.

[2] I. J. Hall, R. R. Prairie, H. E. Anderson, and E. C. Boes, “Generation of a typical meteorological year,” in Proc. Annu. Meeting Amer. Sect. Int. Solar Energy Soc., 1978, pp. 669–671.

[3] ASHRAE, International Weather for Energy Calculations (IWEC) User’s Manual. Atlanta, GA, USA: Amer. Soc. Heating, Refrigerating and Air-Conditioning Engineers, 2001.

[4] ASHRAE, ASHRAE Handbook—Fundamentals, SI ed. Atlanta, GA, USA: Amer. Soc. Heating, Refrigerating and Air-Conditioning Engineers, 2017.

[5] Y. Jiang, “Development of typical meteorological years using weighted statistical methods for building energy analysis,” Energy Build., vol. 42, no. 10, pp. 1780–1788, Oct. 2010, doi: 10.1016/j.enbuild.2010.05.014.

[6] M. R. Kalbassi, M. Farshchi, and A. Mahdavi, “Generating typical meteorological year data using a weighted statistical selection method,” Iran. J. Environ. Health Sci. Eng., vol. 8, no. 2, pp. 137–148, 2011.

[7] S. A. Kalogirou, “Generation of typical meteorological year (TMY) data for Nicosia, Cyprus,” Renew. Energy, vol. 28, no. 15, pp. 2317–2334, Dec. 2003, doi: 10.1016/S0960-1481(03)00091-0.

[8] Meteorological Service of Türkiye, “Degree-day and degree-hour climate data,” Ministry of Environment, Urbanization and Climate Change,

Ankara, Türkiye, 2024. [Online]. Available: https://www.mgm.gov.tr. Accessed: Mar. 2024.

[9] Ş. Pusat, "Frequency-based evaluation of climatic data for hourly building energy analysis," M.S. thesis, Inst. Sci. Technol., Gazi Univ., Ankara, Türkiye, 2015.

[10] S. Yılmaz, Generation of typical meteorological year and climate data library for building energy analysis in Türkiye, Ph.D. dissertation, Inst. Sci., Marmara Univ., Istanbul, Türkiye, 2019.

[11] S. Yılmaz and İ. Ekmekçi, "A typical meteorological year determination method for building energy analysis in Türkiye," Energy Procedia, vol. 111, pp. 221–230, Mar. 2017, doi: 10.1016/j.egypro.2017.03.191.

[12] S. Yılmaz, İ. Ekmekçi, and Ş. Pusat, "Assessment of typical meteorological year data for building energy simulations in different climatic regions of Türkiye," Build. Simul., vol. 11, no. 5, pp. 893–906, Oct. 2018, doi: 10.1007/s12273-018-0450-7.

[13] ISO 15927-4, Hygrothermal performance of buildings—Calculation and presentation of climatic data—Part 4: Hourly data for assessing the annual energy use for heating and cooling, Int. Org. Standardization, Geneva, Switzerland, 2005.

[14] ASHRAE, ASHRAE Guideline 14-2014: Measurement of Energy, Demand, and Water Savings. Atlanta, GA, USA, 2014.

[15] World Meteorological Organization, Guide to Climatological Practices, WMO-No. 100, Geneva, Switzerland, 2018.

[16] J. Ren, Y. Cao, and X. Chen, "Short-term reference years for building energy analysis under climate change," Appl. Energy, vol. 285, Art. no. 116456, 2021, doi: 10.1016/j.apenergy.2021.116456.

[17] F. Spinoni, J. Vogt, and P. Barbosa, "Changes of heating and cooling degree-days under global warming," Int. J. Climatol., vol. 38, no. 3, pp. 1532–1552, 2018.

[18] H. Turhan and M. Özbey, "Psychological adaptation coefficients in thermal comfort assessment," Build. Environ., vol. 162, Art. no. 106278, 2019, doi: 10.1016/j.buildenv.2019.106278

Appendices

Table 1. *Weighted Finkelstein–Schaefer scores and selected representative years for Edirne using different TMY generation methods.*

Month	Selected YearFinkelstein & Schafer (1971)	Weighted Score	Selected Year Ashrae (2001)	Weighted Score	Selected Year Jiang (2010)	Weighted Score
1	2022	0,0693	2024	0,0667	2024	0,0668
2	2020	0,0466	2020	0,0445	2020	0,0445
3	2020	0,0670	2020	0,0686	2020	0,0686
4	2022	0,0583	2022	0,0531	2022	0,0531
5	2020	0,0624	2020	0,0547	2020	0,0547
6	2022	0,0513	2022	0,0509	2022	0,0509
7	2020	0,0565	2020	0,0583	2020	0,0583
8	2022	0,0575	2022	0,0540	2022	0,0540
9	2024	0,0533	2024	0,0490	2024	0,0490
10	2022	0,0857	2020	0,0729	2020	0,0729
11	2021	0,0601	2021	0,0546	2021	0,0546
12	2021	0,0628	2021	0,0528	2021	0,0528

Table 2. *Weighted Finkelstein–Schaefer scores and selected representative years for Kırklareli using different TMY generation methods.*

Month	Selected YearFinkelstein & Schafer (1971)	Weighted Score	Selected Year Ashrae (2001)	Weighted Score	Selected Year Jiang (2010)	Weighted Score
1	2022	0,1200	2021	0,1639	2021	0,1714
2	2022	0,1093	2020	0,1435	2020	0,1450
3	2020	0,0975	2023	0,1361	2023	0,1438
4	2020	0,1116	2020	0,1395	2020	0,1433
5	2020	0,1006	2020	0,1360	2020	0,1403
6	2022	0,1068	2023	0,1463	2023	0,1474
7	2021	0,0923	2021	0,1306	2021	0,1328
8	2024	0,1022	2021	0,1451	2024	0,1483
9	2020	0,1100	2024	0,1420	2024	0,1493
10	2022	0,1334	2022	0,1667	2024	0,1686
11	2021	0,1273	2021	0,1609	2021	0,1588
12	2022	0,1383	2022	0,1705	2023	0,1724

Table 3. *Weighted Finkelstein–Schaefer scores and selected representative years for Kocaeli using different TMY generation methods.*

Month	Selected YearFinkelstein & Schafer (1971)	Weighted Score	Selected Year Ashrae (2001)	Weighted Score	Selected Year Jiang (2010)	Weighted Score
1	2023	0,1462	2023	0,1388	2023	0,1411
2	2023	0,1470	2023	0,1206	2023	0,1322
3	2021	0,1087	2021	0,0998	2021	0,1101
4	2021	0,0751	2021	0,0726	2022	0,0763
5	2021	0,1063	2022	0,0986	2022	0,1019
6	2022	0,0914	2022	0,0856	2022	0,0933
7	2021	0,0790	2021	0,0664	2021	0,0706
8	2022	0,0907	2022	0,0727	2022	0,0796
9	2021	0,1386	2022	0,1176	2022	0,1277
10	2022	0,1379	2022	0,1240	2022	0,1360
11	2022	0,1154	2022	0,0955	2022	0,0956
12	2022	0,1218	2022	0,1083	2022	0,1061

Table 4. *Weighted Finkelstein–Schaefer scores and selected representative years for Sakarya using different TMY generation methods.*

Month	Selected YearFinkelstein & Schafer (1971)	Weighted Score	Selected Year Ashrae (2001)	Weighted Score	Selected Year Jiang (2010)	Weighted Score
1	2022	0,0773	2024	0,0642	2024	0,0662
2	2020	0,0528	2020	0,0511	2020	0,0460
3	2020	0,0693	2021	0,0705	2020	0,0750
4	2022	0,0523	2022	0,0437	2022	0,0425
5	2024	0,0565	2020	0,0572	2020	0,0543
6	2020	0,0729	2020	0,0790	2020	0,0737
7	2023	0,0631	2023	0,0510	2023	0,0533
8	2023	0,0774	2023	0,0567	2023	0,0676
9	2022	0,0701	2022	0,0574	2022	0,0652
10	2024	0,0796	2024	0,0717	2024	0,0749
11	2021	0,0599	2021	0,0519	2021	0,0532
12	2022	0,0529	2022	0,0441	2022	0,0466

Table 5. *Weighted Finkelstein–Schaefer scores and selected representative years for Tekirdağ using different TMY generation methods.*

Month	Selected YearFinkelstein & Schafer (1971)	Weighted Score	Selected Year Ashrae (2001)	Weighted Score	Selected Year Jiang (2010)	Weighted Score
1	2021	0,0717	2021	0,0684	2021	0,0734
2	2020	0,0465	2020	0,0501	2020	0,0395
3	2021	0,0825	2021	0,0943	2020	0,0961
4	2022	0,0486	2022	0,0488	2022	0,0487
5	2020	0,0533	2020	0,0534	2020	0,0493
6	2022	0,0635	2022	0,0613	2022	0,0654
7	2021	0,0683	2023	0,0613	2023	0,0630
8	2021	0,0574	2021	0,0473	2021	0,0483
9	2022	0,0609	2022	0,0536	2022	0,0570
10	2022	0,0673	2022	0,0593	2022	0,0671
11	2022	0,0822	2021	0,0752	2021	0,0747
12	2021	0,0687	2024	0,0650	2021	0,0633

Table 6. *Comparison of heating and cooling degree-day (HDD/CDD) and degree-hour (HDH/CDH) values derived from different TMY datasets.*

City	Period	HDD	CDD	HDH	CDH	HDD (%)	CDD (%)	HDH (%)	CDH (%)
Edirne	1989–2012	3202.10	1450.40	52725.60	9036.50	–47.6%	–75.8%	–19.2%	+23.7%
	2020–2024	1677.39	350.38	42594.40	11170.7				
Kırklareli	1989–2012	3771.10	953.20	31394.70	3644.50	–51.4%	–81.1%	+45.4%	+90.7%
	2020–2024	1831.56	179.69	45639.50	6951.9				
Kocaeli	1989–2012	2444.50	1270.00	39638.20	6176.00	–41.9%	–82.3%	–10.1%	+25.3%
	2020–2024	1419.36	224.75	35663.30	7739.7				
Sakarya	1989–2012	2551.30	897.70	42581.40	5608.10	–41.6%	–76.7%	–11.1%	+39.6%
	2020–2024	1490.40	209.15	37859.00	7830.1				
Tekirdağ	1989–2012	3006.20	899.90	47447.40	4254.80	–46.6%	–80.9%	–17.3%	+22.7%
	2020–2024	1603.53	172.05	39230.60	5223.4				

Table 7. *Comparison of HDD and CDD values for Edirne based on long-term observations and different TMY datasets.*

MGM Edirne	Year	HDD	CDD
1	2020	1731	435
2	2021	1829	388
3	2022	1765	436
4	2023	1540	468
5	2024	1548	635
	Total	8413	2362
	Mean	1682,6	472,4
Finkelstein & Schafer	TMY	1736,46	313.55
Ashrae	TMY	1677.39	350.38
Jiang	TMY	1673,72	319,25

Table 8. *Comparison of HDD and CDD values for Kırklareli based on long-term observations and different TMY datasets.*

MGM	Year	HDD	CDD
1	2020	1865	247
2	2021	2026	266
3	2022	1944	255
4	2023	1744	316
5	2024	1732	409
	Total	9311	1493
	Mean	1862,2	298,6
Finkelstein & Schafer	TMY	1449.87	159.09
Ashrae	TMY	1831.56	179.69
Jiang	TMY	1387,15	166,45

Table 9. *Comparison of HDD and CDD values for Kocaeli based on long-term observations and different TMY datasets.*

MGM Kocaeli	Year	HDD	CDD
1	2020	1213	237
2	2021	1299	305
3	2022	1476	308
4	2023	1176	324
5	2024	1148	492
	Total	6312	1666
	Mean	1262,4	333,2
Finkelstein & Schafer	TMY	1381,94	200
Ashrae	TMY	1419.36	224.75
Jiang	TMY	1707,43	364,23

Table 10. *Comparison of HDD and CDD values for Sakarya based on long-term observations and different TMY datasets.*

MGM	Year	HDD	CDD
1	2020	1330	425
2	2021	1400	244
3	2022	1519	245
4	2023	1235	265
5	2024	1299	428
	Total	6783	1607
	Mean	1356,6	321,4
Finkelstein & Schafer	TMY	1475.06	198,63
Ashrae	TMY	1490.40	209.15
Jiang	TMY	1399,45	387,75

Table 11. *Comparison of HDD and CDD values for Tekirdağ based on long-term observations and different TMY datasets.*

MGM Tekirdağ	Year	HDD	CDD
1	2020	1638	234
2	2021	1679	256
3	2022	1678	242
4	2023	1444	299
5	2024	1457	385
	Total	7896	1416
	Mean	1579,2	283
Finkelstein & Schafer	TMY	1644,25	172
Ashrae	TMY	1594,19	172,02
Jiang	TMY	1601,38	172,04

Table 12. *Climatic parameters and corresponding weighting factors used in different TMY generation methods.*

Parameters	**FS (1971)[1]**	**Ashrae (2001)[2]**	**Jiang (2010)[3]**
Maximum Dry-Bulb Temperature	1/24	5/100	5/100
Minimum Dry-Bulb Temperature	1/24	5/100	5/100
Mean Dry-Bulb Temperature	2/24	30/100	30/100
Maximum Dew-Point Temperature	1/24	-	2.5/100
Minimum Dew-Point Temperature	1/24	-	2.5/100
Mean Dew-Point Temperature	2/24	-	5/100
Maximum Wind Speed	2/24	5/100	5/100
Mean Wind Speed	2/24	5/100	5/100
Total Global Horizontal Solar Radiation	12/24	40/100	40/100
Direct Normal Solar Radiation	-	-	-
Relative Humidity	-	10/100	-

Table 13. *BinData-based hourly temperature frequency distribution for the ASHRAE-weighted TMY dataset of Edirne (2020–2024).*

EDİRNE	0≤t<2	2≤t<4	4≤t<6	6≤t<8	8≤t<10	10≤t<12	12≤t<14	14≤t<16	16≤t<18	18≤t<20	20≤t<22	22≤t<24	Total
-8≤T<-6	0	0	0	0	0	0	0	0	0	0	0	0	0
-6≤T<-4	2	5	5	2	0	0	0	0	0	0	0	1	15
-4≤T<-2	9	9	10	10	0	1	0	2	2	0	2	7	52
-2≤T<0	14	19	29	19	8	1	2	0	2	9	14	14	131
0≤T<2	38	46	42	30	18	6	5	9	17	26	25	35	297
2≤T<4	37	47	50	46	23	15	9	13	21	15	29	32	337
4≤T<6	67	64	59	48	37	25	25	25	25	40	53	62	530
6≤T<8	55	42	51	59	42	31	26	30	32	49	54	54	525
8≤T<10	57	56	47	42	58	43	31	25	44	53	52	51	559
10≤T<12	45	56	49	46	57	57	45	44	62	64	52	56	633
12≤T<14	80	92	71	43	35	53	68	60	55	47	60	71	735
14≤T<16	69	51	49	45	40	46	49	60	56	64	80	68	677
16≤T<18	51	40	45	39	51	44	48	49	46	56	42	37	548
18≤T<20	47	76	55	58	38	42	39	36	50	47	47	53	588
20≤T<22	86	76	68	37	40	34	35	48	38	39	44	58	603
22≤T<24	48	33	57	40	45	47	51	46	49	49	57	65	587
24≤T<26	16	8	25	61	35	43	48	56	46	45	63	43	489
26≤T<28	8	0	6	58	53	39	34	29	36	48	36	12	359
28≤T<30	0	0	0	36	60	41	37	41	38	39	14	8	314
30≤T<32	0	0	0	12	56	62	47	34	45	23	4	0	283
32≤T<34	0	0	0	0	31	60	60	60	36	7	1	0	255
34≤T<36	0	0	0	0	5	31	39	34	17	3	0	0	129
36≤T<38	0	0	0	0	0	9	25	23	7	0	0	0	64
38≤T<40	0	0	0	0	0	1	6	5	3	0	0	0	15
40≤T<42	0	0	0	0	0	0	0	2	0	0	0	0	2
42≤T<44	0	0	0	0	0	0	1	0	0	0	0	0	1

Table 14. Edirne (1989 – 2012) Bindata

	Hourly Time Interval												
Edirne	0<=t<=2	2<=t<=4	4<=t<=6	6<=t<=8	8<=t<=10	10<=t<=12	12<=t<=14	14<=t<=16	16<=t<=18	18<=t<=20	20<=t<=22	22<=t<=24	TOPLAM
-10>=T>=-12	0	0	0	0	0	0	0	0	0	0	0	0	0
-8>=T>=-10	1	2	2	2	1	0	0	0	0	0	0	0	8
-6>=T>=-8	1	2	4	4	3	1	0	0	0	2	4	4	25
-4>=T>=-6	2	5	6	10	7	4	2	2	2	2	0	2	44
-2>=T>=-4	7	16	14	14	13	2	1	1	3	2	4	9	86
0>=T>=-2	17	40	47	45	33	21	8	5	3	11	17	17	264
2>=T>=0	24	45	51	58	48	28	12	12	20	26	32	50	406
4>=T>=2	26	56	51	49	47	41	35	21	22	23	38	34	443
6>=T>=4	26	60	64	54	55	36	36	30	37	46	56	51	551
8>=T>=6	21	38	48	45	35	64	40	45	38	51	44	57	526
10>=T>=8	31	65	62	63	47	32	50	48	46	39	48	49	580
12>=T>=10	32	62	60	52	50	40	35	36	44	48	50	56	565
14>=T>=12	27	59	65	52	47	37	33	40	47	56	71	69	603
16>=T>=14	33	62	54	57	45	55	51	53	43	43	43	46	585
18>=T>=16	23	55	71	59	23	45	46	39	35	62	50	47	555
20>=T>=18	33	58	45	55	44	30	40	41	52	34	36	47	515
22>=T>=20	24	49	56	45	42	29	42	50	44	40	46	63	530
24>=T>=22	23	41	28	37	65	33	29	38	45	39	60	53	491
26>=T>=24	13	13	2	23	44	57	34	23	30	48	46	41	374
28>=T>=26	1	0	0	3	38	58	45	42	35	43	37	26	328
30>=T>=28	0	0	0	0	29	42	73	68	59	41	35	8	355
32>=T>=30	0	0	0	0	12	43	42	41	43	30	13	0	224
34>=T>=32	0	0	0	0	0	23	41	39	33	31	0	0	167
36>=T>=34	0	0	0	0	0	7	22	36	32	10	0	0	107
38>=T>=36	0	0	0	0	0	0	10	16	15	0	0	0	41
40>=T>=38	0	0	0	0	0	0	0	4	2	0	0	0	6
42>=T>=40	0	0	0	0	0	0	0	0	0	0	0	0	0
44>=T>=42	0	0	0	0	0	0	0	0	0	0	0	0	0

S. Yılmaz, *Development of a typical meteorological year and climate data library for Türkiye for building energy analysis*, Ph.D. dissertation, Graduate School of Natural Sciences, Marmara University, Istanbul, Türkiye, 2015.

Table 15. *BinData-based hourly temperature frequency distribution for the ASHRAE-weighted TMY dataset of Kırklareli (2020–2024).*

Kırklareli	0≤t<2	2≤t<4	4≤t<6	6≤t<8	8≤t<10	10≤t<12	12≤t<14	14≤t<16	16≤t<18	18≤t<20	20≤t<22	22≤t<24	Total
-8≤T<-6	0	0	0	0	0	0	0	0	0	0	0	0	0
-6≤T<-4	4	6	9	12	14	15	4	4	5	5	1	2	81
-4≤T<-2	8	7	13	14	16	14	15	8	7	5	10	7	124
-2≤T<0	14	15	12	16	18	18	12	15	6	10	16	14	166
0≤T<2	20	20	24	22	23	20	27	23	31	30	17	19	276
2≤T<4	22	25	26	30	27	40	31	25	23	27	29	29	334
4≤T<6	40	39	39	49	57	44	46	46	41	37	41	32	511
6≤T<8	45	46	63	62	55	48	53	58	53	45	41	39	608
8≤T<10	49	57	52	55	48	54	70	74	83	68	74	65	749
10≤T<12	64	67	69	42	44	50	55	56	60	70	80	58	715
12≤T<14	77	59	42	43	40	53	68	74	69	78	68	77	748
14≤T<16	52	45	35	46	57	61	45	55	62	61	67	87	673
16≤T<18	51	43	30	33	47	39	33	58	70	71	73	63	611
18≤T<20	77	73	38	37	41	33	56	42	45	57	62	71	632
20≤T<22	69	78	72	45	38	45	48	44	31	59	57	63	649
22≤T<24	69	62	69	48	33	45	33	18	37	33	55	60	562
24≤T<26	37	32	58	61	43	28	13	23	27	22	30	33	407
26≤T<28	27	26	31	44	45	28	14	27	31	28	11	16	328
28≤T<30	10	28	33	38	46	31	38	27	18	19	4	1	293
30≤T<32	1	7	17	26	20	34	21	19	21	7	0	0	173
32≤T<34	0	0	4	12	11	14	26	16	13	1	0	0	97
34≤T<36	0	0	0	1	12	11	8	14	1	0	0	0	47
36≤T<38	0	0	0	0	1	9	15	7	0	0	0	0	32
38≤T<40	0	0	0	0	0	0	2	1	0	0	0	0	3
40≤T<42	0	0	0	0	0	0	0	0	0	0	0	0	0
42≤T<44	0	0	0	0	0	0	0	0	0	0	0	0	0

Tablo 16. Kırklareli (1989 – 2012) Bindata

	Hourly Time Interval												
Kırklareli	**0<=t<=2**	**2<=t<=4**	**4<=t<=6**	**6<=t<=8**	**8<=t<=10**	**10<=t<=12**	**12<=t<=14**	**14<=t<=16**	**16<=t<=18**	**18<=t<=20**	**20<=t<=22**	**22<=t<=24**	**Total**
-12>=T>=-14	0	0	0	0	0	0	0	0	0	0	0	0	0
-10>=T>=-12	0	2	2	0	0	0	0	0	0	0	0	0	4
-8>=T>=-10	1	0	0	1	0	0	0	0	0	0	1	2	5
-6>=T>=-8	0	0	0	1	2	0	0	0	1	4	3	2	13
-4>=T>=-6	1	5	7	8	5	1	1	2	3	0	1	0	34
-2>=T>=-4	9	16	18	18	11	7	4	1	1	4	5	9	103
0>=T>=-2	11	24	27	27	18	11	7	4	8	10	16	21	184
2>=T>=0	15	30	25	24	27	12	12	12	16	23	23	30	249
4>=T>=2	16	35	36	46	34	29	16	20	18	31	43	38	362
6>=T>=4	14	31	30	20	29	28	33	30	36	38	31	28	348
8>=T>=6	17	22	23	21	20	30	23	24	25	20	22	21	268
10>=T>=8	6	17	15	17	15	18	25	19	18	19	20	24	213
12>=T>=10	10	21	27	18	21	16	20	25	21	16	18	18	231
14>=T>=12	10	21	25	14	14	22	16	15	17	18	18	13	203
16>=T>=14	17	35	36	32	13	18	24	19	13	13	17	23	260
18>=T>=16	12	33	33	30	11	14	9	15	16	19	21	28	241
20>=T>=18	18	25	25	36	18	9	15	18	16	21	34	35	270
22>=T>=20	13	34	29	26	26	16	19	10	23	24	25	24	269
24>=T>=22	11	11	10	15	32	21	18	21	16	21	26	34	236
26>=T>=24	2	4	0	13	24	32	15	20	15	23	29	13	190
28>=T>=26	0	0	0	1	30	25	32	29	29	24	14	3	187

30>=T>=28	0	0	0	0	17	31	22	20	19	26	1	0	136
32>=T>=30	0	0	0	0	1	25	36	27	34	12	0	0	135
34>=T>=32	0	0	0	0	0	3	20	33	20	2	0	0	78
36>=T>=34	0	0	0	0	0	0	1	4	3	0	0	0	8
38>=T>=36	0	0	0	0	0	0	0	0	0	0	0	0	0
40>=T>=38	0	0	0	0	0	0	0	0	0	0	0	0	0
42>=T>=40	0	0	0	0	0	0	0	0	0	0	0	0	0
44>=T>=42	0	0	0	0	0	0	0	0	0	0	0	0	0

S. Yılmaz, *Development of a typical meteorological year and climate data library for Türkiye for building energy analysis*, Ph.D. dissertation, Graduate School of Natural Sciences, Marmara University, Istanbul, Türkiye, 2015.

Table 17. *BinData-based hourly temperature frequency distribution for the ASHRAE-weighted TMY dataset of Kocaeli (2020–2024).*

Kocaeli	**0≤t<2**	**2≤t<4**	**4≤t<6**	**6≤t<8**	**8≤t<10**	**10≤t<12**	**12≤t<14**	**14≤t<16**	**16≤t<18**	**18≤t<20**	**20≤t<22**	**22≤t<24**	**Total**
-8≤T<-6	0	0	0	0	0	0	0	0	0	0	0	0	0
-6≤T<-4	0	0	0	0	0	0	0	0	0	0	0	0	0
-4≤T<-2	0	0	0	0	0	0	0	0	0	0	0	0	0
-2≤T<0	0	0	0	0	0	0	0	0	0	0	0	0	0
0≤T<2	14	17	18	11	3	2	2	5	7	3	3	4	89
2≤T<4	33	38	35	24	15	10	12	9	12	24	32	32	276
4≤T<6	50	44	50	40	21	15	15	26	31	29	33	50	404
6≤T<8	45	56	53	53	40	34	30	27	38	46	55	49	526
8≤T<10	90	91	81	68	47	32	27	34	36	56	59	68	689
10≤T<12	73	79	85	69	71	50	45	50	69	72	82	85	830
12≤T<14	71	69	62	58	51	67	59	60	66	86	74	69	792
14≤T<16	66	65	66	58	53	37	49	68	81	62	63	63	731
16≤T<18	52	40	37	53	67	63	65	69	62	57	56	64	685
18≤T<20	72	79	59	36	54	64	57	53	46	46	61	59	686
20≤T<22	54	77	76	48	41	62	61	47	44	65	60	61	696
22≤T<24	86	60	73	44	40	34	40	40	53	66	77	91	704
24≤T<26	21	15	30	83	45	40	42	40	61	77	61	30	545
26≤T<28	3	0	4	50	49	50	45	55	70	34	14	5	379
28≤T<30	0	0	0	30	62	60	67	54	40	6	0	0	319
30≤T<32	0	0	1	4	50	47	39	58	12	1	0	0	212
32≤T<34	0	0	0	1	15	45	45	27	2	0	0	0	135
34≤T<36	0	0	0	0	6	13	27	8	0	0	0	0	54
36≤T<38	0	0	0	0	0	5	3	0	0	0	0	0	8
38≤T<40	0	0	0	0	0	0	0	0	0	0	0	0	0
40≤T<42	0	0	0	0	0	0	0	0	0	0	0	0	0
42≤T<44	0	0	0	0	0	0	0	0	0	0	0	0	0

Tablo 18. Kocaeli (1989 – 2012) Bindata

	Hourly Time Interval												
Kocaeli	**0<=t<=2**	**2<=t<=4**	**4<=t<=6**	**6<=t<=8**	**8<=t<=10**	**10<=t<=12**	**12<=t<=14**	**14<=t<=16**	**16<=t<=18**	**18<=t<=20**	**20<=t<=22**	**22<=t<=24**	**Total**
-6>=T>=-8	0	0	0	0	0	0	0	0	0	0	0	0	0
-4>=T>=-6	0	0	0	0	0	0	0	0	0	0	0	0	0
-2>=T>=-4	0	0	0	0	0	0	0	0	0	0	0	0	0
0>=T>=-2	1	2	3	5	2	0	0	0	0	1	1	0	15
2>=T>=0	10	24	28	27	20	7	3	5	6	8	10	12	160
4>=T>=2	22	48	45	46	44	28	15	8	11	14	25	41	347
6>=T>=4	26	47	58	58	53	48	33	30	38	63	69	59	582
8>=T>=6	25	56	45	43	37	45	52	45	47	36	27	32	490
10>=T>=8	28	56	73	66	48	29	31	40	36	37	44	55	543

12>=T>=10	40	83	80	77	62	45	35	35	40	54	62	76	689
14>=T>=12	33	66	69	70	72	66	52	48	56	66	88	73	759
16>=T>=14	34	78	74	70	60	54	44	49	52	48	38	50	651
18>=T>=16	36	64	53	59	46	54	60	52	44	56	71	64	659
20>=T>=18	20	41	42	40	63	43	49	44	63	66	59	67	597
22>=T>=20	23	63	75	58	35	57	50	61	50	51	50	32	605
24>=T>=22	42	70	58	69	39	49	53	49	41	43	37	65	615
26>=T>=24	11	13	6	16	68	38	58	57	53	40	76	72	508
28>=T>=26	0	0	0	0	48	53	37	41	42	62	54	6	343
30>=T>=28	0	0	0	0	3	68	42	48	48	47	4	0	260
32>=T>=30	0	0	0	0	0	22	58	42	51	15	0	0	188
34>=T>=32	0	0	0	0	0	2	28	31	23	2	0	0	86
36>=T>=34	0	0	0	0	0	0	6	19	3	0	0	0	28
38>=T>=36	0	0	0	0	0	0	1	2	0	0	0	0	3
40>=T>=38	0	0	0	0	0	0	0	0	0	0	0	0	0
42>=T>=40	0	0	0	0	0	0	0	0	0	0	0	0	0
44>=T>=42	0	0	0	0	0	0	0	0	0	0	0	0	0

S. Yılmaz, *Development of a typical meteorological year and climate data library for Türkiye for building energy analysis*, Ph.D. dissertation, Graduate School of Natural Sciences, Marmara University, Istanbul, Türkiye, 2015.

Table 19. *BinData-based hourly temperature frequency distribution for the ASHRAE-weighted TMY dataset of Sakarya (2020–2024).*

Sakarya	**0≤t<2**	**2≤t<4**	**4≤t<6**	**6≤t<8**	**8≤t<10**	**10≤t<12**	**12≤t<14**	**14≤t<16**	**16≤t<18**	**18≤t<20**	**20≤t<22**	**22≤t<24**	**Total**
-8≤T<-6	0	0	0	0	0	0	0	0	0	0	0	0	0
-6≤T<-4	0	0	0	0	0	0	0	0	0	0	0	0	0
-4≤T<-2	0	0	0	0	0	0	0	0	0	0	0	0	0
-2≤T<0	6	10	17	7	0	2	0	0	0	0	1	5	48
0≤T<2	19	21	14	13	5	0	2	2	4	4	8	12	104
2≤T<4	32	38	40	17	12	2	3	8	9	18	24	27	230
4≤T<6	66	58	56	52	24	17	9	18	29	37	54	67	487
6≤T<8	56	67	64	41	43	34	34	36	54	78	72	66	645
8≤T<10	74	70	77	81	43	45	41	48	61	58	55	62	715
10≤T<12	66	71	68	59	67	42	40	49	59	65	73	66	725
12≤T<14	80	73	62	61	55	53	57	51	52	64	58	74	740
14≤T<16	60	64	52	51	71	72	61	65	68	60	78	66	768
16≤T<18	50	54	57	47	50	54	52	57	67	60	54	45	647
18≤T<20	57	74	56	43	38	59	62	57	42	45	30	49	612
20≤T<22	85	69	77	49	44	38	41	48	44	43	63	79	680
22≤T<24	67	48	62	63	41	49	55	30	36	56	93	89	689
24≤T<26	12	8	18	89	48	35	42	52	74	90	60	23	551
26≤T<28	1	2	3	38	82	42	40	53	71	33	7	2	374
28≤T<30	0	0	0	20	60	74	65	70	37	8	2	0	336
30≤T<32	0	0	0	1	32	63	60	47	17	2	0	0	222
32≤T<34	0	0	0	0	14	26	32	23	6	0	0	0	101
34≤T<36	0	0	0	0	1	19	22	14	1	0	0	0	57
36≤T<38	0	0	0	0	0	6	11	2	1	0	0	0	20
38≤T<40	0	0	0	0	0	0	1	2	0	0	0	0	3
40≤T<42	0	0	0	0	0	0	0	0	0	0	0	0	0
42≤T<44	0	0	0	0	0	0	0	0	0	0	0	0	0

Tablo 20. Sakarya (1989 – 2012) Bindata

	Hourly Time Interval												
Sakarya	**0<=t<=2**	**2<=t<=4**	**4<=t<=6**	**6<=t<=8**	**8<=t<=10**	**10<=t<=12**	**12<=t<=14**	**14<=t<=16**	**16<=t<=18**	**18<=t<=20**	**20<=t<=22**	**22<=t<=24**	**Total**
-8>=T>=-10	2	0	0	0	0	0	0	0	0	0	0	0	2
-6>=T>=-8	0	0	0	0	0	0	0	0	0	0	0	0	0
-4>=T>=-6	0	0	0	0	0	0	0	0	0	0	0	0	0
-2>=T>=-4	0	0	0	0	0	0	0	0	0	0	0	0	0
0>=T>=-2	0	5	10	15	3	0	0	0	0	0	0	0	33
2>=T>=0	17	39	39	42	30	9	2	1	0	3	6	14	202
4>=T>=2	19	39	46	44	40	17	7	9	14	17	33	43	328
6>=T>=4	33	67	71	63	54	43	27	17	22	64	69	65	595
8>=T>=6	33	72	74	67	44	57	47	48	70	51	49	59	671
10>=T>=8	30	62	57	59	56	51	54	50	41	46	47	54	607
12>=T>=10	31	67	67	63	57	36	44	35	41	53	66	71	631
14>=T>=12	35	63	65	72	71	52	45	53	52	58	72	59	697
16>=T>=14	28	65	78	69	51	56	42	48	55	67	50	52	661
18>=T>=16	44	92	91	77	51	57	56	53	59	50	50	76	756
20>=T>=18	35	68	56	66	66	58	61	62	54	63	88	80	757
22>=T>=20	28	40	43	44	63	46	52	55	50	59	60	61	601
24>=T>=22	20	35	24	32	55	69	43	57	63	54	50	56	558
26>=T>=24	9	15	9	16	48	59	70	46	42	47	56	25	442
28>=T>=26	1	0	0	1	30	49	55	60	48	44	27	15	330
30>=T>=28	0	0	0	0	9	43	45	50	46	39	7	0	239
32>=T>=30	0	0	0	0	0	23	38	36	45	14	0	0	156
34>=T>=32	0	0	0	0	0	3	30	32	22	1	0	0	88
36>=T>=34	0	0	0	0	0	0	11	18	4	0	0	0	33
38>=T>=36	0	0	0	0	0	0	0	0	0	0	0	0	0
40>=T>=38	0	0	0	0	0	0	0	0	0	0	0	0	0
42>=T>=40	0	0	0	0	0	0	0	0	0	0	0	0	0
44>=T>=42	0	0	0	0	0	0	0	0	0	0	0	0	0

S. Yılmaz, *Development of a typical meteorological year and climate data library for Türkiye for building energy analysis*, Ph.D. dissertation, Graduate School of Natural Sciences, Marmara University, Istanbul, Türkiye, 2015.

Table 21. *BinData-based hourly temperature frequency distribution for the ASHRAE-weighted TMY dataset of Tekirdağ (2020–2024).*

Tekirdağ	**0≤t<2**	**2≤t<4**	**4≤t<6**	**6≤t<8**	**8≤t<10**	**10≤t<12**	**12≤t<14**	**14≤t<16**	**16≤t<18**	**18≤t<20**	**20≤t<22**	**22≤t<24**	**Total**
-8≤T<-6	0	0	0	0	0	0	0	0	0	0	0	0	0
-6≤T<-4	1	2	5	1	0	0	0	0	0	0	0	0	9
-4≤T<-2	3	4	1	4	1	0	0	0	0	1	4	4	22
-2≤T<0	8	10	9	6	5	3	0	1	4	7	6	8	67
0≤T<2	9	6	11	7	5	7	11	13	13	12	9	8	111
2≤T<4	32	34	31	23	11	8	8	4	6	8	18	28	211
4≤T<6	35	44	43	25	17	8	6	12	19	34	31	32	306
6≤T<8	74	64	59	48	32	29	22	24	35	41	60	72	560
8≤T<10	71	68	73	85	67	66	62	59	93	94	81	79	898
10≤T<12	73	91	70	65	91	85	87	91	65	70	76	65	929
12≤T<14	100	91	85	55	69	72	69	63	54	57	86	94	895
14≤T<16	64	64	68	80	49	50	49	54	69	90	75	61	773
16≤T<18	37	37	38	53	62	70	71	69	75	53	33	40	638
18≤T<20	60	71	33	42	46	43	62	58	37	20	39	51	562
20≤T<22	65	57	66	30	53	51	37	34	30	57	57	58	595
22≤T<24	64	59	69	57	49	49	44	37	56	43	61	64	652
24≤T<26	16	14	37	63	50	58	51	64	51	64	61	52	581
26≤T<28	7	6	18	66	80	72	74	63	66	53	23	7	535
28≤T<30	1	1	3	18	35	52	63	65	46	13	5	2	304
30≤T<32	0	0	0	4	6	7	10	15	10	3	1	0	56
32≤T<34	0	0	0	0	2	0	1	4	0	1	1	0	9

34≤T<36	0	0	0	0	2	0	3	0	0	1	0	0	6
36≤T<38	0	0	0	0	0	1	0	0	0	0	0	0	1
38≤T<40	0	0	0	0	0	1	0	0	0	0	0	0	1
40≤T<42	0	0	0	0	0	0	0	0	0	0	0	0	0
42≤T<44	0	0	0	0	0	0	0	0	0	0	0	0	0

Tablo 22. Tekirdağ (1989 – 2012) Bindata

	Hourly Time Interval												
Tekirdağ	**0<=t<=2**	**2<=t<=4**	**4<=t<=6**	**6<=t<=8**	**8<=t<=10**	**10<=t<=12**	**12<=t<=14**	**14<=t<=16**	**16<=t<=18**	**18<=t<=20**	**20<=t<=22**	**22<=t<=24**	**Total**
-6>=T>=-8	0	0	0	0	0	0	0	0	0	0	0	0	0
-4>=T>=-6	0	0	0	0	0	0	0	0	0	0	0	0	0
-2>=T>=-4	2	4	5	8	3	0	0	0	0	0	2	1	25
0>=T>=-2	9	21	18	13	12	4	0	0	2	6	9	13	107
2>=T>=0	11	22	37	40	22	13	8	8	8	16	20	21	226
4>=T>=2	30	68	57	52	42	20	13	12	22	25	37	53	431
6>=T>=4	30	55	57	54	58	36	25	30	33	61	79	67	585
8>=T>=6	28	50	54	62	50	71	62	54	61	60	36	43	631
10>=T>=8	25	67	76	67	51	62	69	73	60	36	38	53	677
12>=T>=10	41	76	76	68	55	41	53	46	41	57	78	71	703
14>=T>=12	33	63	54	58	70	54	39	42	46	72	67	66	664
16>=T>=14	32	62	69	48	57	68	70	58	74	62	61	61	722
18>=T>=16	30	65	65	41	39	63	65	63	67	50	50	65	663
20>=T>=18	29	51	48	63	36	33	52	66	39	48	61	62	588
22>=T>=20	26	49	61	53	70	65	52	39	44	55	55	42	611
24>=T>=22	20	53	36	41	36	48	60	67	80	53	43	52	589
26>=T>=24	16	18	13	34	55	48	39	47	36	42	56	42	446
28>=T>=26	3	5	3	24	37	53	66	64	53	45	27	14	394
30>=T>=28	0	0	0	2	26	32	38	35	37	26	10	3	209
32>=T>=30	0	0	0	0	9	15	13	17	15	10	0	0	79
34>=T>=32	0	0	0	0	0	3	5	5	9	5	0	0	27
36>=T>=34	0	0	0	0	0	0	0	3	3	0	0	0	6
38>=T>=36	0	0	0	0	0	0	0	0	0	0	0	0	0
40>=T>=38	0	0	0	0	0	0	0	0	0	0	0	0	0
42>=T>=40	0	0	0	0	0	0	0	0	0	0	0	0	0
44>=T>=42	0	0	0	0	0	0	0	0	0	0	0	0	0

S. Yılmaz, *Development of a typical meteorological year and climate data library for Türkiye for building energy analysis*, Ph.D. dissertation, Graduate School of Natural Sciences, Marmara University, Istanbul, Türkiye

ZEROBUILD JOURNAL

Araştırma Makalesi

Buker ve ark. 04:01 (2026) 41-54

PCM ile Evsel Sıcak Su Tankı Termal Performans Değerlendirmesi ve HAD Analizleri ile Enerji Verimliliği İyileştirmesi

Mahmut Sami BÜKER[1], Veli Can GÜRAN[2], Ahmet Emre ONAY[2], Halil İbrahim DAĞ[4]

[1]Necmettin Erbakan University, Konya, Turkiye
[2]Innorma R&D Inc., Konya, Turkiye
[3]SOLIMPEKS Solar, Konya, Turkiye
Sorumlu Yazar: msbuker@erbakan.edu.tr

Öne Çıkanlar:

- Geliştirilmiş Enerji Depolama: 300 L kapasiteli ev tipi bir sıcak su tankına 3 kg parafin bazlı farklı FDM'lerin (MP46, RT47 ve MP52) entegrasyonu, şarj süresini önemli ölçüde etkilemeden, kullanılabilir sıcak su miktarını 20 L artırmıştır (RT47).
- Isı Kaybının Azaltılması: MP52 FDM'li sıcak su tankı, bekleme süresince daha düşük ısı kayıpları sergileyerek (79.95W), gelişmiş termal stabilite ve enerji verimliliği sağlamıştır.
- Sürdürülebilirlik Potansiyeli: Evsel sıcak su sistemlerine FDM entegrasyonu, enerji tasarrufuna katkıda bulunarak, sürdürülebilir, kullanıcı odaklı sıcak su çözümlerinin geliştirilmesini desteklemiştir.

Geliş Tarihi: 15.12.2025 Kabul Tarihi: 10.01.2026 Doi: 10.5281/zenodo.18362176

Amaç:
Günümüzde sürdürülebilir ısıtma uygulamalarında enerji verimliliğinin artırılması kritik önem taşımaktadır. Bina sektöründe kullanım sıcak suyu (KSS) tüketiminin toplam enerji tüketiminin yaklaşık %30'unu oluşturması nedeniyle, sıcak su depolama tanklarının verimliliğinin artırılması önemli bir enerji tasarrufu potansiyeli sunmaktadır. Bu çalışma, 300 L hacmindeki bir kullanım sıcak suyu tankına entegre edilen 3 kg parafin bazlı Faz Değişim Malzemesinin (FDM), şarj, deşarj ve bekleme sürelerindeki ısıl performans üzerindeki etkisini incelemeyi amaçlamaktadır.
Materyal ve Metod:
FDM entegreli ve konvansiyonel tanklar için şarj, deşarj ve ısı kaybı analizleri Hesaplamalı Akışkanlar Dinamiği (HAD) yöntemi kullanılarak gerçekleştirilmiştir. Deneysel bulgular da değerlendirilerek sayısal model doğrulanmıştır. Isı kaybı analizleri TS EN 12897+A1:2020-03 standardına uygun olarak yapılmış ve FDM'li ve FDM'siz tankların 180 dakikalık bekleme süresi sonundaki performansı karşılaştırılmıştır.
Sonuç:
Yapılan analizler, FDM'li sıcak su depolama tanklarında genel performansı belirgin şekilde iyileştirdiğini göstermektedir. Şarj süresinde FDM'lerin etkisi sınırlı olup, konvansiyonel tank 100 dakikada 50 °C'ye ulaşırken FDM'li tankların 105 dakika ile benzer sonuç vermesi, şarj sürecinin olumsuz etkilenmediğini ortaya koymuştur. Deşarj aşamasında ise FDM'ler önemli bir avantaj sağlayarak, RT47 için 16.40 dk, MP46 için 16.20 dk ve MP52 için 15.30 dk boyunca sıcak su temini sunmuş; bu değerler konvansiyonel tanka göre (14.10 dk) yaklaşık 2.5 dakika (~20 L) daha uzun kullanım süresi anlamına gelmiştir. Ayrıca, 55 °C'de 180 dakikalık bekleme süresinde konvansiyonel tankın 86.9 W olan ısı kaybı FDM'li tanklarda 79.95–82.3 W aralığına düşmüştür.
Anahtar Kelimeler: Faz değiştiren malzeme; termal enerji depolama; kullanım sıcak suyu; enerji verimliliği; hesaplamalı akışkanlar dinamiği.

ZEROBUILD JOURNAL

Research Article

Buker et al. 04:01 (2026) 41-54

Thermal Performance Assessment of Domestic Hot Water Tanks with PCM and Energy Efficiency Improvement Through CFD Analyses

Mahmut Sami BÜKER[1], Veli Can GÜRAN[2], Ahmet Emre ONAY[2], Halil İbrahim DAĞ[4]

[1]Necmettin Erbakan University, Konya, Turkiye
[2]Innorma R&D Inc., Konya, Turkiye
[3]SOLIMPEKS Solar, Konya, Turkiye
Sorumlu Yazar: msbuker@erbakan.edu.tr

Highlights:

- Enhanced Energy Storage: Integrating 3 kg of different paraffin-based PCMs (MP46, RT47 and MP52) into a 300 L capacity domestic hot water tanks increased the usable hot water volume by 20 L without significantly affecting charging time (RT47).
- Reduced Heat Loss: The MP52 PCM-enhanced hot water tank exhibits lower heat loss (79.95 W) in standby mode, resulting in improved thermal stability and energy efficiency.
- Sustainability Potential: Integrating PCMs into domestic hot water systems has contributed to energy savings and supporting the development of sustainable, user-oriented hot water solutions.

Received: 15.12.2025 Accepted: 10.01.2026 Doi: 10.5281/zenodo.18362176

Abstract: Energy efficiency has become increasingly critical in domestic hot water tank (DHWT) systems, as DHWT use accounts for approximately 30% of total energy consumption in buildings. Phase Change Material (PCM) integrated systems offer significant potential for improving thermal performance compared to conventional water-based storage. In this study, the charging, discharging, and heat loss behaviour of PCM-integrated DHWT were evaluated using Computational Fluid Dynamics (CFD). The results showed that adding 3 kg of paraffin-based PCM to a 300 L DHWT increased the usable hot water volume by at least 10% without significantly affecting the charging time. While the conventional tank provided usable hot water for 14.10 minutes, PCM integration extended this time by approximately 2 minutes due to the latent heat released during solidification. A heat loss analysis conducted according to the TS EN 12897+A1:2020-03 standard revealed that the conventional system showed a heat loss of 86.9 W at 55 °C, while the MP52 integrated tank reduced this value to 79.95 W after a 180-minute retention time. These findings demonstrate that combining sensible and latent heat storage reduces thermal losses, improves discharge performance, and contributes to overall energy savings. The study also offers recommendations for the future optimization of PCM-enhanced hot water systems, emphasizing improved control strategies to increase efficiency, particularly in material selection, PCM deployment, and next-generation hot water storage designs.

Keywords: Phase change material; thermal energy storage; domestic hot water, energy efficiency; computational fluid dynamics

1. Introduction

Increasing energy efficiency in buildings has made the optimization of heating and DHWT systems a key focus in building energy efficiency studies and sustainability strategies in recent years. The European Green Deal, which aims to achieve carbon neutrality by 2050, highlights the development of innovative and highly efficient solutions to reduce energy consumption in buildings. In this context, regulations and directives designed to enhance building energy performance, such as the Energy Performance of Buildings Directive (EPBD), encourage the design and use of energy efficient and low carbon DHWT systems. DHWT systems are particularly critical for energy efficiency, accounting for approximately 30 % of total building energy consumption, making them a focal point in sustainable building design [1, 2].

In addition to the conventional sensible heat storage methods, use of PCMs as heat storage medium offers significant advantages due to their ability to store a higher amount of energy [3]. PCMs store a considerable amount of latent heat during phase change, eventually increasing the overall energy storage capacity of the system [4]. This mechanism is particularly effective in extending the storage duration and increasing the amount of hot water available from the tank, allowing for faster response to user demand and significantly improving system energy efficiency.

Various studies in the literature have examined the use of PCMs in DHWTs contained in different geometries and application scenarios. These studies have analysed mainly the effects of PCM location in the tank, quantity, and container geometry on thermal energy storage performance. For example, in vertical mantle DHWTs, positioning paraffin capsules 400 mm above the bottom of the tank enabled the maximum hot water volume (639 L) to be achieved. In contrast, placing the capsules directly at the bottom of the tank (0 mm) reduced the obtainable hot water volume to 619 L. The data indicate a notable increase in hot water volume up to 400 mm, while exceeding 600 mm led to a decrease in the amount of hot water obtained [10].

Similarly, another study on vertical tanks determined that the optimum 32.5 kg PCM quantity was 13 paraffin capsules, which increased hot water output by approximately 20 % [5]. For horizontal mantle DHWTs, four 1 L paraffin tubes extended the discharge duration by 17 minutes and increased the amount of hot water obtained from the tank [6]. These results demonstrate that PCM location and quantity directly and measurably affect the thermal performance of the DHWT.

Another critical factor influencing DHWT performance is heat loss during standby periods. Thermal bridges at tank connections and insufficient or uneven insulation can negatively impact the preservation of stored energy, significantly reducing system efficiency. Therefore, minimizing heat loss is a fundamental design consideration to both enhance energy efficiency and maximize the effectiveness of PCM-integrated thermal energy storage systems [7].

This hybrid sensible-latent heat storage is also promising concept for renewable energy integration. A study on the energy and exergy flow analysis of primary energy sources has shown that solar collector systems provide the highest total energy and exergy efficiency among existing heating options [8]. They observed that energy efficiency ranges from 24.1% to 46.2% for Izmir and 22.4% to 40.3% for Paris under different scenarios. This finding indicates that integrating PCM-enhanced hot water storage tanks with solar collectors has an important potential for increasing energy efficiency in buildings. Furthermore, since the DHWT can be directly fed by solar collectors, the system reduces dependence on fossil fuel-based heating and consequently contributes to lowering total carbon emissions.

In a preliminary study, charging, discharging, and heat loss analyses were conducted. The results showed that the use of PCM in DHWTs increased the amount of hot water by 20 L compared to DHWTs without PCM. It also extended the hot water discharging time by approximately 2.5 minutes [9].

This study investigates the thermal performance of a 300 L DHWT with a vertical cylindrical configuration, comparing conventional operation with a PCM-integrated design. Unlike many previous studies that primarily focus on large PCM masses (typically 10–40 kg) or non-commercial and idealised tank geometries, the present work evaluates the integration of only 3 kg of paraffin-based PCM into a commercially available coil-type storage tank. The key novelty of this study lies in demonstrating that even a relatively small amount of PCM, when appropriately positioned within a tank configuration, can yield a measurable enhancement in thermal performance. This approach provides a more practical and industry-relevant assessment of PCM integration, addressing the gap between laboratory-scale investigations and real-world DHWT applications.

A validated three-dimensional CFD model was developed for the tank, and charge, discharge, and heat loss scenarios were analysed separately. During the charge analyses, temperature distributions and thermal response times were evaluated under constant inlet temperature and flow rate conditions to understand the tank's dynamic behaviour. During the discharge analyses, the temporal variation of the usable DHWT volume and outlet temperature was monitored. Heat loss analyses were conducted according to the TS EN 12897+A1 standard to assess thermal stability and energy savings during the specified holding period.

In addition to assessing energy storage capacity, the study also examines the impact of PCM integration on charge and discharging times, standby heat losses, and DHWT availability. The results provide a comparison between conventional and PCM-integrated tanks and highlight the performance advantages achieved by adding a small PCM volume. These features distinguish the current study from previous research.

2. Materials and Methods

2.1 System Description

In this study, a 3D model of a conventional 300 L DHWT in a vertical cylindrical geometry was realised (Figure 1). The tank has two separate coils positioned at the top and bottom. The lower coil allows the tank to be charged with thermal energy from an external source (e.g., a heat pump, solar thermal collector). The upper coil, on the other hand, is utilised for DHWT production, facilitating indirect heat transfer between the stored hot water in the tank and the incoming cold mains water. During this process, mains water enters the tank through the lower inlet of the upper coil, interacts thermally with the water inside the tank to increase in temperature, and exits as hot water from the upper outlet. This design approach aims to ensure hygienic DHWT supply while enhancing energy efficiency.

To improve the thermal performance of the tank, the PCM tubes were attached to the coils using clip mechanisms that ensured both the PCM tubes remained in place and efficient heat transfer was ensured. Consequently, the PCM's latent heat storage capacity enhances the tank's energy efficiency through minimising fluctuations in hot water temperature. During heating and cooling processes, the PCM stores energy via phase change (solid-to-liquid transition), helping to maintain the water within the desired temperature range for extended periods. This mechanism is particularly effective in meeting sudden demand, ensuring sufficient hot water is available at a stable temperature.

Figure 1. 300 L domestic hot water tank [16]

2.2 Baseline Experimental Procedure

Charge, discharge, and heat-loss experiments were performed on the conventional DHWT (without PCM) test system, and the resulting data were used to validate the analysis model as reference case. During the charging phase, the storage tank was supplied by a heat pump operating at 50 °C with a volumetric flow rate of 24 L/min. Charging was continued until the tank temperature reached 50 °C.

In the discharging phase, DHWT production was obtained by circulating mains water through the coil at 12.5 °C with a flow rate of 8 L/min. The discharge test was terminated when the temperature measured at the coil outlet dropped below 40 °C.

For the heat-loss tests, the tank temperature was first raised to 55 °C (the maximum temperature attainable by the heat pump). The tank maintained at 55 °C was then left in a stand-by mode under natural convection conditions in accordance with the requirements of the TS EN 12897+A1:2020-03 standard.

2.3 Determination of PCM Properties

The PCM plays a critical role in determining the thermal energy storage capacity and optimising the overall energy efficiency of the tank. In this context, the thermophysical properties of the PCMs were thoroughly examined, and its suitability for the system design was evaluated.

Table 1. Properties of the PCMs [15, 17]

Paraffin based PCM type	RT47	MP46	MP52
Melting Temp. (°C)	48	49.1	54.9
Solidification Temp. (°C)	41	42.5	42.6
Latent heat storage capacity (kJ/kg)	160	214	198.4
Specific Heat Capacity (kJ/kg.K)	2	2.2	2.66
Solid Density (kg/m3)	880	772	808
Fluid Density (kg/m3)	770	750	783
Heat Conduction (W/m.K)	0.2	0.137	0.129

2.4 Determination of PCM Capsule Geometry

Physical and thermal properties of the PCMs, including melting – solidification temperature range, material type, thermal conductivity, density, specific heat, and latent heat capacity were derived from both literature and manufacturer specifications (Table 1). These data were used as input parameters in the CFD analyses, ensuring accurate modelling of the tank's performance during charging, discharging, and standby periods.

The paraffin-based PCMs, with a phase change temperature in the range of 40–50 °C, were selected based on a combination of technical and practical criteria. First, the chosen temperature range aligns with the DHWT requirements. Also, paraffin provides high latent heat capacity and significant enthalpy of solidification per unit temperature during phase change. Additionally, factors such as chemical stability, cycle durability, compatibility with metal containers without causing corrosion, and commercial availability were also considered critical. These properties are vital for long-term stable operation of the system while enhancing energy efficiency.

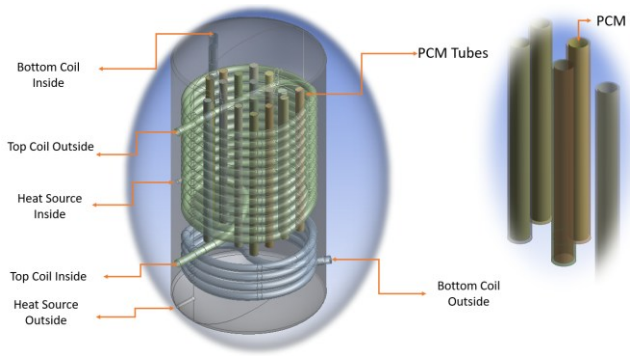

Figure 2. 300 L DHWT with PCM

Table 2. PCM tube details [11]

Material	SAE 304
Length	650 mm
Inside diameter	30 mm
Outside diameter	33.4 mm

The method of integrating PCMs into the DHWT directly affects the thermal performance, particularly in terms of heat transfer surface area. In this study, cylindrical capsules with a relatively higher surface area-to-volume ratio were selected to enhance the heat exchange within the tank (Figure 2) [10]. These cylindrical capsules improve the thermal interaction between the PCM and water due to higher thermal conductivity of the metallic tubes, optimising energy storing and releasing processes and enhancing the overall system efficiency [4].

Capsule diameter is another important factor that has direct impact on the thermal performance of the PCM. Reducing the capsule diameter limits the total heat transfer surface area, which decreases the heat transfer rate. Conversely, excessively increasing the capsule diameter may leave the inner regions of the PCM unmelt. This scenario could result in excessive use of PCM and hinder the tank from delivering hot water at the desired temperature during discharging, negatively impacting system performance. Based on findings from the existing studies in the literature [11], the inner diameter, outer diameter, and length of the PCM tubes were adapted and 12 tubes are used in the system, their specifications are given in Table 2.

In addition to tube dimensions, the placement of PCM capsules within the tank significantly affects thermal performance. In the current design, PCM tubes are positioned vertically at a mid-height between the serpentine and the tank centre. This vertical orientation is chosen to be perpendicular to the upward flow of water due to buoyancy; it enhances convective heat transfer between the PCM capsules and the surrounding water.

The tubes are secured to the serpentines using 37.5 mm clips, resulting in a distance of 54.2 mm from the centre to the serpentine. This configuration ensures uniform spacing and stable flow paths. Careful determination of these size parameters is crucial for enhancing heat transfer while maintaining optimum thermal energy storage. Consequently, capsule geometry and sizing are considered fundamental design factors for improving both energy storage capacity and hot water output performance.

2.5 CFD Modelling

The simulations were governed by the fundamental conservation equations of mass, momentum, and energy. The continuity equation ensures mass balance within the tank, while the momentum equations, formulated as the Reynolds-averaged Navier–Stokes (RANS) equations, account for pressure forces, viscous effects, and buoyancy-driven flow. The energy equation describes transient heat transfer by incorporating both conduction and convection mechanisms, enabling an accurate representation of the thermo-fluid behaviour of the tank during the charging and discharging processes. The fluid flow and thermal behaviour within the tank were evaluated using transient CFD simulations performed in ANSYS Fluent R16.2.

Turbulence effects were modelled using the k–ω turbulence model, a widely adopted two-equation approach in computational fluid dynamics. This model was chosen due to its strong performance in accurately capturing natural and forced convection events under

low to medium Reynolds number conditions. Specifically, the standard k–ω model is better suited for the thermally stratified and mixed convection regimes encountered in the storage tank and provides better handling in the near-wall region and better sensitivity to buoyancy-driven flow structures compared to the k–ε model.

This model resolves two coupled partial differential equations for the turbulence kinetic energy (k) and the specific dissipation rate (ω), where k represents the energy of turbulent velocity fluctuations and ω characterizes the rate at which this energy is dissipated into internal thermal energy.

Mass conservation:

$$\nabla \cdot \vec{V} = 0 \quad (1)$$

Momentum conservation:

$$\rho \frac{\partial \vec{V}}{\partial t} + \rho(\vec{V}\nabla)\vec{V} = -\nabla P + \mu \nabla^2 \vec{V} + \rho\beta\vec{g}\,(T - T_0) + \vec{S} \quad (2)$$

Energy conservation:

$$\frac{\partial}{\partial t}(\rho H) + \nabla \cdot \left(\rho \vec{V} H\right) = \nabla \cdot (k_1 \nabla T) \quad (3)$$

The Darcy source term is used in Eq. (2) due to the porosity change in the soft region [18].

$$\vec{S} = \frac{(1-\lambda)^2}{\lambda^3 + 0.001}\vec{V} A_{mushy} \quad (4)$$

The symbols $V, \rho, P, \beta, t, \mu, g, k_1$ denote velocity, density, pressure, thermal expansion coefficient, time, dynamic viscosity, gravitational acceleration, and thermal conductivity, respectively.

Enthalpy represents the total thermal energy of the PCM and consists of both sensible and latent heat capacities. The sensible heat varies with temperature according to the specific heat capacity, while the latent heat accounts for the energy absorbed or released during phase change at nearly constant temperature. In CFD-based PCM modelling, the enthalpy formulation enables accurate tracking of melting and solidification by coupling temperature-dependent sensible heat with the latent heat source term. This approach ensures a consistent and energy-conserving representation of the phase change process across the computational domain.

$$H = h + \Delta H \quad (5)$$

The sensible heat:

$$h = h_0 + \int_{T_0}^{T} C_p dT \quad (6)$$

The latent heat:

$$\Delta H = \lambda L$$

L is the latent heat of the PCM. λ is the liquid fraction in the soft region, with values between 0 and 1.

$$\lambda = \begin{cases} 0 & T < T_{solid} \\ \frac{T - T_{solid}}{T_{liquid} - T_{solid}} & T_{solid} < T < T_{liquid} \\ 1 & T > T_{liquid} \end{cases} \quad (7)$$

The phase change process in the PCM was modelled based on the classical enthalpy–porosity approach. In this method, the phase transition is defined by accounting for enthalpy variations during the solid-to-liquid transition, and energy transfer within this region is computed [12, 13]. This approach allows the latent heat storage capacity of the PCM and its impact on the overall thermal performance of the tank to be numerically simulated.

2.5.1 Mesh Structure

A locally refined mesh was generated over the geometric model in critical regions. In particular, smaller cell sizes were applied at the coil surfaces, around the PCM tubes, and at the fluid inlet and outlet zones to ensure detailed resolution. This strategy enables accurate modelling of both flow and heat transfer behaviour. The mesh details are presented in Table 3, demonstrating that the simulations are sufficiently stable and resolved numerically (Figure 3, Figure 4). This configuration allows for precise investigation of both energy storage and DHWT supply processes.

A total of 10 iterations were conducted during the simulation process, and the time step size was set to 0.1 s, resulting in a CFL number of 2.66. The primary reason for choosing a time step of 0.1 was to increase temporal resolution while maintaining a stable CFL value within

acceptable limits for incompressible flow, thereby improving the accuracy of the CFD predictions and enabling a more precise representation of transient flow structures, temperature gradients, and convection-driven circulation patterns inside the tank. However, although more precise results were obtained setting time step at 0.1 s has increased the duration tenfold.

Table 3. Model mesh quality values

Element number	1,347,048
Skewness value (max)	0.78
Orthogonal Quality (min)	0.23
Aspect Ratio value (max)	10.6

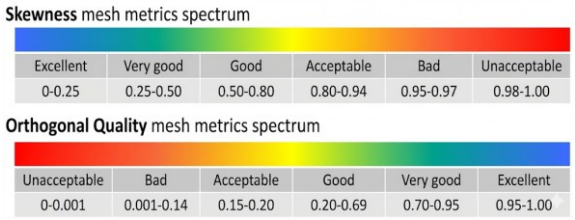

Figure 3. Mesh quality metric

The numerical configuration applied in the transient analyses was as follows:

- Pressure–velocity coupling: SIMPLE
- Time step: 0.1 s
- Courant number: 2.66
- Boundary layer thickness: 0.5 mm
- Convergence criteria: 10^{-5} for continuity and momentum, 10^{-6} for energy
- Under-relaxation factors: default settings (energy=1.0)

Within the framework of the RANS equations, the eddy viscosity ν_T is defined as the ratio of the turbulence kinetic energy to the specific dissipation rate, i.e., $\nu_T = k/\omega$. The transport equations governing the temporal and spatial evolution of the turbulence kinetic energy k and the specific dissipation rate ω are given as follows [19]:

$$\frac{\partial(\rho k)}{\partial t} + \frac{\partial(\rho u_j k)}{\partial x_j} = \rho P - \beta^* \rho \omega k + \frac{\partial}{\partial x_j}\left[\left(\mu + \sigma_k \frac{\rho k}{\omega}\right)\frac{\partial k}{\partial x_j}\right], with\ P = \tau_{ij}\frac{\partial u_i}{\partial x_j} \quad (8)$$

$$\frac{\partial(\rho w)}{\partial t} + \frac{\partial(\rho u_j w)}{\partial x_j} = \frac{\alpha\omega}{k}\rho P - \beta\rho\omega^2 + \frac{\partial}{\partial x_j}\left[\left(\mu + \sigma_k \frac{\rho k}{\omega}\right)\frac{\partial \omega}{\partial x_j}\right] + \frac{\rho\sigma_d}{\omega}\frac{\partial k}{\partial x_j}\frac{\partial \omega}{\partial x_j} \quad (9)$$

The symbols $k, \omega, u_i, u_j, x_i, x_j$ denote Favre-averaged specific turbulence kinetic energy, specific dissipation rate, Favre-averaged velocity vectors (u values), and position vectors (x values), respectively.

2.5.2 Tank Charging Simulation Procedure

For the charging process, both the PCM-integrated and conventional (water based) DHWTs were initially filled with water at a uniform temperature of 12.5 °C. The heating process was simulated to reflect realistic operating conditions, using a heat pump with an outlet temperature of 50 °C at a flow rate of 24 L/min. Firstly, the charging behaviour of the conventional tank was analysed, and the resulting temperature distributions and thermal response were validated against experimental data. This validation ensured the reliability of the simulation model and provided a basis for analysing the PCM-integrated tank.

The melting process of the PCM was specifically accounted for in the simulations, as it directly affects heat transfer within the tank and plays a critical role in determining the charging time. During phase change, the PCM stores latent heat, slowing the temperature rise of the

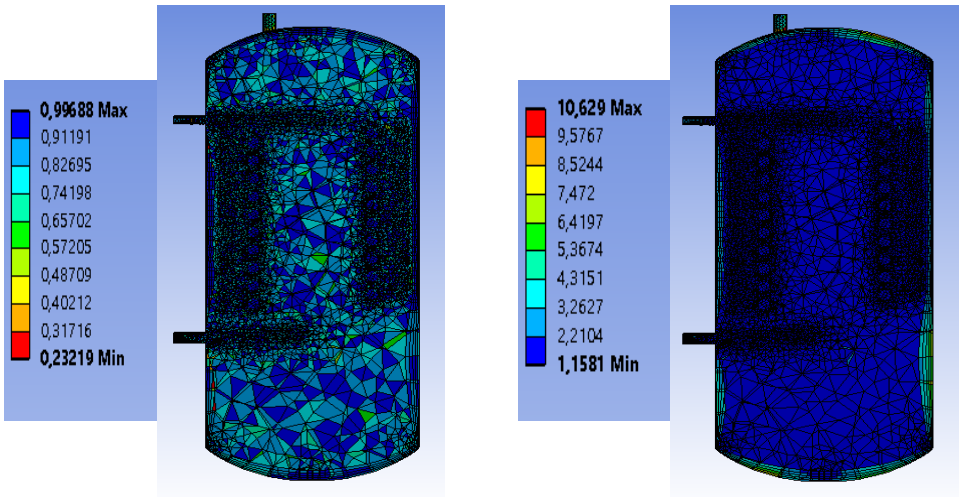

a b

Figure 4. a) Orthogonal quality, b) Aspect ratio views

water and helping maintain thermal homogeneity within the tank. In both tank configurations, the charging process was terminated once the average water temperature reached 50 °C. This approach allowed for a consistent comparison of the thermal effects and energy storage capacity of the PCM with experimental conditions.
This methodology has enabled a detailed assessment of the effects of PCM integration on tank charging time, energy storage efficiency, and hot water output.

2.5.3 Tank Discharging Simulation Procedure

The discharge process was conducted to evaluate the thermal response behaviour of the tanks, which had initially reached an average temperature of 50 °C at the end of the charging phase. For the discharge analysis, both the PCM-integrated and conventional tank were defined with a uniform temperature of 50 °C. Subsequently, mains water at 12.5 °C was supplied to the coil inlet at a constant flow rate of 8 L/min. This scenario simulates real operational conditions of the DHWT consumption.

During the discharge process, the cold water circulating through the coil indirectly transferred heat to the water in the tank, producing usable hot water. As the tank temperature decreased, solidification occurred in the PCM; the molten paraffin solidified, releasing latent heat. This helped maintain the water within the desired temperature range for a longer duration and demonstrated how the energy storage capacity of the PCM stabilizes tank performance during discharge.

The discharge process halted once the outlet temperature of the DHWT dropped below 40 °C. This set temperature was defined as a practical comfort limit and ensured the comparability of the analyses. Temperature distributions, outlet temperature–time profiles, and internal heat transfer data obtained during the discharge period were used to assess the effects of PCM on thermal stability and energy efficiency.

2.5.4 Heat Loss Simulation Procedure

The heat loss analysis was carried out in accordance with the TS EN 12897+A1:2020-03 standard and was designed to evaluate the energy losses occurring when the domestic DHWT tank is left idle for a certain period after the charging process. Within this scope, both the PCM-integrated and conventional tank models were simulated for 180 minutes after the average water temperature reached 55 °C [7, 14].

During the analysis, the tank's inlet and outlet were closed to create a static system, and heat transfer between the tank surface and the environment was limited to natural convection

and surface radiation. No active cooling or additional heating was applied, and the ambient temperature was set to a constant 20 °C in accordance with the TS EN 12897 standard and maintained throughout the simulation.

The tank insulation was modelled based on commonly used polyurethane foam insulation properties, and heat transfer from the tank surface to the surroundings was calculated according to the thermophysical properties of this material. In the PCM-integrated tank, the latent heat storage capacity of the paraffin-based phase change material, near its melting temperature, was utilized to delay the temperature drop and enhance the thermal stability of the tank during the idle period. This approach allowed for a numerical assessment of the effects of PCM on energy storage and heat loss.

3. Results and Discussion

3.1 Charging Process Analysis Results

The charging simulations were carried out by initially setting both the PCM-integrated and conventional tanks to a uniform water temperature of 12.5 °C. A heat pump supplying 50 °C water at a flow rate of 24 L/min was used to evaluate the temperature evolution and charging dynamics. The temperature fields obtained for the conventional and PCM-integrated configurations at their respective charging durations are presented in Figure 4.

To determine the effect of phase change materials on overall thermal performance, PCM temperature variations and corresponding melting rates were evaluated comparatively. Figure 5 shows: (a) initial tank temperature, (b) temperature range of the conventional tank at the end of the charging time (100 min), and (c-e) temperature distributions of the RT47, MP46, and MP52 integrated tanks at their respective charging times (105, 110, and 105 min).

According to Table 4, the simulated charging time of the conventional tank (100 min) showed strong agreement with experimental measurements. Under the same operating conditions, the melting fractions of the integrated PCMs at 105 min were 90 % for RT47, 88 % for MP46, and 75 % for MP52. These results confirm that PCM addition increases the tank's thermal storage capacity without altering the fundamental charging behaviour.

Although the RT47 and MP46 samples required approximately 140 min to reach complete melting, the majority of their latent heat potential had already been activated within the effective charging window. The remaining unmelted fraction did not cause operational delay or degradation in charging performance. Therefore, PCM integration can be considered an effective enhancement strategy that increases storage density while maintaining comparable charging times to the baseline configuration.

Table 4. Test vs simulation charge results

Method (24 L/min)	Charge Temp. (°C)	Charging Time (min)	Diff. (%)	Melting Time (min)
Water (Exp.)	50	100	-	-
Water (Sim.)	50	100	-	-
RT47	50	105	5	105
MP46	50	105	10	110
MP52	50	105	-	105 (75%)

3.2 Discharging Process Analysis Results

During the discharging simulations, mains water at 12.5 °C and 8 L/min was circulated through the upper coil of tanks initially at an average temperature of 50 °C. The process was terminated once the outlet temperature dropped below the comfort threshold of 40 °C. Figure 5 presents the temperature distributions for both the conventional and PCM-integrated tanks at the end of their respective discharge durations.

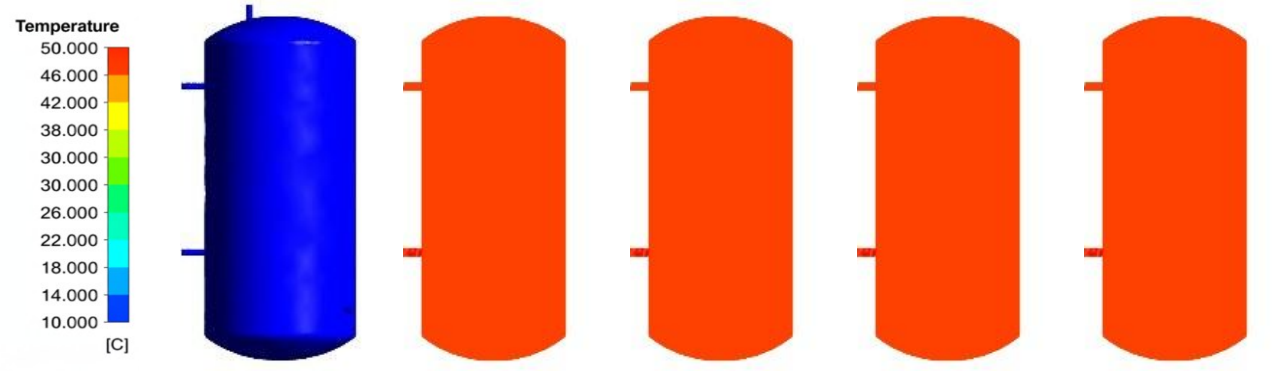

0.min ≈ 12.5˚C a | 100.min ≈ 50˚C b | 105.min ≈ 50˚C c | 110.min ≈ 50˚C d | 105.min ≈ 50˚C e

Figure 5. Standard vs PCMs charging time

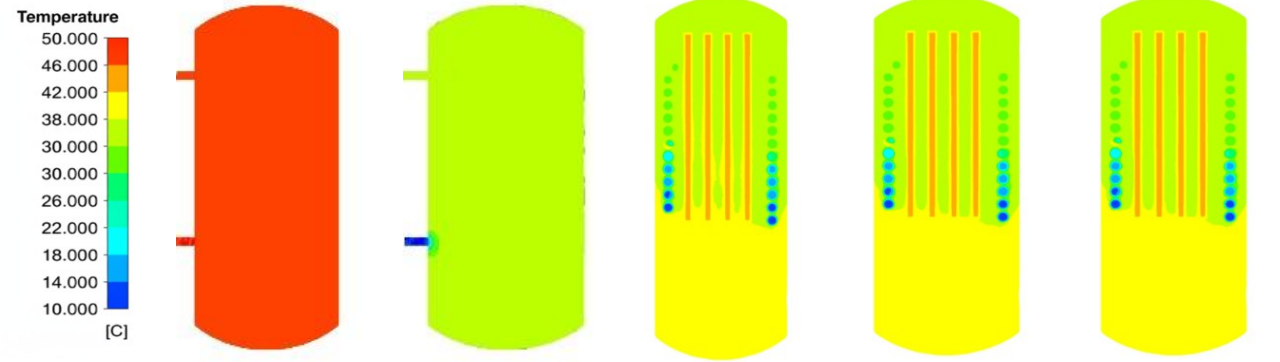

0.min ≈ 50˚C a | 14.10 min ≈ 40˚C b | 16.40 min ≈ 40˚C c | 16.20 min ≈ 40˚C d | 15.30 min ≈ 40˚C e

Figure 6. Standard vs PCMs discharging time

Figure 6 presents: (a) the initial temperature distribution within the tank, (b) the temperature field of the conventional tank at the end of the discharge period (14.10 min), and (c–e) the temperature distributions of the RT47, MP46, and MP52-integrated tanks corresponding to their respective discharge durations (16.40, 16.20, and 15.30 min).

As summarised in Table 5, the simulated discharge time of the conventional tank (14.10 min) closely matched experimental findings.

The RT47, MP46, and MP52-integrated tanks exhibited longer discharge durations of 16.40, 16.20, and 15.30 min, respectively. These increments correspond to approximately 20, 16, and 10 additional litres of usable hot water compared with the reference case.

The extended discharge periods result from the gradual release of latent heat during PCM solidification. As the tank cools, the PCMs transfer stored thermal energy back to the surrounding water, moderating temperature decay and sustaining the outlet temperature above 40 °C. This mechanism enhances the effective hot water volume and contributes to improved thermal efficiency during draw-off periods.

3.3 Heat Loss Analysis Results

Heat loss performance was evaluated according to the TS EN 12897+A1:2020-03 standard. This evaluation was carried out by initially maintaining the average temperature of both conventional and PCM integrated tanks at 55 °C and then applying a 180-minute standby period without water circulation. The

ambient temperature was kept constant at 20 °C, and heat transfer was achieved through natural convection and surface radiation. Figure 6 shows the average temperatures of the tanks at the end of the 180-minute holding period.

Figure 7 shows: (a) the initial temperature of the tank, (b) the temperature distribution of the conventional tank at the end of 180 minutes of analysis, and (c-e) the temperature distribution of the PCM-integrated tanks (RT47, MP46, and MP52) at the end of the same period.

Table 6 indicates that the conventional tank exhibited a heat loss of approximately 86.9 W, consistent with experimental observations. The PCM-integrated tanks demonstrated reduced heat losses of 82.3 W (RT47), 82.24 W (MP46), and 79.95 W (MP52), confirming an improvement in thermal retention.

This enhancement is attributed to the latent heat buffering capacity of the PCMs near their phase change temperatures. As the stored energy is gradually released during cooling, the rate of temperature decay decreases, leading to lower static heat losses and improved standby efficiency. Overall, the integration of PCMs not only increases usable hot water availability but also enhances energy performance by reducing heat losses during no-load conditions.

Table 5. Test vs simulation discharge results

Method (8 L/min)	Discharge Temp. (°C)	Discharge Time (min. s)	Diff. (%)	HW Amount (L)
Water (Exp.)	50	14.10	-	113
Water (Sim.)	50	14.10	-	113
RT47	50	16.40	20	133
MP46	50	16.20	18	132
MP52	50	15.30	9.42	126

Table 6. Test vs simulation heat loss results

Method (Natural Convection)	Heat Loss Temp. (°C)	Heat Loss Time (hour)	Heat Loss (W)	Diff. (%)
Water (Exp.)	55	3	92.7	-5.75
Water (Sim.)	55	3	86.9	-
RT47	55	3	82.3	5.35
MP46	55	3	82.2	5.36
MP52	55	3	79.9	7.99

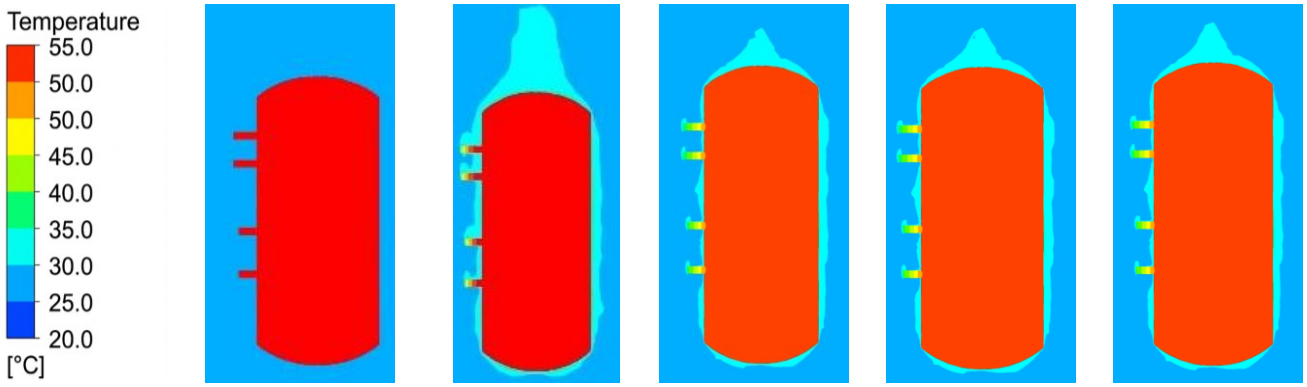

Figure 7. Standard vs PCMs heat loss time

4. Conclusions

This study numerically evaluated the thermal performance of a 300 L DHWT integrated with 3 kg of paraffin-based PCMs under charging, discharging, and standby conditions, and compared the results with those of a conventional configuration. CFD

simulations showed that PCM integration had a negligible influence on charging behaviour. The conventional tank reached 50 °C in 100 minutes, whereas the RT47-integrated tank achieved the same temperature in 105 minutes, indicating only a minor increase of approximately 5 %.

In contrast, PCM incorporation significantly enhanced discharging performance. The useful hot water delivery period of the conventional tank (14.10 min) was extended to 16.40 min with RT47, corresponding to an additional 20 L of water above the comfort threshold. This improvement arises from the latent heat released during solidification, which effectively stabilizes outlet temperature during periods of decreasing tank temperature.

Standby heat-loss analyses conducted in accordance with TS EN 12897+A1:2020 highlighted further thermal advantages. The MP52-integrated tank exhibited a heat loss of 79.95 W after 180 minutes, compared with 86.9 W for the conventional system, confirming superior temperature retention through latent heat buffering.

Among the tested PCMs, RT47 and MP46 demonstrated the most favourable overall performance due to their melting ranges (40–55 °C) aligning well with DHWT operating temperatures and enabling efficient charge–discharge behaviour. Although MP52 contributed less to discharge extension, it performed best in reducing standby heat losses.

Overall, integrating a small PCM quantity (~3 kg) into a 300 L DHWT provides measurable performance gains—extending hot water availability, improving thermal stability, and reducing standby losses—while maintaining comparable charging times. These outcomes indicate that PCM-integrated storage tanks offer a practical and effective pathway for improving energy efficiency in DHWT applications.

Future work will focus on the experimental validation of PCM-integrated hot water tanks under realistic domestic water usage conditions. Furthermore, investigating advanced serpentine and PCM encapsulation techniques in different tank geometries could further enhance heat transfer performance. Moreover, comprehensive studies on the effects of varying PCM quantities and incorporating these findings into energy class assessment procedures could support the development of more efficient storage tank designs.

Acknowledgements

This study was carried out within the framework of project number 3248224, supported by the TÜBİTAK 1832 Green Transformation in Industry Call. We would like to thank the project partners Solimpeks Energy Industry and Trade Inc., Innorma R&D Inc., and Petroyag and Chemicals Industry and Trade Inc. for their valuable contributions throughout the project process.

References

[1] IEA (2023), *Energy Efficiency 2023, IEA, Paris* https://www.iea.org/reports/energy-efficiency-2023, Licence: CC BY 4.0

[2] Energy Performance of Buildings Directive, 2024, Energy Performance of Buildings Directive

[3] Liang, H., Niu, J., & Gan, Y. (2020). Performance optimization for shell-and-tube PCM thermal energy storage. *Journal of Energy Storage*, *30*. https://doi.org/10.1016/j.est.2020.101421

[4] Erdemir, D. (2020). Kapsüllenmiş Faz Değiştiren Malzemelerin Sıcak Su Tankları İçerisindeki Konumlarının Isıl Enerji Depolama Performansı Üzerindeki Etkisi. Erciyes Üniversitesi Fen Bilimleri Enstitüsü Fen Bilimleri Dergisi, 35(3), 24-33.

[5] Erdemir, D., & Altuntop, N., (2019). Experimental Investigation of Phase Change Material Utilization Inside the Horizontal Mantled Hot Water Tank (Accepted Paper). *International Journal Of Exergy* , vol.1, 1-28. https://dx.doi.org/10.1504/IJEX.2020.104722

[6] Erdemir, D., Ozbekler, A., & Altuntop, N. (2022). Experimental investigation on the effect of the ratio of tank volume to total capsulized paraffin volume on hot water output for a mantled hot water tank. *Solar Energy*, *239*, 294–306. https://doi.org/10.1016/j.solener.2022.05.010

[7] Junga, R., Pospolita, J., Kabaciński, M., Sobek, S., Stanisławski, R., Mami, M. A., … Mruk, Z. (2024). Numerical modeling of heat losses from hot water storage tank. *Case Studies in Thermal Engineering*, *62*. https://doi.org/10.1016/j.csite.2024.105146

[8] Yildirim N., Kahraman I. & Umdu E., (2023) Exergetic Performance Assessment of Different Building Heating Systems https://doi.org/10.5281/zenodo.7487556

[9] M. S. Büker, V. C. Güran, A. E. Onay ve H. İ. Dağ, "Thermal performance assessment and energy efficiency improvement of a domestic hot water tank with PCM," in Proc. ULIBTK'25 Uluslararası Katılımlı 25. Isı Bilimi ve Tekniği Kongresi, Adana, Türkiye, 10-12 Eylül 2025, pp. 977-983.

[10] Koželj, R., Mlakar, U., Zavrl, E., Stritih, U., & Stropnik, R. (2021). An experimental and numerical analysis of an improved thermal storage tank with encapsulated PCM for use in retrofitted buildings for heating. *Energy and Buildings*, *248*. https://doi.org/10.1016/j.enbuild.2021.111196

[11] Najafian, A., Haghighat, F., & Moreau, A. (2015). Integration of PCM in domestic hot water tanks: Optimization for shifting peak demand. *Energy and Buildings*, *106*, 59–64. https://doi.org/10.1016/j.enbuild.2015.05.036

[12] Belhadad, T., Draoui, B., & Bouabdallah, S. (2023). CFD investigation of fin design influence on phase change using ANSYS Fluent enthalpy-porosity method. *Journal of Energy Storage, 62*, 107361. https://doi.org/10.1016/j.prime.2023.100306

[13] Saliby, A., Hammami, A., & Sadok, D. (2024). Experimentally based testing of the enthalpy-porosity method for the numerical simulation of phase change of paraffin-type PCMs. *Journal of Building Engineering, 85*, 108467. https://doi.org/10.1016/j.est.2023.107876

[14] TS EN 12897+A1, 2020, *Su temini - Dolaylı olarak ısıtılan havalandırmasız (kapalı) ısıtıcılı su depoları için özellikler,* Standard Detayı

[15] Rubitherm, Rubitherm Technologies GmbH, https://www.rubitherm.eu/produktkategorie/organische-pcm-rt (accessed Nov. 18, 2025).

[16] Solimpeks, "Solikombi 300 Hijyenik Boyler - Serpantinli - Akümülasyon tankı - boiler," Solimpeks Güneş Enerjisi Sistemleri | Isı Pompası - Fotovoltaik Panel - Boyler - Solar Enerji, https://www.solimpeks.com.tr/urun/solikombi-300-hijyenik-boyler/ (accessed Nov. 18, 2025).

[17] Petroyağ, "Endüstriyel Yağlar: Petroyağ ürünler," Endüstriyel Yağlar | Petroyağ Ürünler, https://www.petroyag.com/urunler (accessed Nov. 18, 2025).

[18] A. D. Brent, V. R. Voller, and K. J. Reid, "Enthalpy-porosity technique for modeling convection-diffusion phase change: Application to the melting of a pure metal," Numerical Heat Transfer, vol. 13, no. 3, pp. 297–318, Apr. 1988. doi:10.1080/10407788808913615

[19] Wilcox, D. C. (2008), "Formulation of the k–ω Turbulence Model Revisited", *AIAA Journal*, **46** (11): 2823–2838, Bibcode:2008AIAAJ..46.2823W, doi:10.2514/1.36541

ZEROBUILD JOURNAL

Araştırma Makalesi

Karakoc ve ark. 04:01 (2026) 55-65

TS 825: 2024 ve Pasif Ev Standartlarının Yalıtım Kalınlığı Açısından Karşılaştırılması ve Bina Enerji Performansı Üzerindeki Etkilerinin Değerlendirilmesi

Sümeyra Karakoç, Enes Güngör, Ameer Khan, Adem Görgülü

Yalova Üniversitesi, Yalova Türkiye
Sorumlu Yazar: sumeyrakarakoc11@gmail.com

Öne Çıkanlar

- Pasif Ev standardı, TS 825'e göre yıllık enerji tüketimini iklim bölgesine göre %60 ile %75 oranında düşürmektedir.
- TS 825'te tüketim iklimle ciddi değişkenlik gösterirken, Pasif Ev tasarımı tüm şehirlerde enerji kullanımını 18-22 kWh/m^2 bandında sabitlemektedir.
- Pasif Ev kriterleri, yüksek yalıtım ve güneş kazancı sayesinde sıcak iklim bölgelerinde ısınma ihtiyacını tamamen ortadan kaldırabilmektedir.
- Dinamik simülasyonlar, Pasif Ev'deki sistem etkileşimlerini modellediği için analitik yöntemlere göre daha optimize ve düşük sonuçlar vermektedir.
- Çalışma, Türkiye'nin enerji hedefleri için TS 825'in "performans sınırlamalı" bir yapıya güncellenmesi gerektiğini vurgulamaktadır.

Geliş Tarihi: 01.01.2026 Kabul Tarihi: 22.01.2026 Doi: 10.5281/zenodo.18366481

Özet

Bu çalışmada, Türkiye'de binalarda enerji verimliliğinin artırılmasında önemli bir rol oynayan TS 825 Isı Yalıtım Gereksinimleri Standardı ile yüksek performanslı bir yaklaşımı temsil eden Pasif Ev standardı, dış duvarlarda kullanılan EPS yalıtım kalınlığı ve bunun bina enerji performansına etkileri açısından karşılaştırmalı olarak incelenmiştir.

Amaç

Çalışma kapsamında, Türkiye'nin altı farklı iklim bölgesini temsil eden Adana, Manisa, İstanbul, Eskişehir, Sivas ve Kars illerinde konumlandırılmış örnek bir konut binası modeli için OpenStudio –EnergyPlus kullanılarak dinamik enerji simülasyonları gerçekleştirildi. Dış duvar yalıtım kalınlıkları, TS 825:2024 standardının güncellenmiş U-değeri ile Pasif Ev standardına uygun yalıtımın U değerlerinin kıyaslanması amaçlandı. Simülasyon ve analitik hesaplama sonuçları karşılaştırıldı.

Sonuç

Bulgular, TS 825'in iklime bağlı değişken yalıtım kalınlıklarına karşın Pasif Ev standardının sabit ve daha yüksek performanslı bir yapı kabuğu talep etiğini gösterdi. Pasif Ev yaklaşımı, özellikle soğuk bölgelerde TS 825'e göre %60-75 oranında enerji tasarrufu sağlamaktadır. Çalışmada, Türkiye'nin verimlilik hedefleri için TS 825'in asgari şartlardan ziyade, bina performansını doğrudan sınırlayan bütüncül ve yüksek standartlı bir yapıya güncellenmesinin faydalı olacağı değerlendirilmiştir.

Anahtar Kelimeler: TS 825, Pasif Ev, Optimum Yalıtım Kalınlığı, Bina Enerji Performansı, Enerji Simülasyonu

ZEROBUILD JOURNAL

Research Article

Karakoc et al. 04:01 (2026) 55-65

Comparison of TS 825: 2024 and Passive House Standards in Terms of Insulation Thickness and Evaluation of Their Effects on Building Energy Performance

Sümeyra Karakoç, Enes Güngör, Ameer Khan, Adem Görgülü

Yalova Üniversitesi, Yalova Türkiye
Corresponding Author: sumeyrakarakoc11@gmail.com

Highlights:

- The Passive House standard reduces annual energy consumption by 60% to 75% compared to TS 825, depending on the climate zone.
- While consumption varies significantly with climate in TS 825, Passive House design stabilizes energy use between 18–22 kWh/m² across all cities.
- Passive House criteria can completely eliminate heating demand in warm climates through high insulation and optimized solar gains.
- Dynamic simulations yield more optimized and lower energy results than analytical methods by accurately modeling Passive House system interactions.
- The study emphasizes the need to update TS 825 toward a "performance-limited" framework to meet Turkey's national energy targets.

Received: 01.01.2026 Accepted: 22.01.2026 Doi: 10.5281/zenodo.18366481

ABSTRACT

This study comparatively examines the TS 825 Thermal Insulation Requirements Standard, a cornerstone of energy efficiency in Türkiye, and the high-performance Passive House standard regarding EPS insulation thickness in external walls and its impact on building energy performance. Dynamic energy simulations were conducted using OpenStudio–EnergyPlus for a representative residential building model across six distinct climate zones in Türkiye: Adana, Manisa, Istanbul, Eskişehir, Sivas, and Kars. Insulation thicknesses were determined based on the updated 2024 TS 825 U-value limits and Passive House performance criteria, with simulation results compared against analytical calculations. Findings reveal that while TS 825 insulation thicknesses fluctuate based on climatic conditions, the Passive House standard maintains consistently high insulation levels regardless of the climate. In terms of annual energy demand, the Passive House standard achieves a 60–75% reduction compared to TS 825, particularly in cold regions. The results demonstrate that TS 825 focuses on minimum requirements, whereas the Passive House standard provides a more rigorous and holistic framework that directly limits energy consumption. Consequently, the study emphasizes the necessity of evolving the TS 825 standard toward high-performance approaches to meet Türkiye’s energy efficiency targets.

Keywords: TS 825, Passive House Standard, Optimum Insulation Thickness, Building Energy Performance, Energy Simulation

1. Introduction

Proper application of thermal insulation in buildings leads to both economic and energy savings. Thermal insulation reduces heating and cooling costs and provides a more comfortable indoor environment, resulting in lower energy consumption [1]. The external envelope of a structure—comprising walls, floors, roofs, and windows—exerts a critical influence on building energy efficiency, as approximately 70% of total heat loss occurs through these components [2]. Inadequate thermal transmittance values in practice can cause heat losses in building components and lead to moisture and mold formation on interior surfaces, thereby negatively affecting building performance. In addition, thermal bridges disturb thermal comfort, reduce thermal resistance, and increase overall energy consumption. As insulation thickness increases, heat loss decreases and energy efficiency improves; however, increased thickness also leads to higher costs. Therefore, the optimum insulation thickness should be targeted to balance energy savings and cost [3]. In Türkiye, the significant difference between energy production and consumption levels makes efficient energy use more important [4]. For this purpose, the TS 825 Thermal Insulation Requirements Standard is applied in Türkiye. Although this standard defines higher U-value limits compared to the Passive House approach, it serves as a mandatory reference for determining insulation thicknesses. In this study, the insulation thickness requirements proposed by the Passive House standard are compared with the limits defined by TS 825, and the effects of insulation thickness on building energy performance are evaluated.

When the sectoral distribution of energy consumption in Türkiye is examined, the residential sector accounts for a significant share of final energy consumption (20–22%), and this consumption mainly arises from residential energy needs such as space heating and air conditioning [5]. In building energy performance and energy consumption calculations, the largest share belongs to energy used to ensure thermal comfort [6]. Therefore, reducing heat losses in residential buildings is directly related to determining the appropriate insulation thickness. Studies on insulation thickness determination have shown different results for different climate regions in Türkiye. In a study conducted for Yalova, the required insulation thickness was found to be at the lowest level (approximately 2 cm) when the İZO TD wall type was used, whereas higher insulation thicknesses (approximately 3.3 cm) were required for BIMS block wall elements. In addition, it was observed that insulation was not required at an outdoor temperature of 15.5 °C, while the insulation demand increased as the temperature decreased, reaching approximately 4.5 cm at an outdoor temperature of −11 °C [7]. Economic evaluations carried out for Bursa climate conditions using EPS insulation resulted in optimum insulation thickness values ranging from 5.3 to 12.4 cm [8]. In a study considering different insulation materials and varying heating degree-day values for the provinces of Tunceli, Hakkari, and Kars, the optimum insulation thicknesses were determined as 0.079 m, 0.082 m, and 0.104 m, respectively. The same study reported that the ideal insulation thickness across Türkiye varies between 0.028 and 0.096 m [9]. In another study, it was stated that optimum insulation thickness increases with the severity of climate in different climate regions, and that the calculated values for Antalya, İstanbul, Elazığ, and Kayseri vary depending on wall type, insulation material, and fuel type [10].

Other studies in literature analyzed optimum insulation thicknesses for six insulation materials, different energy sources, and four climate regions, reporting that the optimum values vary over a wide range from 2.8 cm to 45.1 cm [11]. In a comprehensive evaluation covering all 81 provinces of Türkiye, optimum EPS insulation thicknesses ranging from 1 to 20 cm were calculated; however, it was stated that these thicknesses do not reach the levels required by the Passive House standard [12]. Previous studies have reported that optimum insulation thickness depends on climatic conditions and that higher insulation thickness is required in colder regions [13]. Similarly, studies conducted for different wall types and insulation materials have shown that optimum insulation thickness varies significantly with

climate region, and that thickness exceeding 20 cm can be optimum for EPS and XPS in some regions [14]. Existing studies mostly focus only on optimum insulation thickness and do not provide a comprehensive comparison that jointly evaluates the current U-value requirements, wall components, and required insulation thicknesses of TS 825:2024, a national standard, and the Passive House standard, an international high-performance standard. The approach adopted in this study quantitatively examines how the two standards produce different results in terms of EPS insulation thickness across different climate regions in Türkiye by comparing the updated 2024 values of TS 825 with the U-values prescribed by the Passive House standard. In this way, the effects of insulation thickness selection on building energy performance are evaluated in a more systematic manner.

2. Material And Method

2.1. Simulation Method

Simulations were conducted to determine the optimum insulation thickness in accordance with the TS 825 and Passive House standards for six climate regions. The definition of simulation parameters and the modeling processes were carried out using the OpenStudio software interface, while the calculations were performed with the EnergyPlus simulation engine integrated into OpenStudio. In this study, a detached residential building with a usable floor area of 103 m² and a 2+1 floor plan was defined as the reference building, and this dwelling was in cities representing six different climate regions, positioned near the city center. The floor plan of the reference building is shown in Figure 1.

In the residential building, the insulation materials used for the roof, floor, and external walls are glass wool, XPS, and EPS, respectively. The properties of the materials used in the building were determined in accordance with the values specified in the TS 825 standard. The construction layers and material properties of the roof, floor, and external walls used in the simulated building are presented in Figures 2, 3, and 4, and in Tables 1, 2, 3, 4, 5, and 6, respectively.

Table 1. Roof Construction Material Properties

Material	Thickness (cm)	Thermal Conductivity (W/m·K)	Density (kg/m³)	Specific Heat (J/kg·K)
Glass Wool	Variable	0.04	70	1030
Reinforced Concrete	15	2.5	2400	2000
Interior Plaster	2	1	1800	1000

Table 2. Total Roof U-Value

Material	Adana	Manisa	İstanbul	Eskişehir	Sivas	Kars
Total Roof U-Value (TS 825)	0.337	0.299	0.299	0.237	0.196	0.192
Total Roof U-Value (Passive House Standard)	0.149	0.149	0.149	0.149	0.149	0.149

Table 3. Floor Construction Material Properties

Material	Thickness (cm)	Thermal Conductivity (W/m·K)	Density (kg/m³)	Specific Heat (J/kg·K)
Lightweight Concrete	10	1.1	1800	1000
Leveling screed	2	1.4	2000	1000
XPS insulation	variable	0.035	35	1450
Screed	3	1.4	2000	1000
Hardwood fiberboard	0.5	0.13	600	1700

Table 4. Total Floor U-Value

Material	Adana	Manisa	İstanbul	Eskişehir	Sivas	Kars
Total Floor U-Value (TS 825)	0.4	0.345	0.345	0.288	0.224	0.231
Total Floor U-Value (Passive House Standard)	0.148	0.148	0.148	0.148	0.148	0.148

Table 5. External Wall Construction Material Properties

Material	Thickness (cm)	Thermal Conductivity (W/m·K)	Density (kg/m³)	Specific Heat (J/kg·K)
Exterior plaster	0.8	0.35	900	1000
EPS insulation	variable	0.05	35	1450
Intermediate plaster	3	1.6	2000	1000
Horizontally perforated brick	25	0.36	700	1000
İnterior plaster	2	1	1800	1000

Table 6. Total External Wall U-Value

Material	Adana	Manisa	İstanbul	Eskişehir	Sivas	Kars
Total External Wall U-Value (TS 825)	0.45	0.399	0.399	0.247	0.183	0.118
Total External Wall U-Value (Passive House Standard)	0.149	0.149	0.149	0.149	0.149	0.149

In this study, a standard three-person household model with an average energy consumption profile was adopted. The simulations were carried out for the provinces of Adana, Manisa, İstanbul, Eskişehir, Sivas, and Kars, representing six different climate regions of Türkiye, and hourly meteorological data sets in EPW (EnergyPlus Weather) format were used for each climate region. The residential geometry was created using the OpenStudio software. The dimensions of the building components used in the simulation model were determined based on standard architectural dimensions; accordingly, door dimensions were defined as 0.90 × 2.10 m. Window dimensions vary depending on room size: living room windows are 2.50 × 1.50 m, room windows are 2.00 × 1.50 m, and bathroom windows are 0.50 × 0.50 m. The definitions of per-capita floor area usage, average internal heat gains per person, lighting, and annual electricity consumption used in the calculation of the total energy use of the dwelling were based on the internal heat gain values specified in the TS 825 standard. In the simulation, a scenario assuming continuous occupancy of the dwelling was considered, and the weekday occupancy schedule was defined as full occupancy between 17:00 and 09:00 (all household members at home) and partial occupancy between 09:00 and 17:00 (one person at home). Energy consumption profile was defined as follows:

- **00:00–07:00:** Minimum consumption due to sleeping hours (base load),
- **09:00–17:00:** Daytime use (variable load between 15% and 60%),
- **19:00–23:00:** Peak usage (80% load).

For Sundays, a special schedule was defined with high energy use throughout the day (09:00–23:00).

In defining the building envelope properties, the TS 825 standard was taken as the basis. The U-values (thermal transmittance coefficients) of windows and doors were assigned according to the relevant climate region. Roof and floor insulation thicknesses were determined based on the minimum thickness values that satisfy the maximum U-value limits specified in the TS 825 standard. To determine the optimum insulation thickness for external walls, the thickness of the EPS insulation material varied iteratively in increments of 0.5 cm, starting

from the initial value that meets TS 825 requirements, and a series of simulations was conducted. In the mechanical system configuration, a natural gas-fired boiler was defined as the heating source, while electric air-conditioning units were used for cooling. The capacities of the heating and cooling systems were calculated based on the peak thermal loads of the building using the auto sizing function of the simulation software. An efficiency value of 0.913 was assigned for the boiler, and a COP value of 3.0 was used for the electric air-conditioning system. Thermostat set points were adjusted in accordance with TS 825 assumptions, with 20 °C for heating and 26 °C for cooling. In addition, the limit values prescribed by the Passive House standard were analyzed comparatively together with the TS 825 standards. The Passive House standard imposes limits on annual total heating and cooling energy demand and primary energy consumption rather than component-based U-value restrictions. In this context, the simulations were evaluated comparatively by also considering window performance criteria that vary according to climate regions.

2.2. Analytical Calculation Method

2.2.1. Layer Thermal Resistance

The thermal resistance of each material layer against heat transfer is calculated by dividing the layer thickness (d) by the thermal conductivity of the material (λ):

$$R_i = \frac{d_i}{\lambda_i} \quad (1)$$

This expression is applied separately to each layer that forms the building element. In the TS 825 standard, internal and external surface resistances (Rsi and Rse) are also mandatory parameters. Although the same calculation method is used in the Passive House standard, much lower U-value targets are defined. Therefore, layer thicknesses and the thermal conductivity values of insulation materials are determined according to stricter criteria.

2.2.2. Total Thermal Resistance

The total thermal resistance of a building element is obtained by summing the resistances of all layers together with the internal and external surface heat transfer resistances:

$$R_{toplam} = R_{si} + \sum R_i + R_{se} \quad (2)$$

In the TS 825 standard, the internal and external surface heat transfer resistances (Rsi and Rse) are defined as constant values (Rsi = 0.13 m²·K/W, Rse = 0.04 m²·K/W). The Passive House approach is also based on the same fundamental principles for total thermal resistance calculation. In this study, to ensure comparability, the Rsi and Rse values defined in TS 825 were also used for the Passive House evaluations.

2.2.3. Thermal Transmittance Coefficient (U-Value)

The thermal transmittance coefficient (U-value) of a building element is calculated as the inverse of the total thermal resistance:

$$U = \frac{1}{R_{total}} \quad (3)$$

The U-value represents the amount of heat transferred per unit area and per unit temperature difference through a building element (W/m²·K). The TS 825 standard defines maximum allowable U-value limits for specific climate regions. In contrast, the Passive House standard adopts a very high-performance approach, with U-values reduced to levels below 0.15 W/m²·K. Therefore, as insulation thickness increases, the U-value significantly improves, leading to a reduction in annual energy demand.

2.2.4. Annual Heating and Cooling Energy

The annual heating or cooling energy demand of a building is calculated using the total heat transfer coefficient of the building elements and Degree-Day data [15].

$$Q = \frac{K_{top}}{\eta} * HDD * \frac{24}{1000} \quad (4)$$

In Equation (4), Q represents the annual heating or cooling energy demand of the building (kWh/year). K_{top} is the total heat loss coefficient of the building envelope (W/K). HDD represents the heating degree-day value

of the related climate region (K·day), while η indicates the overall efficiency of the system.

3. Results And Discussion

Within the scope of the TS 825 and Passive House standards, external wall insulation thicknesses and window thermal transmittance (U-value) limits were examined comparatively. Our findings are specific to the building that is simulated in this study. The data obtained were evaluated in terms of their effects on the thermal performance of the building envelope and annual energy consumption. In addition, the approaches adopted by the standards for different climate regions were discussed. The differences between the results obtained by analytical calculations and simulation methods were also examined.

3.1. Evaluation of Insulation Thicknesses According to the TS 825 Standard

According to the TS 825 standard, insulation thicknesses increase depending on the climatic conditions of the cities. As shown in Table 7, the EPS insulation thickness is 5.6 cm in Adana, which represents a hot climate region, and gradually increases toward colder climate regions, reaching 23 cm in Kars. Similarly, XPS and glass wool insulation thicknesses also show an increasing trend as the climate becomes colder. This indicates that TS 825 adopts an approach focused on reducing heat losses through the building envelope. When the window U-values are evaluated, it is observed that the same value (1.8 W/m²·K) is used for Adana, Manisa, İstanbul, Eskişehir, and Sivas, while a lower limit value of 1.5 W/m²·K is defined only for Kars. This shows that, within the scope of TS 825, window thermal performance requirements are defined similarly for most cities, and stricter window U-value requirements are applied only for Kars, which represents the coldest climate region. In contrast, insulation thicknesses in the TS 825 standard show more significant variations depending on climate conditions and are treated as a more variable design parameter compared to window performance.

3.2. Evaluation of Insulation Thicknesses According to the Passive House Standard

As shown in Table 8, the Passive House standard specifies the same insulation thicknesses and window U-values for all evaluated cities. For all regions, the insulation thicknesses are defined as 29 cm for EPS, 22.5 cm for XPS, and 26 cm for glass wool. For the window component, a U-value range of 0.5–1.3 W/m²·K is used for all cities. This indicates that the Passive House standard aims for a high and constant thermal performance of the building envelopes rather than defining minimum requirements that vary by climate region. The fact that insulation thicknesses do not change regionally shows that the standard adopts a performance-based and standardized design approach. The window U-value of 0.7 W/m²·K, although higher than that of opaque building elements, allows a balanced overall thermal performance of the building envelope when combined with high-performance window frame systems. When the results in Table 2 are evaluated in general, it is clearly seen that the main objective of the Passive House standard is to achieve low and consistent energy performance independent of climatic conditions.

3.3. Comparison of annual energy consumption according to standards

When the annual energy consumption values calculated according to TS 825 and Passive House standards in Table 9 are examined, it is seen that the differences are related to the building envelope properties and the results obtained for different climate zones. In TS 825 standard, insulation and building envelope performance are defined within the framework of minimum requirements. Therefore, as outdoor temperatures decrease, heat losses increase, leading to higher annual energy consumption. According to simulation results, the annual energy consumption under TS 825 is 53.52 kWh/m² in Adana, while it reaches 88.21 kWh/m² in Kars, which represents the cold climate region. A similar trend is observed in analytical calculations; the value calculated as 27.91 kWh/m² for Adana rises to 45.5 kWh/m² in Kars.

Table 7. Insulation Thicknesses According to TS 825 Standards

City	EPS (cm)	XPS (cm)	Glass Wool (cm)	window U value (W/m². K)
Adana	5.6	7.6	11	1.8
Manisa	5.6	9	12.5	1.8
İstanbul	5.6	9	12.5	1.8
Eskişehir	11	11	16	1.8
Sivas	16	14.5	19.5	1.8
Kars	23	17	20	1.5

Table 8. Insulation Thicknesses According to Passive House Standards

City	EPS (cm)	XPS (cm)	Glass Wool (cm)	Window U value (W/m². K)
Adana	29	22.5	26	1.1
Manisa	29	22.5	26	1.3
İstanbul	29	22.5	26	1.1
Eskisehir	29	22.5	26	1.0
Sivas	29	22.5	26	0.7
Kars	29	22.5	26	0.5

Table 9. Comparison of Annual Total Energy Consumption: TS 825 vs. Passive House

City	Total Annual Energy Consumption (TS825) (kWh/m²)	Total Annual Energy Demand (Passive House) (kWh/m²)	Annual Total Energy Use (TS825) (kWh/m²)	Annual Total Energy Demand (Passive House) (kWh/m²)
	Simulation		**Analytical**	
Adana	53.52	21.72	27.91	18.49
Manisa	61.52	20.39	33.9	23.12
İstanbul	78.02	19.42	40.3	25.90
Eskisehir	79.40	20.95	45.4	30.52
Sivas	83.12	21.34	42.3	36.99
Kars	88.21	22.17	45.5	41.62

In contrast, the Passive House standard limits the impact of climate conditions on energy consumption significantly. This is because building envelope performance is determined by high insulation levels, the reduction of thermal bridges, and high air tightness criteria. This situation is clearly seen in the simulation results, where annual energy consumption in all cities remains within a range of 18–22 kWh/m². This demonstrates that the Passive House standard provides balanced and climate-independent energy performance. When the standards are directly compared, the primary reason why the Passive House standard provides lower energy consumption than TS 825 is that heat losses are more limited due to stricter design requirements. According to simulation results, the Passive House standard reduces annual energy consumption by approximately 60% in Adana and 75% in Kars compared to TS 825. This higher reduction in cold regions occurs because Passive House design criteria limit heat losses more effectively when the temperature difference between the indoor and outdoor environments increases. It should be noted that the findings obtained in this study are valid for the specific reference residential building considered and may differ for buildings with different architectural layouts, usage patterns, or construction characteristics.

3.4. Comparison of analytical and simulation results in TS 825 and Passive House standards

In Table 9, it is observed that annual energy consumption values obtained through the simulation method are higher than the analytical method for all cities under the TS 825 standard. For example, in Adana, the simulation result is 53.52 kWh/m², while the analytical calculation is 27.91 kWh/m², representing an increase of 91.8%. Similarly,

the difference is 81% in Manisa, 94% in Istanbul, and 75% in Eskişehir. In Kars, which represents the cold climate region, the difference between simulation and analytical results is 42.71 kWh/m², reaching a percentage difference of 93.9%.

The TS 825 analytical analysis provides a simplified approach by only considering transmission heat losses through the building envelope. In contrast, simulation-based TS 825 calculations include window losses, infiltration, internal and solar gains, and utilization coefficients, leading to higher annual heating energy demands. Therefore, while manual calculations and simulation results do not match exactly, they remain consistent and within the same order of magnitude. When examining the results for the Passive House standard, the relationship between the analytical and simulation methods is reversed. In Adana, the simulation result is 21.72 kWh/m² and the analytical result is 18.49 kWh/m², a difference of approximately 17.5%. However, in Istanbul, the simulation value is 19.42 kWh/m² while the analytical value is 25.90 kWh/m², meaning the simulation result is 25% lower. This difference increases up to 48% in Kars. The lower energy consumption predicted by the simulation method in the Passive House standard is due to the dynamic modeling of high insulation levels, heat recovery ventilation, and system interactions. Since analytical methods represent these interactions only to a limited extent, they predict higher energy consumption, especially in cold climates.

3.5. Analysis of heating and cooling energy use within the scope of Passive House and TS 825 performance criteria

In Table 10, annual heating and cooling energy consumption for different degree-day regions are compared based on the Passive House standard and the TS 825 approach. A fundamental criterion of the Passive House standard is that the annual heating and cooling energy demand must not exceed 15 kWh/m²·year.The table results show that energy consumption remains within these limits under the Passive House approach, especially in low and medium degree-day regions. For example, in Adana, the annual heating energy consumption is calculated as 0 kWh/m² according to the Passive House standard, while it is 20 kWh/m² according to TS 825.The main reason for this difference is that the Passive House approach can eliminate heating demand through high insulation levels, heat recovery ventilation, and the effective use of solar gains. In contrast, the TS 825 standard is based on minimum insulation requirements and does not define a performance goal to reduce heating energy near zero, even in warm climate regions. Furthermore, TS 825 does not set a numerical upper limit for heating and cooling energy consumption. For instance, the heating energy consumption of 66 kWh/m² year calculated for Istanbul according to TS 825 is well above the Passive House limit and is considered high in terms of energy efficiency.

Table 10. Heating and cooling energy demand according to Passive House Standards

Region	Heating Load (kWh/m²)	Cooling Load (kWh/m²)	Heating Load (kWh/m²)	Cooling Load (kWh/m²)
	Passive House		TS 825	
1. Degree-Day Region (Adana)	0	15	21	20
2. Degree-Day Region (Manisa)	0.5	14	33	15
3. Degree-Day Region (İstanbul)	1	13	66	6
4. Degree-Day Region (Eskisehir)	4	11	63	8
5.Degree-Day Region (Sivas)	9	5	60	8
6. Degree-Day Region (Kars)	11	5	71	2

4. Conclusions

In this study, simulation results for TS 825 and Passive House standards were compared. Additionally, the differences between simulation and analytical calculation methods were evaluated for both standards. The results show that energy consumption calculated via simulation is higher than analytical calculations under TS 825. In contrast, for the Passive House standard, simulation methods provide lower and more optimized results. This indicates that both the chosen standard and the calculation method play a decisive role in evaluating a building's energy performance. Findings regarding heating and cooling energy use show that the Passive House standard follows a stricter approach by setting a clear numerical limit on annual energy consumption. On the other hand, TS 825 focuses on minimum requirements and does not include criteria to limit total energy consumption.

In conclusion, while the Passive House standard provides a stricter framework that directly limits building energy performance, TS 825 ensures minimum insulation requirements without limiting total energy use. Therefore, to meet energy efficiency goals in Turkey, it is essential to update TS 825 with a more holistic approach and increase its compatibility with high-performance standards.

5. References

[1] Ünver, Ü., Adıgüzel, E., Adıgüzel, E., Çivi, S., &Roshangnez, K. (2020). Thermal insulation applications in buildings according to climate regions in Turkey. *Journal of Advanced Engineering Studiesand Technologies*, 1(2), 171–187.

[2] Chen, G., Hou, Y., Ge, H., Zhang, S., Liu, X., Guo, X., & Xie, D. (2025). Effect of thermal bridges on the energy performance of Chinese residential buildings. Energy and Built Environment, 6(3), 545-554.

[3] Karakaya, H. (2018). Determination of optimum insulation thickness for heating and cooling in different wall and fuel types and its environmental effects. *Batman University Journal of Life Sciences*, 8(2), 161–172.

[4] Aytaç, A., & Aksoy, U. T. (2006). Relationship between optimum insulation thickness on external walls and heating cost for energy saving. *Journal of the Faculty of Engineering and Architecture of Gazi University*, 21(4), 753–758.

[5] International Energy Agency (IEA). (2023). Turkey – *Energy Efficiencyand Final Consumption Profile.*

[6] Sezer, F. Ş. (2005). Development of thermal insulation in Turkey and external wall insulation systems applied in residential buildings. *Journal of the Faculty of Engineering and Architecture of Uludağ University*, 10(2), 1–12.

[7] Ünlüer, H. C., Değirmenci, A., Üstüntürk, A., Keleşoğlu, A., & Ünver, Ü. (2021).Simulation-based evaluation of insulation thickness in buildings for Yalova. *International Journal of Multidisciplinary Studies and Innovative Technologies*, 5(1), 114–122.

[8] Bolattürk, A. (2008). Optimum insulation thicknesses for building walls with respect to cooling and heating degree-hours in the warmest zone of Turkey. *Building and Environment, 43(6), 1055–1064.*

[9] Işık, E. & Tuğan, V. (2017). The Calculation of the Optimum Thermal Insulation Thickness for the Provinces of Tunceli, Hakkâri, and Kars. *International Journal of Pureand Applied Sciences, 3(2), 50–57.*

[10] Ekici, B. B., Gülten, A. A. & Aksoy, U. T. (2012). A study on the optimum insulation thickness of various types of external walls with respect to different materials, fuels and climate zones in Turkey. *Applied Energy,* 92, 211–217. https://doi.org/10.1016/j.apenergy.2011.10.008.

[11] Aktemur, C. &Atikol, U. (2017). Optimum insulation thickness for the exterior walls of buildings in Turkey based on different materials, energy sources and climate regions. *International Journal of Energy Technology*, 3(2), 72–82. https://doi.org/10.19072/ijet.307239.

[12] Çağlayan, S., Özorhon, B. ve Kurnaz, L. (2022). Natıonwıde mappıng of optımum wall ınsulatıon thıcknesses: a stochastıc approach.Journal of Heat Science and Technology,42(2),169-202. https://doi.org/10.47480/isibted.1194977

[13] Kürekçi, N. A. (2020). Determination of optimum insulation thickness for building walls using degree-day values. *Journal of Thermal Engineering*, 6(5), 873–887.

[14] Timuralp, C. (2025). Evaluation of optimum insulation thickness according to external wall typesto be used in buildings to be reconstructed in Turkey. *Applied Sciences*, 15(5), 2497.

[15] Büyükalaca, O., Bulut, H. & Yılmaz, T. (2001). Analysis of variable-base heating and cooling degree-daysfor Turkey. *Applied Energy*, 69, 269–283.

6. Appendices

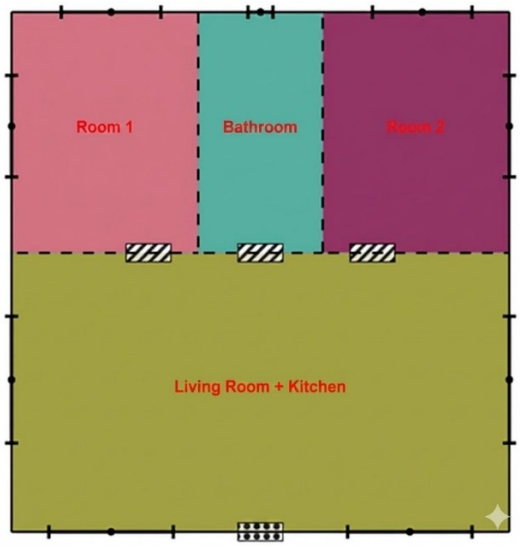

Figure 1. Residential Floor Plan

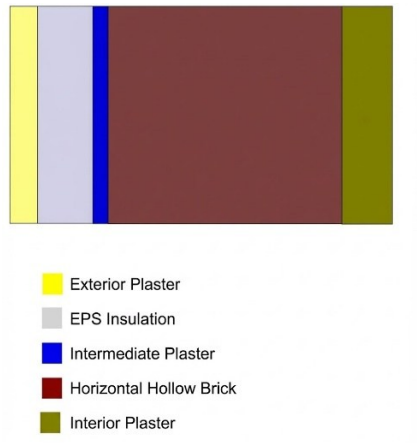

Figure 2. Roof Construction Materials

Figure 3. Floor Construction Materials

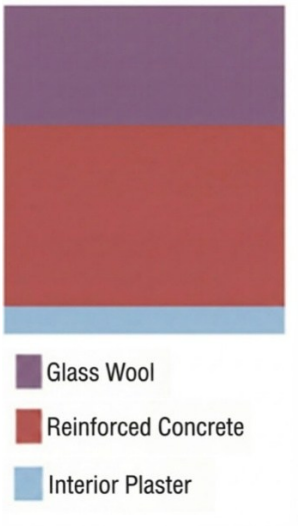

Figure 4. External Wall Construction Materials

ZEROBUILD JOURNAL

Araştırma Makalesi

Seziş ve ark. 04:01 (2026) 66-83

Farklı Duvar Malzemelerinin Bina Enerji Performansı Üzerindeki Etkilerinin Karşılaştırmalı Analizi

Helin Seziş **Kerem Eser** **Mehmet Taşkın**
Sadık Baştürk **Mustafa Aydın**

Yalova Üniversitesi, Yalova, Türkiye
Sorumlu Yazar: kerem.eserr@gmail-com

Öne Çıkanlar

- Çalışma, TS 825 (2024) hedeflerini altı farklı iklim bölgesinde statik ve dinamik yöntemleri kıyaslayarak değerlendirmektedir.
- Yeni standardın zorunlu kıldığı 80 kWh/m^2 enerji hedefinin doğrulanması için dinamik modellemenin şart olduğu belirlenmiştir.
- Statik hesaplar soğuk bölgelerde uygulanamaz duvar kalınlıkları (örn. 341 cm) iken, dinamik simülasyonlar farklı çözümler (örn. 42 cm) sunmaktadır.
- Dinamik simülasyonlar, statik yöntemin genellikle hafife aldığı ısıl kütle ve güneş kazancının kritik önemini ortaya koymaktadır.

Geliş Tarihi: 31.12.2025 Kabul Tarihi: 28.01.2026 Doi: 10.5281/zenodo.18422576

Amaç
Bu çalışmada, Türkiye'nin Adana (Köppen-Geiger: Csa) ve Erzurum (Köppen-Geiger: Dsb) iklimleri ve arasında kalan altı farklı iklim bölgesindeki konut için, farklı duvar malzemelerinin 2024 yılında revize edilen TS 825 standardına göre analitik ve dinamik enerji simülasyon yöntemleriyle karşılaştırması amaçlanmıştır.

Metot
Çalışmada OpenStudio simülasyon programı ve TS 825 (2024) Binalarda Isı Yalıtım Kuralları standardında tarif edilen analitik yöntemler kullanılarak, 103 m2 alana sahip bir evin enerji performansı analiz edilmiştir. Analizde beş farklı ana duvar malzemesi (ahşap, delikli tuğla, gaz beton, kerpiç, perde beton) için yalıtım durumu karşılaştırmalı olarak incelenmiştir.

Sonuçlar
Özellikle soğuk iklim bölgelerinde statik analitik yöntemin güneş kazancı ve malzemenin ısıl kütle etkisini tam olarak modelleyememesi nedeniyle 5. Bölge (Van) gibi illerde kerpiç duvar için 341 cm gibi uygulanabilirliği olmayan kalınlıklar öngördüğünü, buna karşın dinamik simülasyonun (OpenStudio/EnergyPlus) 42 cm gibi makul çözümler sunduğunu ortaya koymaktadır. Ayrıca, düşük ısıl iletkenliğe sahip gaz beton ve ahşap gibi malzemelerin enerji hedeflerine daha ince kesitlerle ulaştığı saptanırken; Erzurum gibi ekstrem iklimlerde hedeflenen enerji limitlerine sadece opak yüzey yalıtımıyla ulaşmanın fiziksel sınırlarına değinilerek, enerji verimliliği optimizasyonunda dinamik simülasyon yöntemlerinin politika ve uygulama süreçlerine entegre edilmesinin kritik önemi vurgulanmaktadır.

Anahtar Kelimeler: TS 825 (2024), Enerji performansı, Duvar malzemeleri, Isı yalıtımı, Dinamik Enerji Simülasyonu.

ZEROBUILD JOURNAL

Araştırma Makalesi

Seziş ve ark. 04:01 (2026) 66-83

Comparative Analysis of the Effects of Different Wall Materials on Building Energy Performance

Helin Seziş **Kerem Eser** **Mehmet Taşkın**
Sadık Baştürk **Mustafa Aydın**

Yalova Üniversitesi, Yalova, Türkiye
Corresponding Author: kerem.eserr@gmail-com

Highlights

- The study evaluates TS 825 (2024) targets by comparing static and dynamic methods across six climate zones.
- Dynamic modeling is identified as essential for verifying the mandated 80 kWh/m² energy target.
- Dynamic simulations offer feasible wall thicknesses in cold regions, whereas static calculations yield impractical results.
- Dynamic simulation highlights the critical importance of thermal mass and solar gain, which are often underestimated by static methods.

Received: 31.12.2025 Accepted: 28.01.2026 Doi: 10.5281/zenodo.18422576

Abstract

Based on the 80 kWh/m² annual energy consumption target introduced by the revised TS 825 (2024) standard, this study comparatively examines the performance of five different main wall materials (wood, perforated brick, autoclaved aerated concrete, sun-dried earth brick, and shear wall) for residences in six different climate zones of Türkiye using analytical calculation and dynamic energy simulation methods. Research findings reveal that the static analytical method fails to fully model solar heat gain and the thermal mass effect of materials in cold climate regions, leading to impractical thickness predictions such as 341 cm for sun-dried earth brick in provinces like Van (5th Zone); in contrast, dynamic simulation (OpenStudio/EnergyPlus) provides feasible solutions such as 42 cm. Furthermore, while it is observed that materials with lower thermal conductivity, such as autoclaved aerated concrete and wood, reach energy targets with thinner sections, the study highlights the physical limits of reaching targeted energy levels solely through opaque surface insulation in extreme climates like Erzurum. Consequently, the critical importance of integrating dynamic simulation methods into policy and implementation processes for energy efficiency optimization is emphasized.

Keywords: TS 825 (2024), Energy performance, Wall materials, Thermal insulation, Dynamic Energy Simulation.

Nomenclature

Symbol	Definition
λ	Thermal Conductivity (W/mK)
ρ	Density (kg/m³)
Cp	Specific Heat (J/kgK)
U	Thermal Transmittance Coefficient (W/m²K)
U_{wall}	Thermal Transmittance of Wall (W/m²K)
U_{ceil}	Thermal Transmittance of Ceiling (W/m²K)
U_{max}	Maximum Heat Transfer Coefficient (W/m²K)
H_{tot}	Specific Heat Loss Coefficient (Total) (W/K)
H_t	Specific Heat Loss Coefficient due to Transmission (W/K)
H_v	Specific Heat Loss Coefficient due to Ventilation (W/K)
V	Ventilation Volume (m³)
n	Air Infiltration Rate (ACH) (h^{-1})
Ψ	Linear Thermal Transmittance (Thermal Bridge) (W/mK)
L	Length of Thermal Bridge (m)
ρ cp	Heat Capacity of Air per Volume (Constant 0.33) (Wh/m³K)
A_n	Net Floor Area (m²)
A_d	Area of Transparent Component (m²)
Q_g	Monthly Total Heat Gain (kWh)
Q_s	Sky Radiation Loss Rate (W)
Q_w	Solar Gains Through Windows Rate (W)
Q_o	Solar Gain from Opaque Surfaces Rate (W)
Q_i	Internal Heat Gains Rate (W)
$Q_{tr,h}$	Heat Transfer for Heating (kWh)
$Q_{tr,c}$	Heat Transfer for Cooling (kWh)
$Q_{req,h}$	Net Heating Energy Requirement (kWh)
$Q_{req,c}$	Net Cooling Energy Requirement (kWh)
Q_y	Specific Annual Energy Consumption (kWh/m²y)
I_d	Solar Radiation Intensity (Direct) (W/m²)
I_{ort}	Average Solar Radiation Intensity (Opaque) (W/m²)
I_{hor}	Solar Radiation on Horizontal Surface (W/m²)
g_{gl}	Solar Energy Transmittance Factor (0.401) (-)
F_{sh}	Shading Factor (0.8) (-)
F_{fr}	Frame Factor (0.25) (-)
R_{se}	External Surface Thermal Resistance (0.04) (m²K/W)
α	Absorption Coefficient (0.60) (-)
t_m	Time Period of the Month (h)
T_o	Monthly Average Outdoor Temperature (°C)
τ	Time Constant (h)
C_m	Thermal Mass of the Building (J/K)
α_H	Alpha Value (Heating) (-)
γ_H	Gain/Loss Ratio (Heating) (-)
η_H	Usage Factor (Heating) (-)
γ_C	Gain/Loss Ratio (Cooling) (-)
η_C	Usage Factor (Cooling) (-)
COP	Coefficient of Performance (-)

1. Introduction

Today, the sustainable use of energy resources and the reduction of environmental impacts are among the primary agenda items for the entire world. According to International Energy Agency (IEA) data, a very large share of global energy consumption and carbon emissions originates from the building sector [1]. Energy consumption in the building sector accounts for approximately 30% of global total energy consumption [2], and it has been calculated that 80% of energy in buildings is consumed for heating and cooling [3].

The correct determination of thermal insulation thickness is not only a legal necessity but also carries critical importance in terms of national energy policies. Building construction and operational activities accounted for approximately 38% of global energy-related CO_2 emissions in 2019, continuing their critical impact on the environment [5]. Adequate insulation offers an energy saving potential of between 30% and 50% in buildings, thereby reducing operating costs and providing a structural contribution to Turkey's goal of reducing greenhouse gas emissions by up to 41% by 2030 [4]. Thermal insulation in buildings is not limited to external walls; insulation must also be applied to areas such as the roof, floor, ceiling, attic, etc. [3]. The recently updated TS 825 (2024 Revision) standard has introduced more restrictive conditions compared to previous versions. For example, the maximum heat transfer coefficient (U_{max}) value for external walls in the 1st Climate Zone, which is the warmest region, has been reduced to 0.40 W/(m^2K), and to 0.25 W/(m^2K) in the 6th Climate Zone [5]. These new limits necessitate the updating of insulation thickness calculations and the re-analysis specific to different wall materials.

In literature, research conducted on the effectiveness of insulation and the determination of thickness shows that insulation dramatically reduces energy consumption. Dombaycı (2010) emphasized that the use of optimum insulation thickness not only reduces fuel costs but also directly contributes to environmental sustainability by reducing CO_2 and SO_2 emissions resulting from combustion by over 40% [7]. Bolattürk (2006), in a comprehensive analysis conducted across different degree-day regions of Turkey, determined that insulation thicknesses vary between 2 cm and 17 cm depending on fuel type and climate zone; and if these thicknesses are applied, energy savings occur in the range of 22% to 79% [8]. However, not only the climate zone but also the orientation of the building is effective in determining the insulation thickness. Özel (2011) stated that wall orientation (north, south, etc.) has a decisive effect on insulation thickness and that solar radiation should be included in these calculations [9]. Similarly, scientific research reports that the annual heating energy requirement of an insulated building compliant with TS 825 standards (29.47 kWh/m^3) is reduced to one-third compared to an uninsulated building (91.84 kWh/m^3) [10]. Economic optimization studies, in analyses conducted for provinces in the reconstruction process after earthquakes, emphasize that insulation thickness varies depending on the Degree-Day (DD) value of the region and the fuel type [11]. As the number of degree-days increases (as the climate gets colder), the required insulation thickness increases. As the number of degree-days increases (as the climate gets colder), the required insulation thickness increases. Colder provinces such as Kars and Erzurum require thicker insulation compared to Erzincan [12]. In other words, as the number of degree-days increases, the insulation thickness increases [13].

Although heating loads are generally prioritized in insulation optimization, the importance of cooling loads is gradually increasing with global warming. Studies have emphasized that to correctly determine insulation thickness, the cooling load must also be included in insulation thickness calculations in DD1 and DD2 regions [14]. Insulation provides energy savings not only for heating but also for cooling loads and is effective in reducing costs [15].

Not only insulation thickness but also the thermal mass of the wall, material properties, and architectural configuration directly affect performance. Yüksel et al. (2021) proved that materials with high thermal mass (e.g., cut stone) are much more successful in damping indoor temperature fluctuations compared to modern aerated concrete walls (temperature amplitude difference: 0.18°C vs. 0.59°C) [16]. Elias-Özkan (2006) stated that local materials such as adobe and straw bales provide a more balanced indoor environment compared to reinforced concrete due to their high heat capacities [17]. In another study on traditional materials, Binici et al. (2005) revealed that the thermal insulation properties and mechanical strength of fiber-reinforced adobe can be improved, thus offering a sustainable building material alternative [18]. In contrast, the moisture factor is also important in the application of modern materials. Pehlivanlı (2009) determined that when the mass moisture content of aerated concrete reaches 48%, its thermal conductivity increases approximately 3 times compared to the dry state [19]. Özer and Özgünler (2019) mentioned that thermal insulation materials lose their thermal insulation properties when they absorb water [20]. This is because the thermal conductivity value of water filling the air gaps is 20 times higher than that of air. Regarding wall configuration, it has been reported that the sandwich wall (aerated concrete) model has the lowest heat loss (3300 W/m^2), while uninsulated brick walls yield the highest loss [21].

This study, shaped in the light of existing literature, aims to provide multifaceted contributions to the field of energy efficiency for the Turkish construction sector. The main objective of the study is to determine the required wall thicknesses for five different wall materials (adobe, shear wall concrete, aerated concrete, perforated brick, and wood) to meet the restrictive U_{max} values introduced by the TS 825 standard revised in 2024. The most important element that distinguishes this paper from other studies is that it is not limited to the new static U-value calculations determined according to TS 825 (2024 revision) but also utilizes dynamic energy simulation tools such as OpenStudio. This study aims to provide a guide based on objective data for architects and engineers in choosing the most economically appropriate wall/insulation combination compatible with the new standards.

2. Material and Method

In this study, an energy performance analysis of a typical 2+1 (100 m^2) residence was conducted in order to meet the thermal insulation conditions determined by the latest 2024 revision of the TS 825 standard. For some of the 5 different construction materials (Wood, Perforated Brick, Aerated Concrete, Adobe, Shear Wall Concrete) across the 6 different climate zones revised according to the TS 825 (2024) standard, wall thicknesses that bring the energy performance of the building to the target of 80 kWh/m^2 were calculated by using EPS (Expanded Polystyrene) insulation material. Energy simulations were performed using the OpenStudio and EnergyPlus engines. In the simulations, TMY (Typical Meteorological Year) weather data in EPW format belonging to the city centers of Adana (1st Zone), Izmir (2nd Zone), Istanbul (3rd Zone), Ankara (4th Zone), Van (5th Zone), and Erzurum (6th Zone) were used to represent the 6 climate zones of Turkey, respectively.

2.1. Building Geometry and Enclosure

The external wall area of the reference building was calculated as 105.89 m^2 and the roof area as 100 m^2, and it was modeled as a single-story detached house. The geometry can be seen in Figure 1. In all building types, the ceiling and floor materials were kept constant; insulation thicknesses were adjusted to provide the U-values compliant with TS 825 (2024) standards in the relevant climate zone (Table 1). Although different wall materials (wood, adobe, etc.) were examined in this study, the floor and ceiling systems were assumed to be standard reinforced concrete in all scenarios. Since the high thermal mass formed by these reinforced concrete elements is dominant, the building heat capacity (C_m) was considered constant

and classified as 'Heavy Building' for all types in the TS 825 calculations.

The building air infiltration rate was assumed to be at a constant value of 0.3 ACH (air changes per hour). Since the brick used in the 1st and 2nd zones exhibits standard and sufficient thermal performance, it was modeled without insulation. The thermophysical properties of the analyzed construction materials are presented in Table 2, and the insulation thicknesses, whose variation according to climate zones was examined, are presented in Table 3.

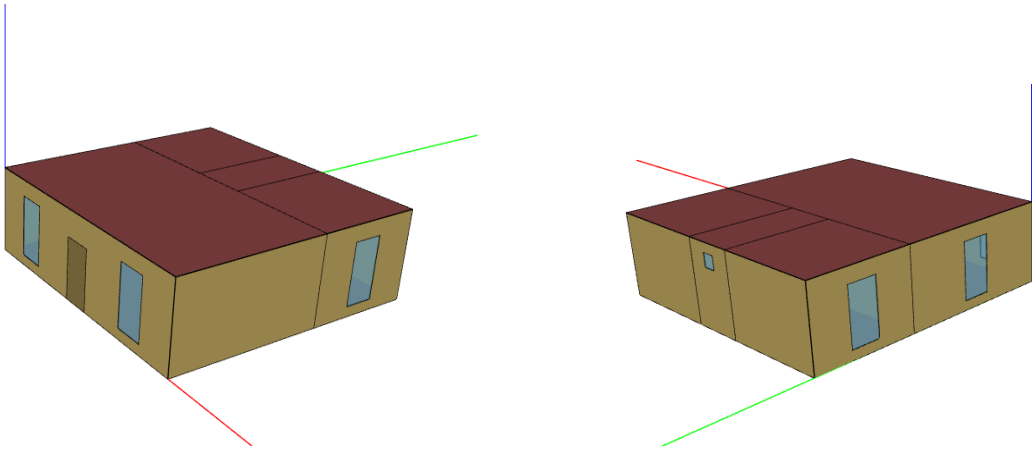

Figure 1. Geometry of the reference building

Table 1. Ceiling and Floor U-values used according to climate zones (W/m^{2}K)

Zones	Ceiling	Floor	Window
Zone 1 (Adana)	0,35	0,4	1,8
Zone 2 (İzmir)	0,3	0,35	1,8
Zone 3 (İstanbul)	0,3	0,35	1,8
Zone 4 (Ankara)	0,25	0,29	1,8
Zone 5 (Van)	0,2	0,24	1,8
Zone 6 (Erzurum)	0,2	0,24	1,8

Table 2. Thermophysical Properties of Building Materials

Material Name	Thermal Conductivity (λ) [W/mK]	Density (ρ) [kg/m³]	Specific Heat (Cp) [J/kgK]
EPS Insulation	0,035	30	1450
Aerated Concrete	0,1	500	1000
Wood (Laminated)	0,13	600	1700
Adobe Block / Mud Plaster	0,2	1000	1000
Perforated Brick	0,29	1000	1000
Interior Plaster (Shear Wall / Aerated Concrete)	1	1800	1000
Exterior Plaster (Brick)	1	1800	1000
Exterior Plaster (Shear Wall / Aerated Concrete)	1,6	2000	1000
Concrete	2,5	2400	1000

Table 3. Thicknesses vary by climate zones according to TS 825 (2024) Standard (m)

Building Type	Variable Layer	Adana (Z1)	İzmir (Z2)	İst. (Z3)	Ankara (Z4)	Van (Z5)	Erzurum (Z6)
Wooden House	Wood Thickness	0,065	0,08	0,11	0,195	0,29	0,7
Brick Wall	EPS Thickness	0	0	0,0025	0,025	0,05	0,17
Shear Wall Concrete	EPS Thickness	0,009	0,014	0,022	0,045	0,069	0,185
Adobe House	Adobe Thickness	0,04	0,078	0,104	0,14	0,37	1
Aerated Concrete	Aerated Concrete Thickness	0,085	0,085	0,085	0,135	0,2	0,54

2.2. Internal Loads and Operating Schedules

The internal gains and usage schedules that determine the energy consumption profile of the residence were established by considering the daily life cycle of an average family. The lighting profile used in the simulations was defined to be off between 08:00-17:00 when daylight is utilized, at full capacity (100%) from 17:00 in the evening until midnight, and at a 10% level during the 00:00-08:00 interval at night. The use of electrical equipment was kept at a minimum 40% load throughout the day, while the usage rate was increased to 100% capacity during the morning (08:00-09:00) and evening (19:00-24:00) hours. While the activity level was kept at a constant value of 70W throughout the simulation, the indoor occupancy hours were structured to intensify in the morning and evening, in harmony with the lighting and equipment profiles.

2.3. Mechanical Systems and Air Conditioning

Constant temperature setpoints were used for the control of air conditioning systems. The indoor design temperature was determined as a constant 20°C for all hours of the day during the winter period (heating) and a constant 26°C for the summer period (cooling). The heating and cooling systems were autosized according to the building dimensions. For the heating system, a combi boiler with a nominal thermal efficiency of 80% and a radiator distribution system were preferred. Furthermore, the boiler water temperature feeding the heating system was kept constant at 67°C. The circulation pump was defined as variable speed with a pressure drop of 60,000 Pa and a motor efficiency of 90%. For cooling requirements, a Packaged Terminal Air Conditioner (PTAC) system with a COP value of 3.0, a fan efficiency of 60%, and a pressure rise of 250 Pa was included in the model. The fan mode was set to operate cyclically, and its heating feature was disabled due to the use of the combi boiler.

2.4. Analytical Calculation Method

The algorithm used in this study is presented in Fig. 2. In these calculations, the "Monthly Calculation Method" defined in the TS 825 (2024) standard was used to determine the energy performance of buildings. Calculations for Zone 3 (Istanbul) are provided as an example. All coefficients and constants used in the equations were taken from Annex C and Annex D of the TS 825 (2024) standard. In the calculations, the thermal transmittance coefficient of the building's opaque component (U_{wall}) was accepted as a variable parameter, while other building components and operating conditions were kept constant.

Fixed Heat Loss (H) Values:

First, the Specific Heat Loss Coefficient (H_{tot}), which consists of transmission (H_t) and ventilation (H_v) heat losses, is defined as follows:

$$H_{tot} = H_t + H_v \qquad (1)$$

The transmission heat loss coefficient (H_t) represents the losses from surfaces and thermal bridges:

$$H_t = \sum(U \times A) + \sum(L + \Psi) \qquad (2)$$

In this study, the effect of thermal bridges (Ψ) was neglected and assumed to be zero in both the analytical calculations and the dynamic simulations to ensure consistency between the two approaches and to focus solely on the performance of the wall materials.

For reference building, the heat loss coefficients of fixed components (excluding external walls) were calculated and summed up to obtain a constant value. These components are detailed in the table below:

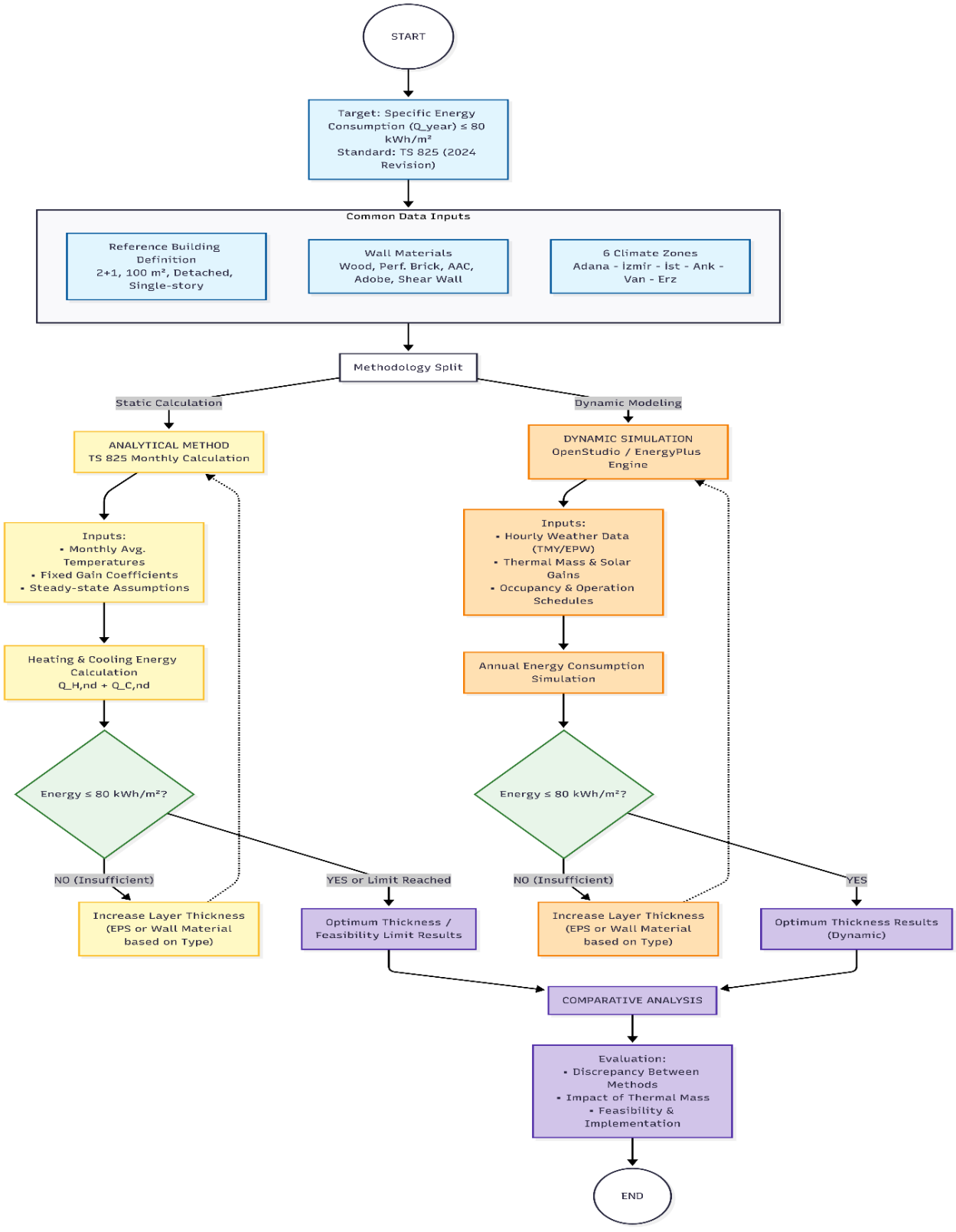

Figure 2. Wall Thickness Analysis Flowchart

Table 4. Fixed heat loss coefficients of the reference building components

Component	Calculation Method	Value (W/K)
Ventilation (H_v)	$0.33 \times A_{net} \times 0.7$ (0.7:m^3/h.m^2 area-based flow rate)	23.10
Ground/Floor(H_g)	Effective U Calculation (($U_{eff} \approx 0.173$)	17.30
Ceiling(H_{ceil})	$100m^2 \times 0.192\, W/m^2\, K$	19.20
Window(H_w)	$11.80m^2 \times 1.801\, W/m^2\, K$	21.25
Door(H_{door})	$2.31m^2 \times 0.870\, W/m^2\, K$	2.01
Fixed Total ($H_{tot/}$)	(Total Excluding Wall)	82.86 W/K

Using this constant value (82.86 W/K), the total Specific Heat Loss Coefficient (H_{tot}) is expressed as a function of the wall thermal transmittance (U_{wall}):

- Specific Heat Loss Coefficient (H):

$$H_{tot} = (U_{wall} \times 105.89) + 82.86 \quad (3)$$

The Total Heat Gains (Q_{gn}) affecting the building's heating and cooling loads were obtained by subtracting sky radiation losses (Q_s) from the sum of solar gains from transparent components (Q_w), solar gains from opaque components (Q_o), and internal heat gains (Q_i). In these calculations, the monthly average solar radiation intensities provided in TS 825 (2024) Annex C (I_d) and outdoor temperature data were used:

- Solar Gains Through Windows (Q_w):

$$Q_w = \sum[A_d \times I_d \times g_{gl(0.401)} \times F_{sh(0.8)} \times (1 - F_{fr(0.25)})] \quad (4)$$

- Solar Gain from Opaque Surfaces (Q_o):

$$Q_o = R_{se(0.04)} \times \alpha(0.60) \times [(U_{wall} \times 105.89 \times I_{ort}) + (U_{ceil} \times 100 \times I_{hor})] \quad (5)$$

- Sky Radiation Loss (Q_s):

$$Q_s = R_{se(0.04)} \times 4.14 \times 11 \times [(0.5 \times U_{wall} \times 105.89) + (U_{ceil} \times 100 \times I_{hor})] \quad (6)$$

- Internal Gains (Q_i):

$$Q_i = 2.75 \times 100 \quad (7)$$

- Monthly Total Heat Gain (Q_{gn}):

$$Q_{gn} = [(Q_w + Q_o - Q_s) + Q_i] \times t_m \times 0.001 \quad (8)$$

Heating Energy Calculation:

The design indoor temperature for the heating season is assumed to be 20°C. The Heat Transfer for Heating ($Q_{tr,h}$) was calculated using monthly average outdoor temperatures (T_o), and the Time Constant (τ) and Alpha Value (α_H) were determined based on the building's thermal mass (C_m) and specific heat loss:

- Heat Transfer Coefficient for Heating ($Q_{tr,h}$):

$$Q_{tr,h} = [(H_{tot} - 17.30) \times (20 - T_o) + 17.30 \times (20 - (13.54))] \times t_m \times 0.001 \quad (9)$$

- Net Heating Energy Requirement ($Q_{req,h}$):

$$Q_{req,h} = Max\left(0; Q_{tr,h} - \left(\eta_H \times Q_{gn}\right)\right) \quad (10)$$

Cooling Energy Calculation:

In cooling period calculations, the indoor design temperature is taken as 26°C. Similar to the heating calculation, but considering conditions specific to the cooling period, Heat Transfer for Cooling ($Q_{tr,c}$)is calculated:

- Heat Transfer for Cooling ($Q_{tr,c}$):

$$Q_{tr,c} = [(H_{tot} - 17.30) \times (26 - T_o) + 17.30 \times (26 - (13.54))] \times t_m \times 0.001 \quad (11)$$

The Cooling Gain/Loss Ratio (γ_C) and the Cooling Utilization Factor (η_C) were determined to account for factors that reduce the cooling load. The Net Cooling Energy Requirement ($Q_{req,c}$) was obtained by subtracting the heat transferred out through building elements and ventilation from the total heat gains:

Similar to Net Heating Energy Requirement, Net Cooling Energy Requirement can be calculated by Eq. (12) considering Cooling Gain/Loss ratio.

- Net Cooling Energy Requirement ($Q_{req,c}$):

$$Q_{req,c} = Max(0; Q_{gn} - (\eta_C \times Q_{tr,c})) \quad (12)$$

Optimization:

To achieve the minimum wall insulation value that provides the limit value, which is the main objective of the study, the annual sum of heating and cooling energies is defined as the Specific Energy Consumption (Q_y). The U_{wall} value at the point where this value equals the limit value ($\frac{80kWh}{m^2 \times year}$) was determined separately for each climate zone using an iterative calculation method:

- Specific Energy Consumption (Q_y):

$$Q_y = \frac{\sum Q_{req,h} + \sum Q_{req,c}}{A_n} \quad (13)$$

In the calculations performed according to the TS 825 standard, insulation thickness was not selected as an independent variable; instead, the annual energy consumption limit of 80 kWh/m², introduced by the 2024 update, was set as the objective function. Using the Excel 'Goal Seek' optimization tool, the maximum thermal transmittance coefficient U_{wall} and the corresponding minimum wall thickness required to meet this energy limit were calculated iteratively.

3. Results

In this study, the minimum wall thicknesses and U-values required to ensure energy performance (80 kWh/m^2) in compliance with the TS 825 (2024) standard in provinces representing 6 different climate zones of Turkey were analyzed using the analytical method and the EnergyPlus program.

3.1. Required Thermal Transmittance (U) Values in Different Climate Zones According to the Analytical Calculation Method

As a result of the analytical calculations performed using the TS 825 (2024 revision), the wall U-values that must be provided in the building envelope to avoid exceeding the targeted annual energy consumption limit are presented in Table 4. It was observed that as the climate zones get colder, the required insulation performance (lower U-value) increases significantly to meet the energy performance target.

While a value of 0.432 kW/m^2 is sufficient for the 1st Zone (Adana), this value must decrease to the level of 0.058 kW/m^2 for the

5th Zone (Van). This situation reveals the critical role of the building envelope in preventing heat loss in cold climate zones.

In the calculations for Erzurum (Zone 6), due to the TS 825 standard being based on critical climatic conditions and the resulting increase in constant heat losses (windows and ventilation), the annual energy consumption could not be reduced below the level of 81.65 kWh/m^2, even if the wall thermal transmittance coefficient was lowered to the theoretical lower limit of 0.00 W/m^{2}K Therefore, a wall U-value that achieves the 80 kWh/m^2 target for Erzurum could not be derived with the specified design parameters. While heat losses originating from windows and ventilation appear high in TS 825 calculations because outdoor climatic conditions are fixed based on critical boundary values (the lowest 25th percentile in winter), the hourly dynamic data used by OpenStudio allows for the optimization of these constant loads by reflecting climatic variability more realistically.

3.2. Wall Thicknesses Compliant with U-values Determined According to TS 825

The wall thickness required according to material types to provide the U-values determined by the analytical method are presented in Table 5 and Figure 3. The differences between the thermal conductivity coefficients (λ) of the materials are clearly reflected in the wall thickness, especially in cold climate zones:

Table 5. Wall U-values provide the required energy performance across different climate zones

Zone	Reference City	Required Wall U-Value (W/m^{2}K)
Zone1	Adana	**0.432**
Zone 2	İzmir	**0.383**
Zone 3	İstanbul	**0.338**
Zone 4	Ankara	**0.209**
Zone 5	Van	**0.058**

Table 6. Wall thickness calculated according to climate zones and house types

Zone	Wooden House (cm)	Aerated Concrete (cm)	Adobe (cm)	Shear Wall Concrete (cm)	Brick Wall(cm)
Zone 1 (Adana)	27,88	26,06	42,9	32,09	29,06
Zone 2 (İzmir)	31,73	29,02	48,82	33,13	30,1
Zone 3 (İstanbul)	36,25	32,5	55,77	34,34	31,32
Zone 4 (Ankara)	59,99	50,76	92,29	40,74	37,71
Zone 5 (Van)	221,93	175,33	341,43	84,33	81,31

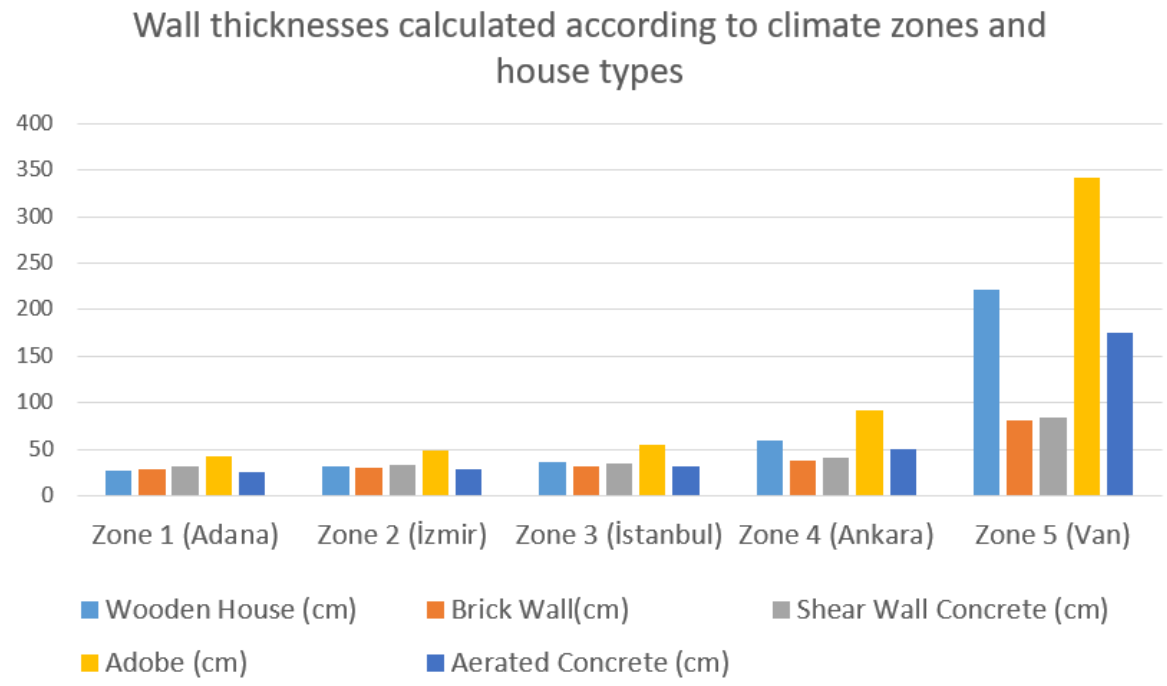

Figure 3. Wall thicknesses calculated with analytically determined wall U-values

3.3. OpenStudio Simulation Results and Thicknesses

The wall thicknesses obtained as a result of OpenStudio simulations, which take dynamic parameters (solar gain, thermal mass, etc.) into account and calculate weather data on an hourly basis, have yielded more feasible results compared to the analytical method (See Table 6 and Figure 4).

- In all regions, materials with better insulation values, such as Aerated Concrete and Wood, achieved the energy target with thinner sections compared to Adobe and Shear Wall Concrete.

- **Erzurum (Zone 6):** According to the simulation results, to meet the energy limit in Erzurum; the wooden wall should be 70 cm, the aerated concrete 59 cm, and the adobe wall 105 cm thick. Although these results are high, they provide a solution set, unlike the analytical method.

- **Comparison of Methods (The Case of Van):** The difference between the methods is seen most clearly in the province of Van. While the analytical method predicts a thickness of 341 cm for the adobe wall, the dynamic simulation calculated this value as 42 cm. This difference demonstrates that dynamic simulation reduces the heating load by using solar gains and the thermal capacity of the building more effectively, and it also highlights the difference between the monthly outdoor temperature data of TS 825 and the outdoor temperatures used in the simulations.

Table 7. Wall thickness obtained because of OpenStudio simulations

Zone	Wood (cm)	Brick (cm)	Shear Wall Concrete (cm)	Adobe (cm)	Aerated Concrete (cm)
Zone 1 (Adana)	6,5	24	25,9	9	13,5
Zone 2 (İzmir)	8	24	26,4	12,8	13,5
Zone 3 (İstanbul)	11	24,25	27,2	15,4	13,5
Zone 4 (Ankara)	19,5	26,5	29,5	19	18,5
Zone 5(Van)	29	29	31,9	42	25
Zone 6 (Erzurum)	70	41	43,5	105	59

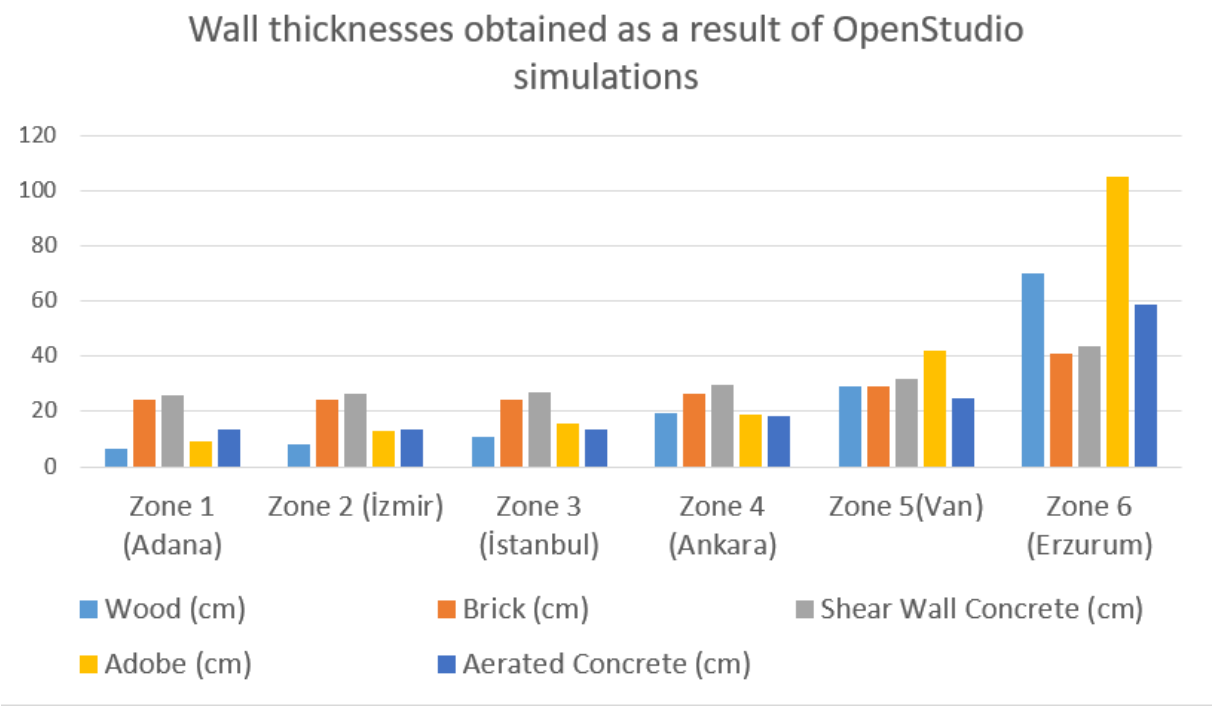

Figure 4. Graphical analysis of the data presented in Table 6.

4. Discussion

The findings obtained in this study reveal significant discrepancies between the analytical calculation method used within the scope of the TS 825 (2024) standard and dynamic energy simulations. Although both approaches confirm that higher wall thicknesses are required to limit heat losses of the building envelopes as climate zones become colder, the quantitative differences between the calculated values are noteworthy. Specifically, the analytical method was observed to predict significantly higher wall thicknesses compared to dynamic simulations

across all climate zones and for all construction materials.

This distinction is clear even in temperate climate zones (Zones 1 and 2). In hot-temperate climatic conditions such as Adana and Izmir, it was determined that the wall thicknesses suggested by the analytical method are two to four times greater than the OpenStudio simulation results. For instance, while the analytical method calculated a wall thickness of approximately 28 cm for wooden residences in Adana, dynamic simulations demonstrated that a thickness of approximately 6.5 cm is sufficient in terms of energy performance. This suggests that the analytical approach maintains excessively high safety margins, even in milder climates.

As climatic conditions become more severe, the divergence between the two methods becomes even more pronounced. In the fourth and fifth climate zones, particularly in the province of Van, it was observed that the wall thickness calculated by the analytical method reached values exceeding practical application limits. For Van, the analytical method's prediction of approximately 222 cm for wooden structures and 341 cm for adobe (mudbrick) structures renders the direct applicability of this method in cold climates controversial. In contrast, dynamic simulations offer reasonable and feasible solutions for the same energy performance target, such as 29 cm for wood and 42 cm for adobe, which are viable in terms of construction techniques.

The basis of this difference lies in the calculation logic of the two approaches. The analytical method based on TS 825 relies on monthly average climate data and steady-state assumptions. In this method, solar gains, internal heat gains, and the time-dependent thermal behavior of structural elements are represented to a limited extent. Conversely, OpenStudio/EnergyPlus-based dynamic simulations provide a modeling approach closer to the actual operating conditions of the building by utilizing hourly climate data.

In particular, the behavior of building materials with high thermal mass plays a crucial role in explaining the difference between the two methods. Materials such as adobe, brick, and concrete can store heat during daylight hours and release it to the interior environment at night, thereby limiting indoor temperature fluctuations. While dynamic simulations account for this "time lag" effect in detail, the analytical method represents this effect largely through fixed coefficients. Consequently, the analytical approach necessitates excessive insulation or wall thickness in most cases to achieve the targeted energy consumption values.

The results obtained for Erzurum, located in the sixth climate zone, clearly demonstrate that merely improving wall insulation is insufficient beyond a certain point. Dynamic simulations revealed that even if the wall heat transfer coefficient is theoretically reduced to near zero, annual energy consumption remains slightly above the 80 kWh/m² target. This finding indicates that heat losses originating from window areas and ventilation become decisive factors in harsh climatic conditions. Nevertheless, dynamic simulations suggest technically feasible wall thicknesses for materials like wood, aerated concrete, and adobe, pointing to the necessity of a holistic design approach.

When evaluated in terms of material type, it was observed that aerated concrete and wooden structures, which possess low thermal conductivity coefficients, can reach energy targets with thinner wall sections compared to materials like adobe and shear wall concrete. For example, a thickness of approximately 25 cm is sufficient for aerated concrete walls in Van, whereas this value increases to 42 cm for adobe walls. This result reconfirms that the direct thermal insulation capacity of the construction material is a determinant for the required wall thickness.

Overall, the results obtained from both analytical and dynamic methods demonstrate that a more robust building envelope is required to meet energy performance targets as climate zones get colder. These findings are

consistent with previous studies by Timuralp et al. [10] and Çomaklı and Yüksel [11], supporting the critical role of the building envelope in limiting heat losses in cold climates. However, the results of this study show that dynamic energy simulations have the potential to produce more realistic and applicable design decisions compared to analytical calculation methods, especially under severe climatic conditions.

5. Conclusion

Based on the recently revised TS 825 (2024) standard's Annual Primary Energy Consumption (APEC) target of 80 kWh/m^2, this study analyzed the wall thicknesses of residences in six climate zones of Turkey across five different main wall materials (Wood, Perforated Brick, Aerated Concrete, Adobe, and Shear Wall Concrete) using both the Analytical (Monthly Calculation) Method and Dynamic (OpenStudio/EnergyPlus) Simulation.

The most critical finding of the study is the distinct difference between the two methods. The analytical method predicted wall sections that are too thick to be structurally feasible for achieving energy targets, especially in cold climate zones (Zone 4 and beyond). The most prominent example of this deviation was observed for the Adobe House type in Zone 5 (Van): while the analytical calculation determined a thickness of 341.43 cm (Table 5), the dynamic simulation calculated this value as 42 cm (Table 6). This difference proves that dynamic simulations model the heating load reduction effects of high thermal mass and solar gains more accurately than the analytical method.

For Zone 6 (Erzurum), Turkey's coldest region, the analytical method failed to derive a feasible wall U-value and thickness to meet the targeted 80 kWh/m^2 limit. This is thought to be because heat losses from windows and ventilation appear high in TS 825 calculations—where outdoor climatic conditions are fixed based on critical boundary values (the lowest 25th percentile in winter) whereas the hourly dynamic data used by OpenStudio reflects climatic variability more realistically, allowing for the optimization of these constant loads. In contrast, dynamic simulations were able to offer technically feasible solutions for Wood (70 cm), Aerated Concrete (59 cm), and Adobe (105 cm). According to simulation results, materials with naturally better insulation values, such as Aerated Concrete (λ=0.1W/mK) and Wood (λ=0.13W/mK), achieved the energy target with thinner wall sections.

In conclusion, to reach the 80 kWh/m^2 APEC target set by the TS 825 (2024) standard, the Analytical Calculation Method produces overly cautious results, particularly for high-thermal-mass structures and cold climate zones. The use of Dynamic Energy Simulation methods in energy efficiency optimization is of critical importance for providing applicable and feasible building solutions.

6. References

[1] IEA. (2023). World Energy Outlook 2023. International Energy Agency, Paris.

[2] Erbıyık, H., Çatal, T., Durukan, S., Topaloğlu, D. G., & Ünver, Ü. (2021). Assessment of Yalova University Campus according to LEED V. 4 certification system. *Environmental Research and Technology*, 4(1), 18-28. doi: 10.35208/ert.812339.

[3] Ünver, Ü., Adıgüzel, E., Adıgüzel, E., Çivi, S., & Roshanaei, K. (2020). Thermal Insulation Applications in Buildings According to Climate Zones in Turkey. *Journal of Advanced Engineering Studies and Technologies*, 1(2), 171-187. (In Turkish).

[4] Republic of Turkey Ministry of Environment, Urbanization and Climate Change. (2023). Turkey's Updated First Nationally Determined Contribution (NDC). Ankara.

[5] United Nations Environment Programme (UNEP). (2020). 2020 Global status report for buildings and construction: Towards zero-

emissions, efficient and resilient buildings and construction sector. Retrieved from https://wedocs.unep.org/handle/20.500.11822/34572. (Accessed October 4, 2023).

[6] TS 825. (2024). Thermal Insulation Requirements for Buildings (Revised Standard). Turkish Standards Institution (TSE), Ankara.

[7] Dombaycı, Ö. A. (2010). The environmental impact of optimum insulation thickness for external walls of buildings. *Building and Environment*, 45(7), 1746-1751. doi: 10.1016/j.buildenv.2006.10.054

[8] Bolattürk, A. (2006). Determination of optimum insulation thickness for building walls with respect to various fuels and climate zones in Turkey. *Applied Thermal Engineering*, 26(11-12), 1301-1309. doi: 10.1016/j.applthermaleng.2005.10.019

[9] Özel, M. (2011). Effect of wall orientation on the optimum insulation thickness of building walls. *Energy Conversion and Management*, 52(1), 485-489. doi: 10.1016/j.apenergy.2011.01.049

[10] Yüksek, İ., & Sıvacılar, S. (2016). Comparison of thermal performance of traditional buildings and reinforced concrete buildings based on TS 825 (Thermal insulation requirements for buildings). *International Advanced Technologies Symposium (IATS'16)*, Elazığ, Turkey.

[11] Timuralp, C., Aras, N., Şişman, N., & Aras, H. (2025). Evaluation of Optimum Insulation Thickness According to External Wall Types to be Used in Reconstructed Buildings in Turkey. *Applied Sciences*, 15, 2497. doi:10.3390/app15052497

[12] Çomaklı, K., & Yüksel, B. (2003). Optimum insulation thickness of external walls for energy saving. *Applied Thermal Engineering*, 23(4), 473-479.

[13] Geliş, K., & Yeşildal, F. (2020). Determination of Minimum Insulation Thickness with the Change of Heat Conduction Coefficient in Case of Using Conventional and Modern Construction Elements. *Gümüşhane University Journal of Science and Technology Institute*, DOI:10.17714/gumusfenbil.725909. (In Turkish).

[14] Aydın, N., & Bıyıkoğlu, A. (2020). Effect of Cooling Load on Optimum Insulation Thickness in Residential Buildings. *Journal of Thermal Science and Technology*, 40(2), 281-291. (In Turkish). doi:10.47480/isibted.817036

[15] Uçar, A., & Balo, F. (2010). Determination of the energy savings and the optimum insulation thickness in the four different insulated exterior walls. *Energy*, 35(1), 88-94. doi: 10.1016/j.renene.2009.07.009

[16] Yüksel, A., Arıcı, M., & Karabay, H. (2021). Comparison of thermal response times of historical and modern building wall materials. *Journal of Thermal Engineering*, 7(6), 1506-1518. doi: 10.18186/thermal.991093

[17] Elias-Ozkan, S. T. (2006). **A** Comparative Study of the Thermal Performance of Building Materials. *PLEA 2006 - 23rd Conference on Passive and Low Energy Architecture*, Geneva, Switzerland, September 6-8, 2006.

[18] Binici, H., Aksogan, O., & Shah, T. (2005). Investigation of fiber reinforced mud brick as a building material. *Construction and Building Materials*, 19(4), 313-318. doi: 10.1016/j.conbuildmat.2004.07.013

[19] Pehlivanlı, Z. (2009). Investigation of the Change of Thermal Conductivity of Autoclaved Aerated Concrete with Moisture and Temperature. *International Journal of Engineering Research & Development*, 1(2), June 2009. (In Turkish).

[20] Özer, N., & Özgünler, S. (2019). Evaluation of Performance Characteristics of Commonly Used Thermal Insulation Materials in Buildings on Wall Sections.

Uludağ University Journal of the Faculty of Engineering, 24(2). (In Turkish). doi: 10.17482/uumfd.438738

[21] Kan, A. (2024). Numerical Investigation of the Effect of Thermal Insulation in Different Exterior Wall Models. *BSEU Journal of Science*, 11(2), 385-393. (In Turkish). doi: 10.35193/bseufbd.1379760